DELFT UNIVERSITY OF TECHNOLOGY

MSC THESIS

BY RENEKE KOLFF

Converting the LNG-Peakshaver to be fit for processing LH_2

gasunie transport services

TU Delft

Converting the LNG-Peakshaver to be fit for processing LH_2

By

Reneke Kolff

in partial fulfillment of the requirements for the degree of

Master of Science
in **Mechanical Engineering**

at the Delft University of Technology,
to be defended publicly on Thursday 15 July, 2021.

Student number:	4333837	
Project duration:	October 1, 2020 - July 15, 2021	
Thesis committee:	Prof. Dr. A.J.M. van Wijk	TU Delft, supervisor
	Prof. Dr. J.J.C. Geerlings	TU Delft, supervisor
	Dr. S.A. Saadabadi	TU Delft
	Ir. A. G. de Bakker	Gasunie, supervisor

gasunie transport services

TU Delft

Preface

This thesis is my final work to complete the Master's degree in Mechanical Engineering (track Energy & Process Technology) from the Delft University of Technology. During the past ten months, I have conducted scientific research for Gasunie to determine if their current LNG-Peakshaver can be retrofitted to a liquid hydrogen import terminal. This thesis could not have been completed without the support of several people, who I would like to thank beforehand.

I would like to express my gratitude to my supervisors from the TU Delft, Prof. Dr. Ad van Wijk and Prof. Dr. Hans Geerlings, for their excellent guidance and support throughout my research. The endless knowledge from Ad about hydrogen, his extensive network and his gentle pressure to complete this thesis in time have been of immense value. This was very well complemented by the in-depth process know-how of Hans and his guidance regarding the technical aspects of the study. Both have been essential for accomplishing this research.

Furthermore, I would like to thank Gasunie for giving me the opportunity of conducting my graduation research in these difficult times. During this period, I could join the weekly team meetings, consisting of Adriaan de Bakker, Daan Velter, Martijn Theelen, Wim Tichelaar, Peter Verkerke, Marcel Adrichem, Jan Bezuijen and Johan Douma. I have genuinely enjoyed these meetings and discussions, which have significantly contributed to the success of this research. In addition, special thanks to Adriaan de Bakker, who was my daily supervisor at Gasunie. I appreciated the time and the fruitful meetings we had. Adriaan's vision and input gave me new insights and helped me focus on the essential aspects, keeping me on track. Lastly, I would like to thank Geert Jager for supporting me with the Aspen simulations. I had never used Aspen Plus, so all the time and effort from Geert was really valuable.

I look back at an exciting and worthwhile period in which I acquired an enormous amount of knowledge in the field of hydrogen. It also taught me how working in and with a diverse team can accelerate the speed and quality of developing new solutions and innovation. I sincerely hope this research will provide a small contribution to successful hydrogen projects for Gasunie in the future.

Reneke Kolff
Amsterdam, July 2021

Abstract

To reach the goals of the European Green Deal (CO_2 emission reduction of 55% by 2030 and climate neutral by 2050), North-Western Europe has to import sustainable energy as locally produced renewable energy will not be sufficient to meet the total demand. This will be realised by importing green hydrogen from areas with a surplus of renewable energy. If those areas are in another continent, the hydrogen is expected to be imported by vessel and received and stored at a hydrogen import terminal. Since Gasunie has an LNG plant in the Port of Rotterdam that becomes available within a few years, they want to investigate the possibilities to retrofit this plant into a hydrogen import terminal.

This research has investigated if the current LNG-Peakshaver, owned by Gasunie, can be retrofitted to an LH_2 import terminal. This import terminal will receive, store and process LH_2 to be delivered to the hydrogen Backbone (future hydrogen grid in the Netherlands owned by Gasunie). The imported LH_2 will be received from maritime vessels at conditions just above ambient pressure and below its boiling point (-253°C). It will be stored in the retrofitted LNG storage tanks, and depending on the hydrogen demands of the grid, LH_2 will be processed (regasified) to the requirements of the grid (5°C and 50 bar). This send-out process is very similar to LNG and requires pumps, BOG compressors and evaporators as process equipment.

The **differences in physical and chemical properties** have been analysed to determine if retrofitting LNG process equipment into LH_2 application is feasible. The three main property differences that most affect the processes at the terminal are 1. the lower temperature (-253°C instead of -162°C), 2. the lower density and 3. the lower latent heat of vaporization of LH_2 as compared to LNG. In view of these differences, it has been established that the reuse of the current LNG equipment is not possible. Even the pipes cannot be reused, as the LH_2 pipes must be vacuum insulated to prevent liquid oxygen formation at the outside of these pipes.

Enhanced research has been carried out into the **required process equipment**. For the LH_2 pumps, cavitation and the low pressure-head of the centrifugal pump are a problem. To overcome these, a special inducer is used, and three HP pumps in series to reach the desired pressure of 50 bar. Regarding the hydrogen BOG compressors, a vertical labyrinth (reciprocating) type is considered. However, manufacturers cannot yet design compressors that operate at temperatures as low as -250°C. For the evaporator, a Super-ORV design with seawater as the heat source is considered the best option to evaporate the LH_2. This design is an enhanced ORV that improves the heat transfer, which is desirable considering the lower temperatures of LH_2.

Retrofitting the LNG tank is essential since it is the most expensive part of the plant. The current inner tank material and insulation are not capable of handling LH_2. Therefore, two solutions have been explored to retrofit the storage tank. The more expensive solution -resulting in a lower BOR- is implementing a new vacuum insulated storage tank inside the existing concrete construction. The other option is to attach membrane insulation panels at the inside of the current storage tank.

Simulations have been performed to analyse the desired terminal configuration with regard to energy efficiency. The differences in configuration depend on the tank's insulation method, BOG processing, and cold exergy utilization. From these results, it is concluded that a compressor that can handle temperatures as low as -250°C is essential for an LH_2 terminal as it dramatically improves energy efficiency. Considering the terminal configuration, it is concluded that a membrane insulated tank combined with a recondenser to process the BOG flow is the desired solution if the terminal has baseload send-out. However, when a low minimum flow is required, a vacuum insulated tank in combination with "cold" BOG compressors is the best solution. Both configurations have an energy efficiency loss for baseload send-out of 0,13% of the HHV. To determine the feasibility of the terminal configuration, a further cost-efficiency evaluation is essential, next to this energy efficiency analysis.

The **overall conclusion** is that for the storage tank, the most expensive part of the plant, potential solutions to retrofit it exists. Especially the membrane insulation method is very promising and deserves more in-depth research. However, reusing the LNG process equipment is not possible. The equipment for the LH_2 process is not yet commercially available except for the LH_2 pumps. Further research is recommended because an LH_2 import terminal has many advantages over other hydrogen import terminals, namely a relatively simple and flexible send-out process that requires little energy input.

Contents

List of Figures

List of Tables

Acronyms

BC	Brayton cycle
BOG	Boil-off gas
BOR	Boil-off rate
BS	Baseload
BWRS	Benedict-Webb-Rubin-Starling
CAPEX	Capital Expenditure
EOS	Equation of state
EU	European Union
G-gas	Groningen-gas
GTT	Gaztransport Technigas
H_2	Hydrogen
H-gas	High calorific gas
HEX	Heat exchanger
HHV	Higher heating value
HP	High pressure
LH_2	Liquid hydrogen
LHV	Lower heating value
LIN	Liquid nitrogen
LNG	Liquid natural gas
LNG-PS	LNG-Peakshaver
LOHC	Liquid organic hydrogen carrier
LP	Low pressure
MBWR	Modified-Benedict-Webb-Rubin
$NPSH_A$	Net positive suction head available
$NPSH_R$	Net positive suction head required
OPEX	Operating Expenses
ORV	Open rack vaporizer
PC	Power cycle
PEM	Polymer Electrolyte Membrane
PS	Peakshaver
PSA	Pressure swing adsorption
RC	Rankine cycle
REFPROP	NIST Reference Fluid Thermodynamic and Transport Properties Database
SG	Specific gravity
SOFI	Spray on foam insulation
SRK	Soave-Redlich-Kwong
SW	Seawater
WF	Working fluid

1 Introduction

The global energy market will change rapidly due to enhanced international environmental regulations. These enhanced regulations are outlined in the Paris Agreement, which was adopted in December 2015. The Netherlands joined this agreement and agreed to reduce the CO_2-emissions by 40% in 2030, compared to the CO_2-emission levels of 1990 [1]. In addition, the EU recently presented the European Green Deal and plans to reduce emissions by at least 55% by the end of 2030 [2]. The aim of the European Green Deal is to be the first continent to be climate neutral in 2050 [3].

Regarding the recent developments in the transition to a carbon-neutral society, an important role is expected from hydrogen as a clean and sustainable energy carrier [4]. The Dutch government recently conducted research to determine the importance of hydrogen in the future [5]. This study showed that both the large industrial clusters as well as the ports of the Netherlands consider green hydrogen as an essential part of achieving the environmental goals of 2050. In industry, renewable hydrogen should replace fossil fuels in processes where electrification is not a viable option [6].

In the ideal situation, the green hydrogen is produced with locally generated renewable electricity. In case of the Netherlands, most of the green hydrogen will be produced with offshore wind energy [7]. However, considering the massive demand for energy in industry, the Dutch produced green energy will not be sufficient for the total hydrogen demands [7]. Furthermore, the production of green hydrogen in the Netherlands is more expensive than in other parts of the world [8], [9]. This is not only the case for the Netherlands but for all of North-Western Europe [8], [9]. So to reach the environmental goals, North-Western Europe, including the Netherlands, has to import green hydrogen on a large-scale [8], [9], [10].

Currently, there are no large-scale green hydrogen production facilities; but it is a matter of time before these facilities will be built [11], [12]. The location of these facilities will be at places around the world where there is a surplus of renewable energy, e.g. solar energy in Australia, the Middle East, North Africa, Latin America, and Southern Europe [9]. Large-scale hydrogen transport to Europe is possible in two ways, either by pipeline or ships [13]. The Dutch government expects hydrogen import from other continents will be done by large maritime vessels [5]. This also offers the possibility to import hydrogen independently from other countries, which is not the case when using pipelines. Furthermore, the Netherlands has the opportunity to operate as the hydrogen hub for North-Western Europe, thanks to its favourable location, the ports and the extensive gas network and storage capacity [5]. In order to enable the import of hydrogen with the use of maritime vessels, a hydrogen receiving terminal is necessary.

1.1 Background - LH_2 import

For long-distance overseas transport, it is necessary to reduce volume by converting gaseous hydrogen into a higher energy-dense state per unit volume [14]. Many different forms to store hydrogen at a higher energy-dense state can be distinguished [15]. However, at the moment, three options are most promising for overseas transport by maritime vessels. Those options are: liquification to liquid hydrogen (LH_2), converting to (liquid) ammonia (NH_3) or Liquid Organic Hydrogen Carriers (LOHC) [6].

A worldwide transportation infrastructure exists for ammonia already, as ammonia is consumed in large quantities by the fertiliser industry [16]. Therefore, it has a lot of potential in the early phase of large-scale hydrogen transportation [16]. Furthermore, the storage conditions of liquid ammonia are near ambient conditions; stored refrigerated at -33,3°C or in the pressurised case at around 9 bar [14], [17]. The disadvantage of this option is that substantial energy is needed for converting ammonia back to hydrogen at the location of the receiving terminal, i.e. in an area where energy cost are high.

The advantage of a LOHC is that the hydrogen is stored in liquid form under atmospheric conditions, and no CO_2 is released when the hydrogen is released from the carrier [6]. Another benefit of most LOHCs is the fact that it has similar properties as crude oil-based liquids, so existing infrastructure can be used for transportation and storage [18]. However, also this option requires high energy for conversion at the receiving terminal.

Transporting LH_2 has many similarities with LNG transport, which has already been proven as a good way of importing gas [6]. However, due to the lower temperature and the ease of evaporation of LH_2, the current infrastructure cannot be used [6], [19]. This is a disadvantage compared to the other hydrogen carriers. On the other hand, a significant advantage of the option with LH_2 is that conversion to the higher energy-dense state (liquefication) happens at the location of the hydrogen production – before transportation [20]. This conversion energy will be sourced at the production location where a lot of green energy is available and at low costs. This makes the LH_2 solution a very (cost) efficient one, even if the overall round-trip conversion efficiency is not the highest. Figure 1 gives an overview of the conversion efficiencies to convert hydrogen to the higher energy-dense state (hydrogen carrier) and vice versa.

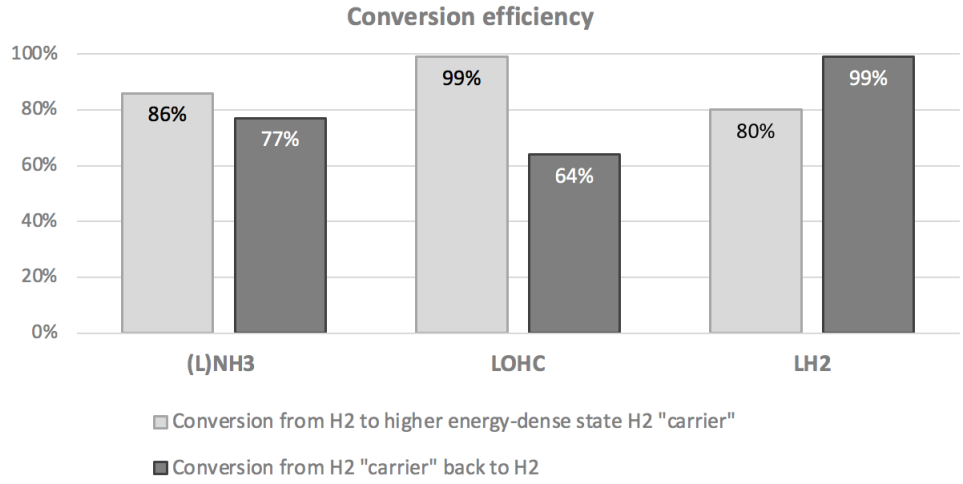

Figure 1: The efficiency to convert hydrogen into a higher energy-dense state for overseas transport, and convert it back to hydrogen gas. The conversion efficiencies are related to the HHV of hydrogen. [20], [21], [22], [23], [24], [25], [26]

In addition to the higher energy demands to recover hydrogen from NH_3 or LOHC, these processes are also more complicated than for LH_2. For the hydrogen retrieval process out of NH_3 or LOHC, a cracking or dehydrogenation reaction is required [22]. Both are catalytic endothermic reactions, which require high temperatures. After the decomposition reaction, hydrogen separation is necessary to generate pure hydrogen. For the decomposition as well as for the separation reaction, a lot of research is still being done to improve the efficiencies and scalability [16], [18].

For the LH_2 case, the processes at the import terminal site are comparable to an LNG import terminal [27]. The LH_2 terminal requires only LH_2 pumping and evaporation to deliver pure hydrogen to the grid. The advantage of this send-out process over the other terminals is the ease with which the transmission speed can be adjusted. Having a hydrogen terminal that can quickly scale up and down the output capacity is beneficial as it provides flexibility. This is valuable for the hydrogen supply to the grid, for example, to absorb the fluctuating hydrogen production from wind energy in the Netherlands.

1.2 Background - Gasunie & LNG-Peakshaver

Gasunie is a European energy network operator that manages natural gas transport infrastructure in the Netherlands and the Northern part of Germany. Gasunie's network is one of the most extensive gas transport high-pressure networks in Europe. It consists of more than 15,000 km of pipelines, dozens of installations, and approximately 1,300 gas receiving stations. The annual throughput of gas is around 125 billion cubic meters [28].

It is expected that natural gas throughput will decrease in the coming years, due to the energy transition as well as the decommissioning of the Groningen gas field [29], [30].

The transition to renewable hydrogen significantly affects the existing energy infrastructure in the Netherlands [4], [31]. Therefore, Gasunie is developing a hydrogen gas grid in the Netherlands, which has recently been supported by the Dutch government [32]. With this grid, called Hydrogen Backbone, Gasunie aims to maintain its key position as an energy infrastructure company in the future [29].

The reduced throughput of natural gas is favourable for constructing the Hydrogen Backbone because many existing natural gas pipes will become available for reuse. Gasunie estimates that approximately 90% of the Hydrogen Backbone will consist of reused natural gas pipeline [29], making it relatively easy to deploy the hydrogen network quickly at affordable costs.

Besides their gas transportation network, Gasunie also owns several installations. One of these is the LNG-Peakshaver (LNG-PS), located at the Maasvlakte in the Port of Rotterdam (see figure 2). This plant converts pipeline natural gas into LNG via its on-site purification, liquefaction, and storage facility. At periods of low ambient temperatures and high natural gas off-take, the stored LNG can be pumped to high pipeline pressure, evaporated and injected into the gas grid. Therefore, the Peakshaver is operational during winter, on days when severe frost requires extra gas for domestic consumers. The LNG-PS has a storage capacity of 78 million normal cubic meters of natural gas, and the maximum send-out capacity is equal to 1,3 million normal cubic meters per hour [28].

Due to the reduction in natural gas supply, the function of the Peakshaver to act as a natural gas buffer for domestic consumers is no longer needed in the near future. Meaning another purpose has to be determined for this site in the Port of Rotterdam.

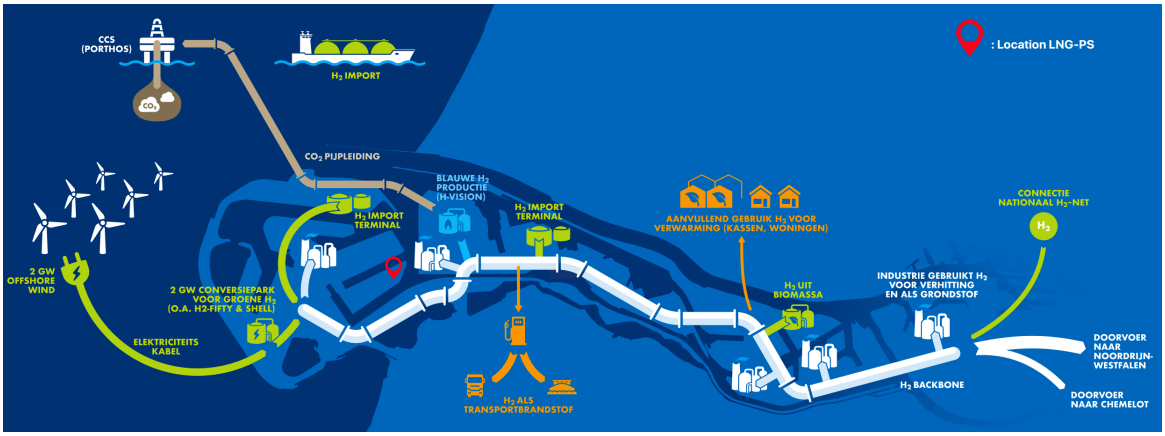

Figure 2: Shows the ideal location of the LNG-PS and the future projects in the Port of Rotterdam regarding the hydrogen economy [10].

As shown in figure 2, the Peakshaver and its location provide various opportunities to play a role in the energy transition. It can be a part of the Porthos project, for example, by liquefying the captured CO_2 or compress the CO_2 to the offshore well. Another option is utilising offshore wind energy to produce hydrogen. However, the most promising new function for the LNG-PS is a hydrogen import terminal. A preliminary investigation has determined that two options are feasible for retrofitting the LNG-PS into a hydrogen import terminal, namely an NH_3 or LH_2 terminal. Of these, LH_2 is considered the most promising, as the process philosophy has many similarities with the current LNG installation, the energy demand for the conversion to hydrogen is low and the system has high flexibility in scaling up and down the output.

For all of the above reasons, an LH_2 terminal as future utilization of the current LNG-Peakshaver is selected to further investigate in this research.

1.3 Purpose of this research

The purpose of this research is to provide Gasunie with meaningful insights that can contribute to maintaining its key position as an energy infrastructure company in the -fossil free- future. This investigation into the conversion of the LNG-Peakshaver into an LH_2 terminal will do so by providing the following aspects:

1. **Knowledge of the process and the design of LH_2 storage**
   Investigating an LH_2 import terminal is of great importance for Gasunie. As Gasunie is committed to the hydrogen distribution grid in the Netherlands, it is necessary to acquire knowledge about hydrogen import terminals in general. As there is no commercially operating LH_2 terminal yet anywhere in the world, there is no blueprint available, but this research provides a comprehensive overview of existing knowledge.

2. **Knowledge needed to retrofit the Peakshaver as an LH_2 terminal**
   Acquiring knowledge about LH_2 processing and identifying the possibilities and barriers for converting the LNG installation to an LH_2 terminal is regarded as valuable for Gasunie. This conversion allows Gasunie to contribute to the energy transition.

3. **It will provide a solution to fill the Hydrogen Backbone**
   Gasunie is investigating multiple routes to fill their Hydrogen Backbone. This research will investigate the requirements for enabling the LH_2 terminal to supply the hydrogen to this grid.

4. **Knowledge for the design of the Hydrogen Backbone**
   Understanding the process and equipment needed for an LH_2 terminal, can help make decisions concerning the requirements of the hydrogen conditions in the Hydrogen Backbone grid.

1.4 Research objective

The current utilisation of the LNG-Peakshaver, which has been in use since 1977, is no longer necessary in the near future. However, given the location and the on-site process equipment, Gasunie wants to investigate whether another function can be devised that contributes to the energy transition.

The assumption is that the current LNG storage tanks need to be retrofitted for LH_2 application, and the hydrogen will be supplied to the Hydrogen Backbone of Gasunie. Furthermore, it is assumed that the LNG-PS has been decommissioned before being converted into a hydrogen terminal.

Based on this, the research objective is formulated as follows:

To determine how the current LNG-Peakshaver can be retrofitted to receive, store and process liquid hydrogen in an energy-efficient way.

The research objective can be fulfilled by answering the following sub-questions:

1. What are the physical and chemical properties that influence the processes, and how do they vary between hydrogen and natural gas?
2. Under which conditions is the liquid hydrogen delivered (by the large-scale maritime LH_2 vessels) to the proposed LH_2 terminal?
3. What are the process conditions for hydrogen in the hydrogen network?
4. Which factors impact the send-out capacity of the future LH_2 terminal, and how does this influence the terminal's design?
5. Can the LNG storage tank be retrofitted to store LH_2, and if so, how can this be achieved?
6. What type of process equipment is suited to process LH_2, considering the process conditions of the terminal and can the current LNG equipment be reused for this?
7. What are the required para- and ortho-hydrogen conditions for the supply to the Hydrogen Backbone, and how does this affect the processes at the terminal?
8. What is the potential of utilizing the thermal exergy during LH_2 regasification?
9. What are the possibilities for processing the LH_2 and related boil-off gas most efficiently, and what is the total energy consumption?

1.5 Report outline

This research consists of thirteen chapters. In the first three chapters, the background of the project, the characteristics of the existing LNG-Peakshaver and the basic differences between LNG and LH_2 properties are reviewed.

In Chapter 4, the basis of design for an LH_2 terminal is described, providing insight in the required input and output conditions and different send-out scenario's. Chapter 5 goes into the process of unloading LH_2 from the transportation vessels, detailing the needed facilities (pipes, jetty) as well as the chemical aspects of the process. The details of storing the LH_2 are reviewed in Chapter 6, which describes the required adaptations to transform the terminal from storing LNG to LH_2. Chapter 7 explores the process of pumping the LH_2 as the first step in the send-out process.

Chapter 8 evaluates the topic of BOG processing, outlining how BOG gets formed and different alternatives to process it. The final stage of the send-out process, the regasification, is then described in Chapter 9, including

details of the para-ortho conversion during this process. Chapter 10 deals with the important topic of energy (re-)utilization and how energy of the regasification process can be recovered.

In Chapter 11, the simulation model that has been used and the assumption for the modelling are detailed. With the aid of this simulation model, the efficiency of the various terminal designs has been determined, demonstrating which components have most impact and which bottlenecks need to be addressed. These aspects are described in Chapter 12 as well as the overall results of the research, describing how the research objective has been met and answering the sub research questions.

This leads to the conclusions of the research which are given in Chapter 13. Finally, Chapter 14 gives recommendations for follow up research needed to make the retrofitting of the LNG-Peakshaver into an LH_2 terminal become a reality.

2 LNG-Peakshaver

In this chapter, the current situation of the LNG-Peakshaver, depicted in figure 3, is described. A general overview of the processes at the plant, consisting of three sections, is provided.

Figure 3: Photo of the LNG-Peakshaver from above.

The LNG-PS is operational since 1977 at the Maasvlakte in the Port of Rotterdam (see figure 4). The facility stores natural gas in liquid form and can, after a period, re-emit it as gaseous natural gas. The processes that take place at the Peakshaver can be sub-divided into three main functions.

- Natural Gas liquefaction: The plant is able to convert pipeline natural gas into LNG.
- Storage: At the plant LNG (methane) and liquid nitrogen is stored.
- Send-out process: Inject the stored substances back into the gas network by compressing, evaporating and blending back to its requirements.

As the name suggests, this plant serves as a peak shaver and is intended to support gas transport in situations with high gas demand. The demands are high during winter, on days when severe frost requires extra gas for domestic consumers. Those domestic consumers are mainly located in the west of the Netherlands. Therefore, the LNG-PS is located in the Port of Rotterdam, to handle the fluctuating gas demands in the west. The LNG-PS has a storage capacity of 78 million normal cubic meters of natural gas, and the maximum send-out capacity is equal to 1,3 million normal cubic meters per hour [33].

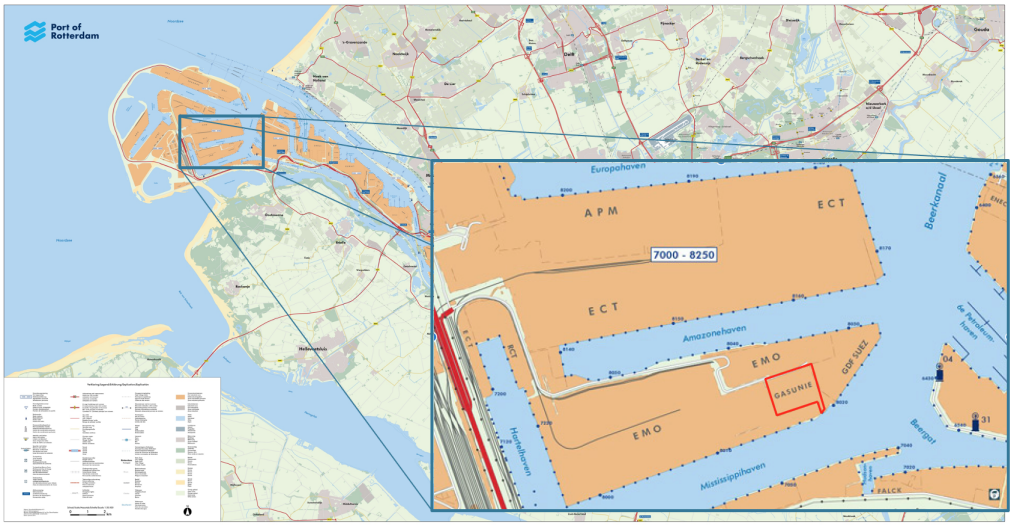

Figure 4: Map of the Port of Rotterdam, with the location of the LNG-PS marked in red [34].

As mentioned above, the LNG-PS is located at the Maasvlakte in the Port of Rotterdam. This location in the west was selected because it gave the opportunity to import LNG with maritime vessels. The figure 4 shows there is excess to the sea, however nowadays this is just a small dock mainly for safety purposes. The neighbours of the Peakshaver are EMO and a coal power plant owned by Riverstone. EMO is one of the largest dry bulk terminals in Europe, importing mainly iron ore and coal [35]. The coal-fired power plant has been operational since 2016, but the Dutch government is trying to shut it down to achieve the CO_2-emission goals.

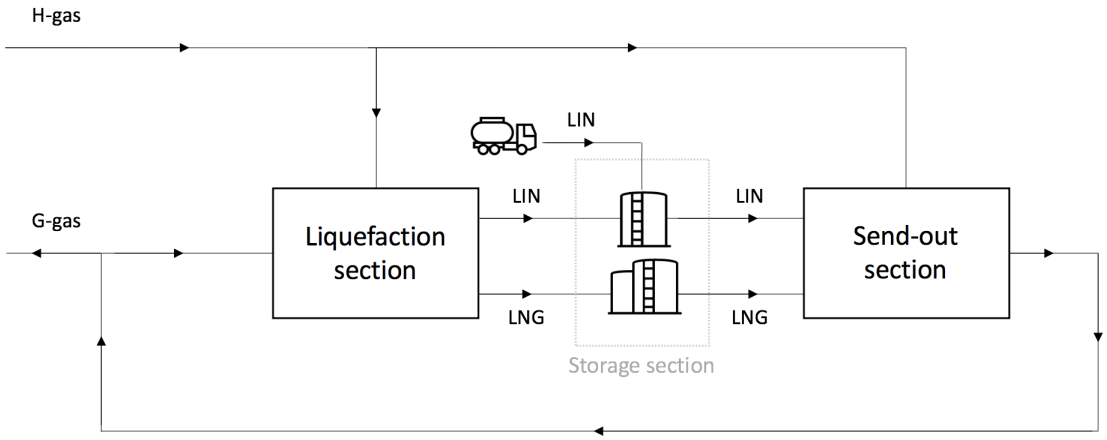

Figure 5: Global overview of the LNG-Peakshaver, with the three main process sections

The figure above gives a global overview of the three process sections of the LNG-PS. It can be seen that the plant is connected to the H-gas (high calorific gas) and G-gas (Groningen-gas, which is consumed by households), which are two separated gas grids in the Netherlands [28]. Both gas streams can be liquefied and stored on site. When liquefying G-gas, also liquid nitrogen is produced because G-gas contains relatively much nitrogen. However, nowadays, mainly H-gas is utilized for the liquefaction process. For this reason additional liquid nitrogen has to be supplied with tank-lorries. Since the LNG-PS acts a buffer for the domestic

consumers, the plant only delivers G-gas to the grid. The send-out is done by either mixing vaporized LNG and LIN or by mixing H-gas directly with vaporized LIN to the specs of the G-gas.

In the next sections of this chapter, a general description is given about the three process sections of the LNG-PS.

2.1 Liquefaction section

In the liquefaction section, pipeline natural gas is liquefied into LNG and also LIN, if the pipeline natural gas contains nitrogen. The first step of this process is to purify the natural gas. Dryers remove the water after which the gas passes through molecular sieves to remove CO_2. Thereafter, the purified natural gas stream is cooled down to -69°C. At that temperature, the higher hydrocarbons still present condense, which can then be removed in the gas separator. The stream is then further cooled to -100°C, creating a mixture of methane, nitrogen and some ethane. This mixture enters a double distillation column to separate the nitrogen from methane and ethane. The obtained methane and some traces of ethane are cooled for the last time and expanded to tank pressure. The LNG is stored at -163°C, which is below the boiling point of methane. The separated nitrogen is liquefied in the same way as the LNG stream and stored at -196°C.

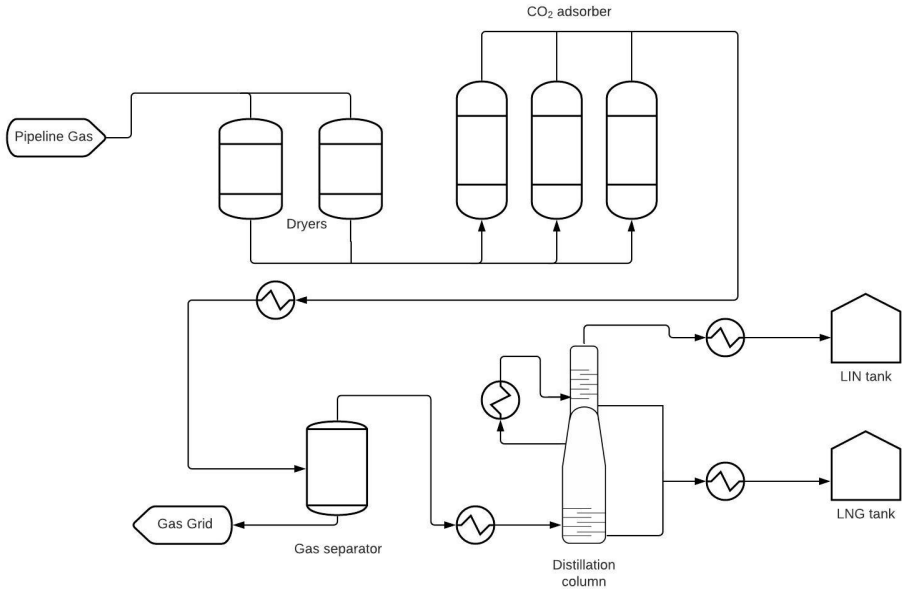

Figure 6: Process flow diagram of the liquefaction process at the LNG-PS site

The cooling process is done with a separate nitrogen refrigeration cycle. For this refrigeration cycle the stored LIN or LIN boil-off gas is utilized as cooling liquid. This process is shown in simplified form in Appendix A, with the essential process components. The nitrogen is compressed first with a two-stage piston compressor and with a two-stage centrifugal compressor. After that, the nitrogen is cooled with an intercooler and fed to a booster compressor that is driven by an expansion turbine. The compressed nitrogen passes through the second intercooler before it is available for cooling purposes. First compressed nitrogen is utilized for heat transfer and after expansion the temperature of the nitrogen drops, allowing additional cooling.

2.2 Storage section

In this section, the storage tank and how the boil-off gas is processed is described. Processing the BOG is evaluated in this section because the boil-off gas is related to the storage tank.

The liquefied natural gas and nitrogen are stored on-site in storage tanks. For LNG storage two tanks are utilized, each with a capacity of 57.250 m^3. The LIN is stored in one tank with a capacity of 19.000 m^3. Both liquids must be stored at low temperatures due to the low boiling-points. The tanks are all insulated well to keep the temperature in the tank low.

(a) Picture of the two LNG storage tanks

(b) Picture of the LIN storage tank

Figure 7: The storage tanks at the Peakshaver site

The LIN storage tank, stores liquid N_2 at an overpressure of 40 mbar and -193°C. The boil-off rate per day is equal to 0,065% of the tank capacity, which is similar as 335 m^3/h. However, in this section, the LNG tanks will be discussed in more detail because the LIN tank is not available for LH_2 storage in the near future.

LNG is stored in the two similar tanks at a pressure of approximately 40 mbarg and a temperature of -163°C. It is a double-containment tank design, as the outer concrete construction is capable of containing the LNG in case of product leakage [36]. The insulation measures to keep the temperature low are shown in figure 8. The tanks are double-walled insulated. The inner tank, which is in contact with LNG, is made of a nickel-steel; the outer tank is made of carbon steel. The space between the inner and outer tank is filled with perlite. Perlite is a volcanic material, which has a lower thermal conductivity when the temperature decreases [37]. At the bottom of the tank, a different insulation material than perlite is used to handle the bearing capacity, namely a strong foam glass. Furthermore, the tank is not in direct contact with the ground to limit heat leakage. Instead the storage tank is carried by 110 concrete pillars. On the roof of the inner tank, insulation blankets are used. Nevertheless, there will always be some heat leakage, which results in the liquid to evaporate. This evaporated gas must be removed from the tank to keep the pressure at the desired level, which is called boil-off gas. The boil-off rate per day for the LNG tank is equal to 0,05% of the tank capacity, which is similar as 710 m^3/h.

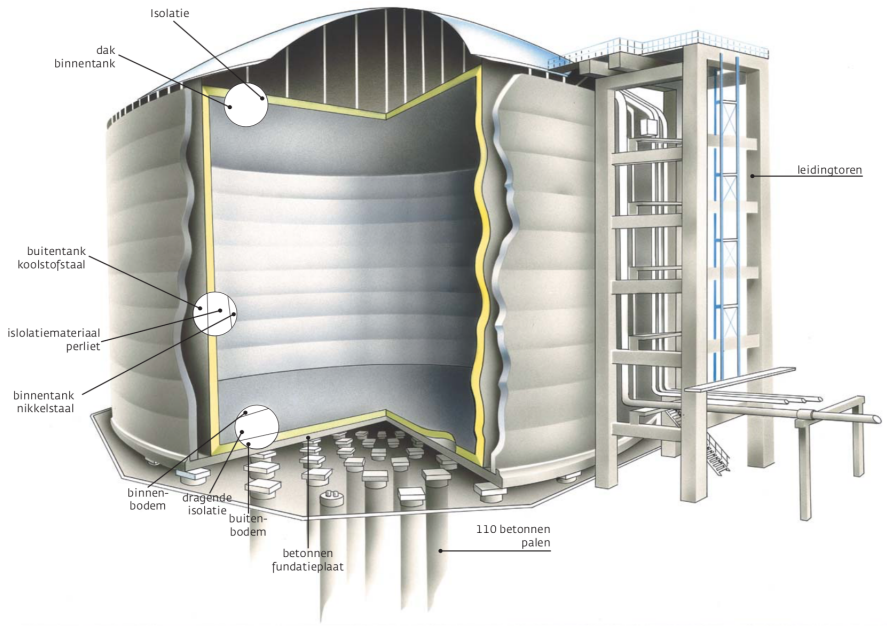

Figure 8: Picture of the insulation technology of the LNG storage tanks at the LNG-PS [38].

The boil-off gas from the LNG tank is considered as pure methane because the boiling point of methane is the lowest compared to the other substance that are stored, such as ethane. When the pressure in the tank is above 40 mbar, the methane BOG compressors increase their capacity to remove the evaporated methane. The first BOG compressors increased the pressure up to 12,95 bar, which is done with five two-stage reciprocating compressors connected in parallel. For the nitrogen BOG compression, it is a similar process only the pressure is increased till 15 bar. A more detailed description about these compressors can be found in Appendix B.

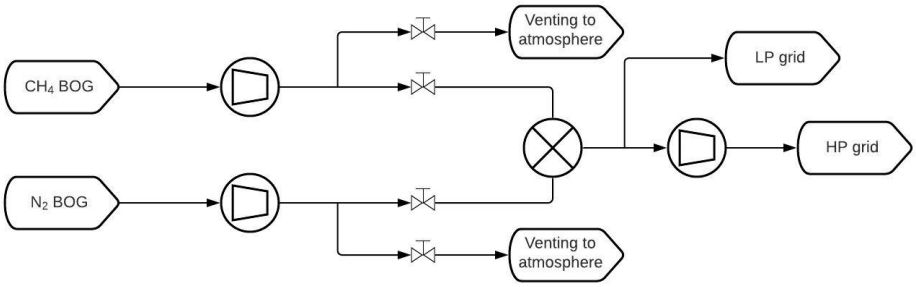

Figure 9: Process flow diagram of the BOG process at the LNG-PS site

Thereafter, the compressed BOG passes through a pressure regulator before entering the blending station. If the CH_4 BOG is over-compressed, the methane would be vented to the atmosphere as depicted in figure 9. The pressure regulator is required to properly mix the compressed nitrogen and methane to the specifications of the G-gas grid. As is shown in figure 9, this pipeline ready G-gas can be fed directly into the low-pressure grid (around 9 bar). Otherwise it goes through an extra compression section for the high-pressure G-gas grid.

The high-pressure BOG compressor compresses G-gas up to 80 bar to be capable of handling the flow two compressors are parallel connected. The compressor is again a two-stage reciprocating compressor with intermittent cooling. More information regarding this compressor type can be found in Appendix B.

2.3 Send-out section

The processes required to feed the liquefied gases back into the gas grid, are the components that fall under the send-out section. A global overview of the process steps is shown in figure 10.

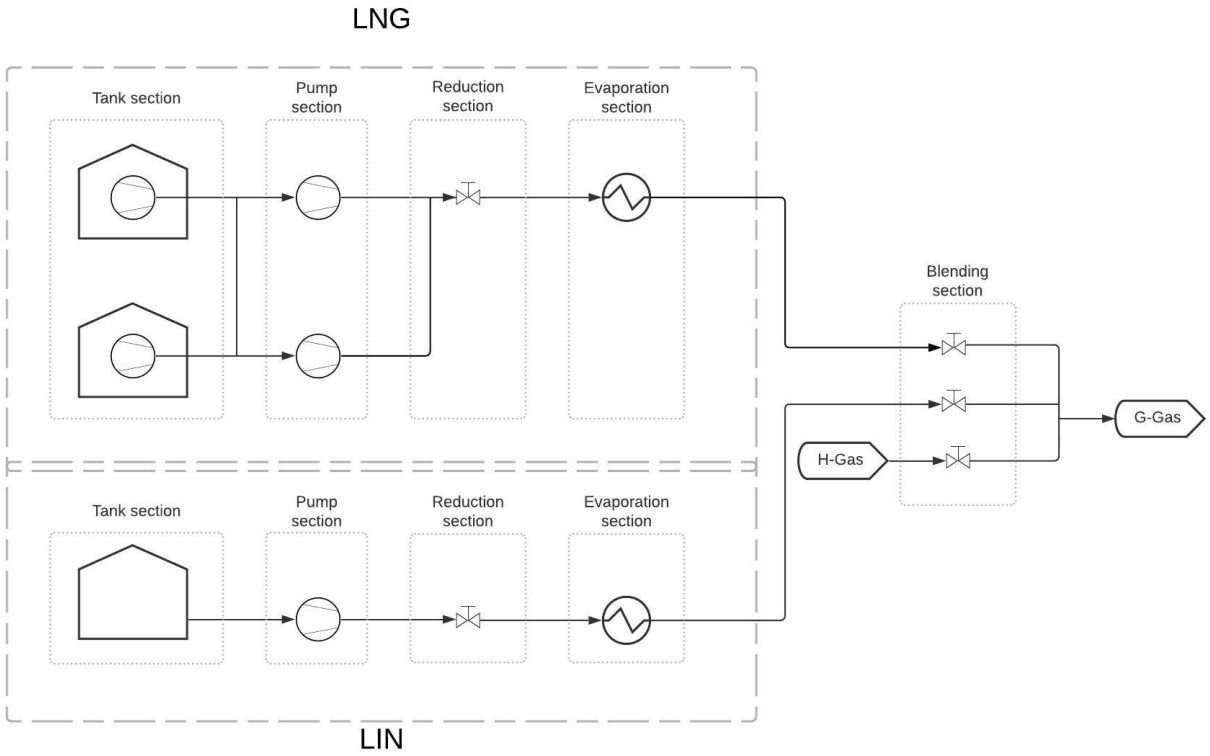

Figure 10: General overview of the send-out process at the LNG-PS

The first step of the send-out process, is pumping the liquid out of the storage tank. In case of the LIN, however, no pumping is required because there is an opening at the bottom of the LIN tank to take it out. As can be seen in the figure 10, the LNG tanks do have pumps to get the LNG out of the tank. Each LNG tank has four submerged pumps, which are called LNG-boosterpumps. Those pumps are centrifugal type of pumps, each with a capacity of 240 m^3/h (156.000 Nm^3/h) and a head of 72 meter at 2900 rpm.

After that, the liquids are pumped up to higher pressures for the high-pressure grid application. The LNG main pumps receive the liquid methane under low pressure from the low pressure boosterpumps. The main pumps pressurize the liquid (up to approximately 90 bar) and transport it via the liquid reducer to the LNG evaporators. They are centrifugal pumps and mounted in a barrel with a capacity of 325 m^3/h (192.000 Nm^3/h). In total there are six main LNG pumps, three pumps for each tank. The pumps are fitted with a vapour return line and a minimum flow line. The LIN pumps operate similar with a capacity of 115 m^3/h (71.900 m^3/h) at a head of 80 bar. For the LIN pumping, four pumps are utilized.

The liquid reduction section is added to control the pressure. Because the pumps deliver too high discharge pressure at low flow for good controllability during the blending process. The liquid reduction system ensures a constant pressure difference of 7-10 bar over the mixing station.

Next is the evaporation section. The evaporators heat the LNG and LIN to 15°C so that the liquid change into the vapour phase. Combustion heat vaporizers are used for the evaporation process of both liquids, with natural gas as the combustion gas. For the LNG and LIN evaporation process, ten and four evaporators placed in parallel are used, respectively.

Finally, the last step before the gases can be supplied to the grid is the blending process. The evaporated LNG and LIN are blend to meet the requirements of the G-gas grid. The Wobbe index for the supplied G-gas by the Peakshaver is set at 44,0 MJ/Nm^3. Besides mixing the evaporated LNG with nitrogen, is it also possible to use H-gas directly from the grid and blend it with nitrogen for the send-out process.

When all pumps and vaporizers are operational, the total send-out capacity of G-gas is equal to 1,3 million Nm^3/h. In Appendix B, additional specifications regarding the main process components of the LNG-PS (tank, compressors, pumps and evaporators) can be found.

3 LNG-LH_2 differences

To determine the possibilities of retrofitting the LNG installation into an LH_2 terminal, it is necessary to point out the differences between LNG and LH_2. For this reason, the physical and chemical properties of LNG and LH_2, which influence the processes at the receiving terminal, are compared. In addition, a unique phenomenon of hydrogen is discussed, the spin-isomers. Finally, the process conditions on both terminals are evaluated to gain insight into the process equipment requirements.

3.1 The physical and chemical properties

In this section, the physical and chemical properties of LNG and LH_2 are compared. The properties that do not influence the processes at the receiving terminal are not taken into account.

Table 1: Properties, * NTP (normal temperature and pressure) = 20°C and 1 atm [39], [19], [40], [41]

Properties	**LH_2**	**LNG**	**Units**
Molar mass	2,02	16,5 - 18,88	kg/kmol
Boiling point, @ 1 bar	-253	-162	°C
Liquid density, @ 1 bar	70,8	430 - 470	kg/m^3
Gas density, NTP*	0,0838	0,70 - 0,79	kg/m^3
Critical Temperature	-240	-83	°C
Critical Pressure	1,28	4,60	MPa
Higher heating value, mass	141,9	55,2	MJ/kg
Higher heating value, volume	10,05	23,6	MJ/L
Latent heat of vaporization, mass	444	510	kJ/kg
Latent heat of vaporization, volume	31,4	226	kJ/L
Flammable range in air	4 - 75	5 - 15	vol%
Flammable range in Oxygen	4 - 95	5 - 61	vol%
Minimum ignition energy	0,02	0,3	mJ
Diffusion coefficient in air, NTP*	0,61	0,016	cm^2/s

LNG is a natural gas fossil fuel mixture mainly consisting of methane and a few other organic compounds like ethane. When importing LNG from overseas locations, the percentage of methane in LNG can vary between 85 and 99% [42], [43]. However, the LNG stored at the Peakshaver site, is natural gas from the Dutch grid that has been liquefied on-site, as is described in chapter 2. Unlike imported LNG from overseas locations, the LNG produced at the Peakshaver site always has a similar composition with high methane concentrations. Furthermore, methane is considered as the second most important greenhouse gas [44].

The composition of liquid hydrogen consists of pure hydrogen molecules with a molecular weight of 2,02 kg/kmol. Hydrogen -in contrast to methane- is not considered as a direct greenhouse gas. However, hydrogen can indirectly contribute to the formation of greenhouse gases in the atmosphere in three ways. Hydrogen in the stratosphere produces water vapour which absorbs Infra-Red [45]. Secondly, hydrogen reacts with the hydroxyl radical (OH) resulting in a decrease of the hydroxyl radical in the atmosphere [44]. The hydroxyl radical is required to destruct Fluor and Chlorine containing greenhouse gases and methane [46]. For this reason, a decrease in the hydroxyl radical in the atmosphere will lead to an increase in greenhouse gases [44]. And lastly, hydrogen interferes with the ozone production cycle. However, this indirect production of greenhouse gases due to hydrogen is much lower than when methane is being used. The global warming potential (GWP) over a 100-year time horizon for hydrogen in comparison with methane is respectively 5,8 [44] and 34 [46].

3.1.1 Temperature

Hydrogen and natural gas are gases when in atmospheric condition. By cooling the substance below the boiling point, the substance becomes liquid. For hydrogen, this boiling point is extremely low, namely -253°C. In the case of LNG, the temperature of the boiling point is at -162°C.

The first issue with the lower operating temperature of LH_2 is the formation of liquid oxygen. The formation of liquid oxygen can occur when air comes into contact with a cold surface whose temperature is below the boiling point of oxygen. Since the boiling point of oxygen is -183°C, this formation of liquid oxygen only occurs at the LH_2 terminal. It will not happen at the LNG terminal because the operating temperature at the LNG terminal will not reach temperatures below -162°C. Liquid oxygen is unwanted in processing hydrogen because it improves the flammable limit as table 1 shows [47]. The formation of liquid oxygen can occur at the outside of LH_2 pipelines, where the temperatures are below the boiling point of the oxygen. To prevent this from happening, the pipelines have to be vacuum insulated, so the oxygen in the air cannot come in contact with temperatures below -183°C. For pipelines that are not vacuum insulated but instead insulated with a non-vacuum-jacket, like most LNG piping. In that case, the air can migrate through the insulation layer and reach the outside of the piping with the risk of inflammation. For this reason, non-vacuum-jacketed insulation should be oxygen-compatible [48].

The lower temperature of liquid hydrogen will also has a significant affect on the material selection, for all process components.

3.1.2 Critical point

The critical point for a substance is the highest temperature and pressure at which the substance has a phase change from liquid to vapour [49]. For pressures and temperatures above the critical point, the substance becomes supercritical. A supercritical fluid behaves differently, so this value is important for the process analysis of the LH_2 receiving terminal.

3.1.3 Density

The density of liquid hydrogen is six times smaller than LNG, as table 1 shows. In the gaseous phase, this difference is almost eight times. With these values, it can be concluded that the expansion ratio from liquid to gaseous hydrogen is nearly 850 and for LNG it is 650.

This lower density influences the energy density per unit volume, which is significantly lower for LH_2 than LNG, as can be seen in table 1. The lower energy density results in a smaller amount of stored energy inside the two storage tanks of the Peakshaver. Furthermore, processing hydrogen is also seen as more difficult due to the lower density; for example, the work for compression will increase [23].

An advantage of the lower density of LH_2 is that the stored mass in the storage tank will be less than LNG. Considering the LNG storage tanks at the LNG-PS having a capacity of 57.250 m^3, the total stored weight for the LNG and LH_2 case is respectively 26.000 ton and 4.050 ton. This provides opportunities to retrofit LNG tanks for LH_2 application.

3.1.4 Energy

For a chemical substance like hydrogen and LNG, the chemical energy of the substance is expressed as the heating value. The heating value of a substance is the amount of heat released during the combustion of this substance [50]. This heating value can be distinguished in the lower heating value (LHV) and the higher heating value (HHV). At the HHV, the heat of vaporization of the water vapour is taken into account, which is not the case for the LHV. In this report, the HHV is used because as hydrogen is considered as a feedstock,

this is the general indication [51].

The heating value of liquid hydrogen per unit mass is more than two times higher than the heating value for LNG, as table 1 shows. However, the heating value per unit volume of liquid hydrogen is lower than LNG due to the lower density. Therefore, to store an equal amount of energy in a storage tank, the total volume of the LH_2 tank must be 2,3 times larger. When looking at the current two LNG storage tanks at the LNG-PS, the total amount of stored energy is equal to 2700 TJ. If these tanks are filled with LH_2 1150 TJ would be stored (around 8.100 ton H_2).

Liquid hydrogen is used during transportation and storage because the energy density is much higher than gaseous hydrogen. As pointed out above in section 3.1.3, the expansion ratio from liquid to gaseous hydrogen is 850. For this reason, the liquid hydrogen energy density per unit volume is 850 times higher, which is desired for storage and transportation with vessels.

3.1.5 Latent heat

For determining the insulation of the liquid hydrogen storage tank, the latent heat of vaporization is an important value [22]. The latent heat of vaporization is the amount of energy absorbed by a substance during the phase change from liquid to vapour that occurs at a constant temperature.

Table 1 shows that the latent heat of vaporization per unit volume for liquid hydrogen is significantly lower than in the case of LNG, respectively 31,4 kJ/L and 226 kJ/L at the boiling point and ambient pressure. This means that a heat leakage of 31,4 kJ results in one litre of liquid hydrogen to evaporate. In comparison with an LNG storage tank, the heat leakage can be seven times as large to generate a gas boil-off of one litre LNG.

3.1.6 Safety

For processing the liquid hydrogen at the receiving terminal, some safety aspects have to be taken into account. As table 1 shows, the flammability limits in air have a broader range for hydrogen, meaning the chance of an explosion is larger. This broader range, in combination with the lower minimum ignition energy of only 0,02 mJ, makes hydrogen a hazardous substance [41]. However, due to the higher diffusion coefficient of hydrogen gas, the dispersion of hydrogen is larger. So with the correct control, it is a safe substance to process [52]. At the LH_2 terminal, nevertheless, also liquid hydrogen is processed. The LH_2 -in contrast to gaseous H2- has a lower diffusion coefficient and will initially behave as a dense gas, meaning the dispersion rate is lower [52]. For this reason, processing LH_2 requires additional safety measurements.

For processing the liquid hydrogen in a safe manner, a different ATEX class is needed. This European classification is used for equipment and protective systems intended for use in potentially explosive atmospheres. The ATEX class for hydrogen is set at IIC, which requires higher standards for the equipment than is the case for LNG (the ATEX class for LNG being I). This higher standard is a result of the very low ignition energy of hydrogen [53].

3.1.7 Joule-Thomson effect

Another phenomenon which is different for a hydrogen substance in comparison with an LNG substance, is the Joule-Thomson effect [54]. The definition of the Joule-Thomson effect is 'The change in temperature that accompanies the expansion of gas without production of work or transfer of heat' [55]. In other words, it is the temperature change of a real gas or liquid when it is forced through a valve while keeping it insulated, meaning no heat is transferred to the surrounding. In figure 11, the J-T inversion curve is shown for hydrogen and for methane (LNG), where the differences between the Joule-Thomson coefficient (μ_{J-T}) is shown. The curve shows a large operating window of the methane substance with a positive Joule-Thomson coefficient. For the hydrogen substance, this operation window is significantly smaller. The positive J-T coefficient results

in a temperature decrease on expansion. Therefore, the negative J-T coefficient will result in a temperature increase on expansion, as is shown in equation 1 for the Joule-Thomson coefficient.

$$\mu_{J-T} = \left(\frac{\partial T}{\partial P}\right)_H \tag{1}$$

For the LH_2 terminal, the negative J-T coefficient as well as the positive J-T coefficient are taken into account. For the liquid hydrogen and for the hydrogen gasses below 200 K the negative J-T coefficient applies. However, for the hydrogen gasses above 200 K the positive coefficient applies, so this also applies for the hydrogen delivered to the hydrogen grid. Due to the pressure drop in the pipelines of the hydrogen grid and because of this positive coefficient of the hydrogen, the temperature of the H_2 rises in the pipelines [56]. For the natural gas case the coefficient is negative, meaning the temperature decreases in the pipelines of the grid due to the pressure drop. However, this temperature increase or decrease in the grid is relatively small and should not cause any problem. For the hydrogen gas, the reducing pressure increases the temperature of the substance with 0,035 °C/bar, whereas the temperature decreases for NG with 0,5 °C/bar [57].

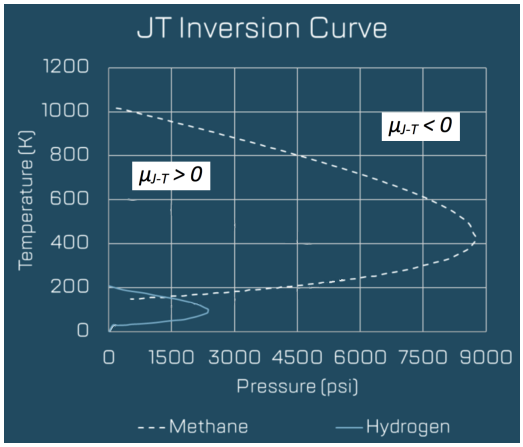

Figure 11: Joule-Thomson inversion curve for the methane and hydrogen substance [54].

3.2 Para- and Ortho-Hydrogen

At the liquid hydrogen receiving terminal, the liquid hydrogen has to be stored and evaporated. The para- and ortho-hydrogen concentration could influence these processes. Therefore, an introduction on the spin isomers of hydrogen is given in this section.

3.2.1 Spin isomers of hydrogen

Molecular hydrogen (H_2) consists of two hydrogen atoms, as figure 12 shows. These atoms can be related in two ways, depending on the direction of the nuclear spins of its two protons [58]. These two types of hydrogen spin isomers are called para-hydrogen and ortho-hydrogen. Para-hydrogen has a lower internal energy and has a symmetric nuclear rotation and anti-symmetric nuclear spin. For ortho-hydrogen, it is the other way round; it has a higher internal energy and the nuclear rotation is anti-symmetric whilst the nuclear spin is symmetric [59].

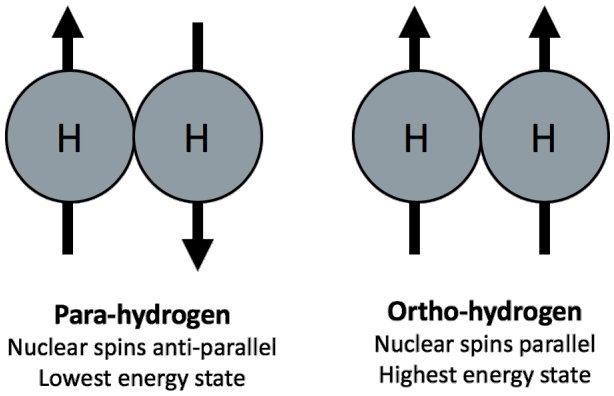

Figure 12: Spin isomers of hydrogen

The equilibrium composition of para- and ortho-hydrogen depends on the temperature as is shown in figure 13. At room temperature and temperatures above, the equilibrium composition consists of 25% para-hydrogen and 75% ortho-hydrogen [60]. This composition, with a concentration of 75% of the higher internal energy component, is called "normal" hydrogen [61].

The percentage of the concentration para-hydrogen increases when the temperature decreases, which means that the equilibrium composition moves toward the lower energy form. For liquid hydrogen, when the temperature is very low (-253°C), the concentration of para-hydrogen is at its highest with 99,8% para-hydrogen and only 0,2% ortho-hydrogen [62].

The difference in concentration of "normal" and liquid hydrogen could potentially also influence the heating value of the substance. Knowing that LH_2 consist mainly of the lower energy state isomer, this would lead to a smaller heating value in comparison to the "normal" hydrogen. However, considering that the enthalpy of conversion is the difference in heating value, the real difference for the heating value in comparison with the HHV is minimal. Since the total enthalpy of conversion is 523 kJ/kg [63] and the HHV of hydrogen is 141,9 MJ/kg, it results in a difference of only 0,37% of the HHV.

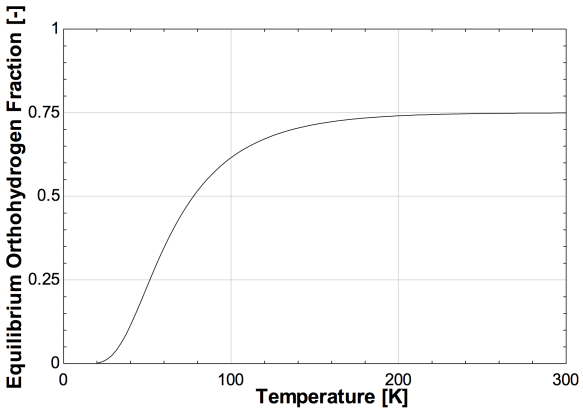

Figure 13: Equilibrium curve of ortho-hydrogen [60]

3.2.2 Influence of spin-isomer conversion on processes

During the liquefaction process, the equilibrium composition of the spin isomers changes, as is shown in figure 13. For this reason, ortho- to para-hydrogen conversion has to take place during liquefaction. In case of the vaporization process from liquid to gaseous hydrogen, para- to ortho- conversion occurs. However, without the use of a catalyst in both processes, the conversions take several days [59], meaning the conversion takes place after the process.

For the liquefaction process, ortho- to para-hydrogen conversion is needed. This conversion from the higher internal energy state (ortho) to the lower (para) is an exothermic reaction, resulting in heat release. The heat released during this conversion is equal to the enthalpy of conversion. In the literature multiple different values can be found ranging from 523 kJ/kg till 702 kJ/kg [62], [63], [64]. In this report, the enthalpy of conversion from "normal" hydrogen to the equilibrium composition of liquid hydrogen is equal to 523 kJ/kg [63]. Since the conversion takes several days, most of the exothermic conversion will happen when hydrogen is in the liquid phase [65]. The heat released during this conversion is enough to vaporize 65% of the liquid hydrogen [59]. For the reason to keep the boil-off losses low when storing liquid hydrogen, a catalyst has to be added in the liquefaction process to speed up the conversion from ortho to para. So the exothermic conversion takes place during the liquefaction process and not in the LH_2 storage tank. This exothermic ortho to para conversion requires 16% of the total minimum liquefaction work at room temperature and ambient pressure (3,90 kWh/kg) [66].

At the LH_2 receiving terminal, a regasification process is employed to convert liquid hydrogen to gaseous hydrogen. During the regasification process, the para and ortho equilibrium composition is changed back to the “normal” hydrogen state with 75% ortho-hydrogen, as is illustrated in figure 13. The para to ortho conversion is the opposite conversion mentioned during liquefaction and therefore is an endothermic reaction. This conversion process absorbs heat from the environment, which is equal to the enthalpy of conversion 523 kJ/kg [63]. Again, the conversion can take several days before the equilibrium composition of “normal” hydrogen is reached [65]. It results in the fact that most of the endothermic conversion is happening after the regasification process. In that case, the LH_2 terminal will supply hydrogen with a large concentration of para-hydrogen to the grid. There are two potential side-effects of delivering para-hydrogen to the grid, namely:

1. The temperature of the hydrogen gas in the grid can potentially drop below 0°C. As the endothermic conversion absorbs heat from the surrounding, the temperature of the hydrogen gas will decrease.
2. The supplied energy content to the hydrogen grid is slightly lower. This is because the energy state of the para-hydrogen is lower than that of the ortho-hydrogen. As mentioned in the previous section, the maximum difference is 0,37% of the HHV of hydrogen.

However, a catalyst can be added to the regasification process so that most of the conversion takes place in the heat exchanger. The catalyst is preferably a metal oxide catalyst, e.g., Fe_2O_3, Ni/SiO_2, or Ru/Al_2O_3, especially iron oxide [67]. If the catalyst is added, the evaporation will consume more energy because the endothermic conversion reaction is added to the process. But when no catalyst is added during the evaporation process, it is realistic to ignore the conversion reaction because it is so slow [61]. These potential side-effects are discussed in more detail in section 9.2.

3.2.3 Composition of the spin-isomers at the LH_2 terminal

Defining the composition of the spin isomers of the hydrogen at the terminal is of interest for the processes. For example, suppose the para concentration of the LH_2 is lower than the equilibrium composition for the liquid phase (as explained above, this is 99,8%). In that case, it will influence the boil-off rate, resulting in more unwanted boil-off gas at the terminal. Furthermore, the required composition of the grid can have an effect on the evaporation process.

The LH_2, which is handled at the terminal, is delivered by maritime tankers. Due to this fact, assumptions can be made on the composition of the spin isomers. During the liquefaction process, a catalyst is used to convert as much ortho- to para-hydrogen [59]. After this liquefaction process, the LH_2 has to be shipped to the Port of Rotterdam, which takes several days. In the course of these days, further conversion into the lower energy state of the spin isomer will take place [62]. Therefore after this transport, it can be assumed that the equilibrium composition of the delivered liquid hydrogen, has a para-hydrogen concentration of at least 98% [62]. Hence, for the liquid hydrogen stored at the terminal, there will be no additional boil-off gas losses due to heat release during the exothermic conversion reaction, as can be seen in figure 14 [62].

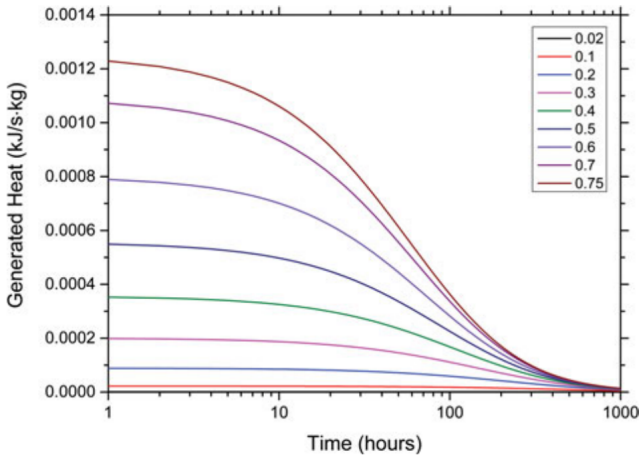

Figure 14: Heat generated by initial ortho concentration [62]

The para-hydrogen concentration of the liquid H_2 at the terminal is assumed to be at least 98%. However, the para-hydrogen concentration of the H_2 in the grid has a concentration of 25% as can be concluded from figure 13, which is called “normal” hydrogen. During the evaporation process, the conversion from liquid hydrogen to “normal” hydrogen does not occur without adding a catalyst [61]. If no catalyst is added, the higher concentration of para-hydrogen supplied to the grid has a negative effect on both the temperature and the energy content of the hydrogen gas. However, adding a catalyst has also side effects, namely the energy consumption and the complexity of the regasification process increases. Currently, no requirements are set for the composition of the hydrogen spin isomers in the grid. So a trade-off has to be made if adding a catalyst to the regasification process is desired for the LH_2 terminal. This trade-off is carried out in section 9.2.

3.3 Process conditions at an LNG and LH_2 terminal

In addition to the differences in properties, it is important to gain insight into the processes at an LH_2 import terminal and to what extent it differs from an LNG terminal. Therefore, the send-out process of the terminal is briefly explained. Also, the process conditions of an LNG and LH_2 terminal have been compared. In order to do this, general assumptions have been made for such an import terminal.

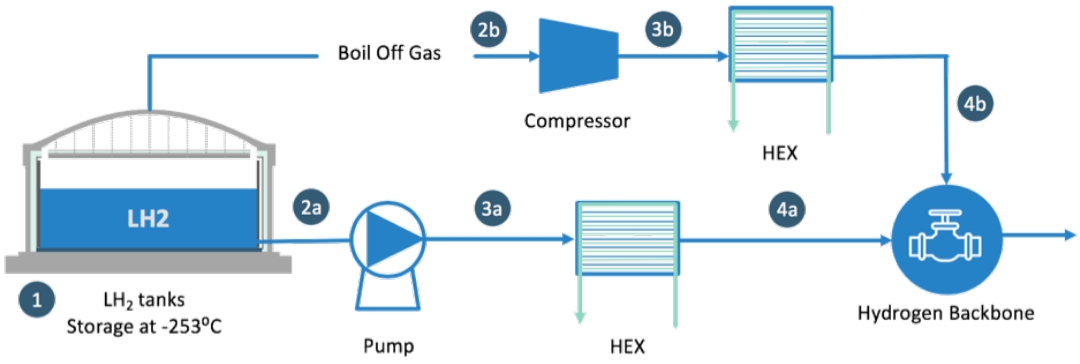

Figure 15: Schematic overview of the send-out processes of the liquid hydrogen terminal

A general overview of how the cryogenic liquid (LH_2 or LNG) is processed at an import terminal, assuming it supplies to the gas grid, is shown in figure 15. The cryogenic liquid is stored in a tank below their boiling point, for LNG and LH_2 respectively -162°C and -253°C. Depending on the demands of the grid, the cryogenic liquid is processed to meet the requirements of the grid. This is achieved by pumping and evaporating the liquid to the desired pressure and temperature of the grid. This process is shown with stream "a" in figure 15. In addition to the liquid stream process, both terminals also have to deal with the boil-off gas of the stored cryogenic liquid. There are multiple ways to process the BOG flow, which will be discussed later on, but in this case, compression is considered, as can be seen in figure 15.

In order to properly analyse the process equipment requirements of an LH_2 terminal, it is important to know the conditions of the different phases of the send-out process. To give this first impression, the general configuration of the terminal has been considered, as shown in figure 15. It is assumed that the pumps and compressors have an isentropic efficiency of 75%, and mechanical losses are neglected. Furthermore, the grid requirements are considered at 50 bar and 5°C.

Table 2: Estimated temperature and pressure conditions for the liquid stream of the LNG- and LH_2-terminal, with the numbers of the streams similar to the numbers in figure 15. Considering 75% isentropic efficiency for both pumps and compressors.

	Stream 'a', liquid stream							
	LNG				**LH_2**			
Stream	P [bar]	T [°C]	ρ [kg/m^3]	E [MJ/L]	P [bar]	T [°C]	ρ [kg/m^3]	E [MJ/L]
1	1,04	-162	423,11	23,36	1,04	-253	71,11	10,09
2a	5	-161,81	423,20	23,36	5	-252,62	71,20	10,10
3a	50	-158,61	424,18	23,41	50	-248,33	72,12	10,23
4a	50	5	38,91	2,15	50	5	4,23	0,60

Table 3: Estimated temperature and pressure conditions for the BOG stream of the LNG- and LH_2-terminal, with the numbers of the streams similar to the numbers in figure 15. Considering 75% isentropic efficiency for both pumps and compressors.

	Stream 'b', BOG stream							
	NG BOG				**H_2 BOG**			
Stream	P [bar]	T [°C]	ρ [kg/m^3]	E [MJ/L]	P [bar]	T [°C]	ρ [kg/m^3]	E [MJ/L]
1	1,04	-162	423,11	23,36	1,04	-253	71,11	10,09
2b	1,04	-161,17	1,86	0,10	1,04	-252,69	1,36	0,19
3b	50	75,89	28,84	1,59	50	-157,90	10,30	1,46
4b	-	-	-	-	50	5	4,23	0,60

The conditions for the various stages of the send-out process are presented in the two tables above. Besides the pressure, also the temperature, density and energy density are depicted. These values are presented because they differ significantly for the LNG and LH_2 case and thereby have a large impact on the processes of the terminal. It can be seen that the temperatures of the hydrogen terminal are significantly lower than in the LNG case. A noticeable difference is the lower temperature of the hydrogen BOG after compression (stream 3b), which remains well below 0°C. Therefore, an additional heat exchanger is required to process the hydrogen BOG, which is not needed for the LNG terminal, as is shown in table 3. Furthermore, these lower temperatures will have a considerable influence on material selection.

The density of LH_2, as mentioned earlier, is significantly lower compared to LNG, as can be seen in tables 2 and 3. Due to the lower density, the power requirement for pumping and compression will be considerably more significant [68]. Furthermore, this will probably also influence the design of this equipment. Another affect of the lower density is the lower energy density per unit volume, as is shown in the two tables above.

4 Basis of design

It is essential to clarify the basis of design in order to design a suitable LH_2 import terminal. The basis of design is the input and output conditions of the proposed hydrogen terminal. Furthermore, the desired send-out capacity of the terminal is also considered as the basis of design. The input condition for the receiving terminal is the condition of the liquid hydrogen delivered by the ships. For the output condition, the hydrogen gas needs to meet the requirements of the hydrogen grid. Finally, a desired send-out scenario of the terminal has been analysed to determine the send-out rate of the terminal. These values are crucial to select proper process equipment and define possible LH_2 processing solutions.

4.1 Input conditions

As stated before, it is assumed that hydrogen will be delivered in the liquid phase at the terminal by liquid hydrogen bulk tankers. In this section, the storage conditions of the LH_2 ships will be analysed to determine the hydrogen input condition at the proposed LH_2 terminal.

To determine the LH_2 conditions of the maritime vessels, the state of the art of large-scale LH_2 ships have been considered. At the time of writing, however, there is no commercial hydrogen shipping yet. Although NASA has transported liquid hydrogen on a barge carrier [69], [70], and KHI recently transports LH_2 from Australia to Japan for a pilot study of the HySTRA project [71], it has not been applied to commercial shipping. And more importantly, no international regulations are set for maritime transportation of hydrogen. The International Gas Carrier Code (IGC Code) lacks specific requirements for hydrogen transport [27]. For this reason, the storage conditions of the LH_2 on board of the ships have to be determined from prototypes. Moreover, the knowledge of the existing LNG ships is also used to analyse the LH_2 conditions, as it has many similarities.

The Euro-Quebec project introduced the liquid hydrogen shipping concept. The barge-mounted tanker used type-C tanks with a capacity of 14.500 m^3 [72]. Another design dating from the same period was the SWATH (small water-plane area twin hull), which also has type-C tanks and a total liquid hydrogen capacity of 12.500 m^3 [73]. For the WE-NET program, Japanese researchers proposed a large-scale liquid hydrogen tanker based on LNG tanker technologies. The cargo capacity was designed at 200.000 m^3, and type-B tanks were used. The type-B tanks, unlike the type-C, cannot build up pressure during transport, so the boil-off gas cannot be kept in the storage tank. The ship was designed to utilise the boil-off gas for propulsion in the same way as an LNG tanker [74]. Moss Maritime is developing an LH_2 bunker vessel concept with two type-C tanks with a total capacity of 9.000 m^3 [75].

Figure 16: Large-scale LH_2 tanker design, [66]

Kawasaki Heavy Industries (KHI) made the most promising designs, both for small- and large-scale LH_2 ships. As mentioned above, their small-scale tanker is already operational since March 2021 for the pilot case of the HySTRA project [71]. This small-scale liquid hydrogen tanker called The Suiso Frontier has one type-C tank with a capacity of 1.250 m^3 [76]. However, the HySTRA pilot project is not commercial yet. It wants

to operate on a commercial-scale with two large-scale LH_2 tankers by 2030. The large-scale LH_2 ship will have four type-B tanks with a total capacity of 160.000 m^3, as illustrated in figure 16. The boil-off gas for the large-scale carrier will be used as propulsion fuel [66].

For the LH_2 terminal, large-scale tankers are expected to arrive at the terminal. When looking at large-scale LNG vessels, the LNG is stored in either type-A or type-B tanks [77]. Both tanks are non-pressurised, meaning the LNG is stored at or near ambient pressure [78]. This is similar to the proposed large-scale LH_2 vessel of Kawasaki and WE-NET [66], [74]. For this reason, it is assumed that the LH_2 will be delivered at conditions just above ambient pressure and below its boiling point. An overview of the LH_2 input conditions can be found in table 4.

Table 4: Input conditions for the liquid hydrogen terminal

Properties	**LH_2**	**Units**
Pressure	1,2	bar
Temperature	-253	°C
Para concentration	>98	%
Hydrogen purity	99,995	%

4.2 Output conditions

The received hydrogen at the import terminal is assumed to be delivered to the hydrogen grid, meaning the output conditions of the terminal have to match the requirements of the grid. Although it is possible that in the future, several different hydrogen grids will run side by side in the Port of Rotterdam, for this study, it is assumed that the hydrogen will be fed to the Hydrogen Backbone [6]. Besides the apparent reason Gasunie will implement the Backbone, another benefit of utilising the Backbone is that it will be the largest hydrogen grid in the Netherlands [79].

The Hydrogen Backbone is not only focussing on the energy cluster of the Port of Rotterdam. It will be a hydrogen supply network for the entire country, connecting the five big energy clusters of the Netherlands, as shown in figure 17. The Hydrogen Backbone will also be connected to Germany and Belgium, which could be in favour of the hydrogen distribution of the hydrogen terminal [79]. The construction of the Backbone is relatively simple because the grid will mainly consist of reused LNG pipelines.

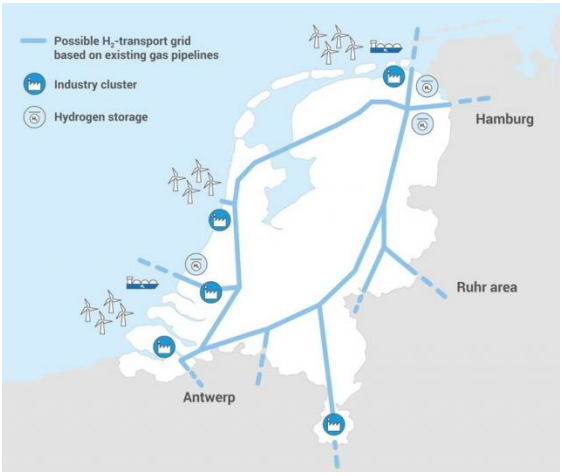

Figure 17: Hydrogen Backbone concept by Gasunie [80]

Gasunie presented recently, in October 2020, a market consultation for the Hydrogen Backbone, which is done to determine the conditions of the grid [33]. This presentation emerged that the grid's pressure regime has already been defined; however, the hydrogen quality specifications have not yet been determined. For the LH_2 terminal, this will be less of a factor, assuming that the LH_2 will be very pure.

Gasunie has done a study to define the ideal system pressure regime for the Backbone. The pressure regime has to be suitable for producers, transportation, and customers. Based on this study, Gasunie has determined that the desired pressure of the grid changes over time [33]. In the first phase, a low-pressure regime between 10-30 bar will be implemented. This is the development phase and will consist mainly of regional ribs. In the second phase, when the hydrogen Backbone is operational, the optimal pressure regime is defined at 30-50 bar. The higher pressure regime is sufficient for hydrogen customers and will enable Gasunie to reach the desired transport capacity.

Regarding the hydrogen quality specification of the Backbone, Gasunie has still to determine the best possible conditions for all parties involved. The market consultation is carried out to determine this question about the ideal quality specification [33]. Hydrogen purity of 100% is not feasible because the gas can be contaminated during transmission [81], and also due to separation limitation during production. To determine what specification below 100% is the ideal solution, Gasunie defined three different purity cases for the market consultation. The hydrogen purity for those three cases are respectively; 98,0; 99,0 and 99,5% [33]. Since these purity conditions are all below the assumed hydrogen concentration at the terminal, the purity requirements will not form a constrain for the LH_2 terminal.

The temperature of gasses in underground pipelines have to be above 0°C because of safety regulations [57]. However, too high temperatures are also not desired. Therefore Gasunie has defined a range for the hydrogen temperature in the Backbone, namely between 5 to 50°C [33], [82].

Concluding, the conditions for the output conditions of the terminal for this research are as followed. The send out pressure is determined at 50 bar because, in this way, the terminal is able to reach the desired pressure in the future. The third case for the hydrogen quality specification is selected, which has the highest hydrogen purity, 99,5% [33]. However, as mentioned before, for the LH_2 terminal, this will not be a constrain. The hydrogen temperature regime of the grid is defined between 5-50°C. An overview of the output conditions is given in table 5.

Table 5: Output conditions for the liquid hydrogen terminal, supplied to the Hydrogen Backbone

Properties	**LH_2**	**Units**
Pressure	50	bar
Temperature	5 - 50	°C
Hydrogen purity	99,5	%

This section does not take into account the limitations for the para-ortho hydrogen concentration, as there are no requirements for the hydrogen backbone yet. However, it is essential to determine this factor, as a higher concentration of para-hydrogen could influence the temperature as well as the HHV of the supplied hydrogen. Furthermore, a catalytic reactor must be added for the isomeric conversion to take place during the regasification process. In section 9.2, a detailed evaluation has been carried out to determine if para to ortho conversion is desired during regasification.

4.3 Send-out scenario

In addition to the input and output conditions, it is desirable to have realistic send-out scenarios of the terminal in order to obtain the most accurate results possible. This is important because the scenario defines the desired send-out rate (minimum and maximum flow) of the terminal and, therefore, significantly influences the regasification installation.

The desired send-out scenario of the proposed LH_2 terminal is influenced by various factors, such as the LH_2 import strategy and the terminal's storage capacity. Furthermore, the function(s) of the terminal also affect the scenario. So to determine the send-out scenario, the factors influencing it have been evaluated. Thereafter, the possible scenarios are determined. Finally, the send-out scenario is selected, which has been used throughout this report.

4.3.1 Factors influencing the send-out scenario

LH_2 import
The liquid hydrogen import strategy of the terminal has an influence on the send-out scenario as well as on the desired storage capacity of the terminal. Considering LNG terminals, two different types of import strategies can be distinguished [83]. The first strategy is a supply contract between the producers (LNG source) and consumers (LNG terminal). This is also known as "dedicated supply", as the frequency, price and the supplied amount are stated in the agreement. The other option is a flexible import strategy, which is mainly driven by the LNG price. In the Netherlands, this type of strategy is used by Gate Terminal because different natural gas supply chains are available [84]. In case the price of LNG is high, natural gas can also be imported from other locations via pipelines. Therefore, a flexible import strategy is currently best suited for LNG import in the Netherlands.

It is difficult to predict what the market for green hydrogen will look like, but for this study it is assumed that the LH_2 supply will be contractually bound, i.e. a dedicated supply strategy. This assumption can be made because if this LH_2 terminal is built, it will be one of the first in the world. With this pioneering function, dedicated supply is evident because the whole LH_2 supply chain still needs to be built and requires a contract of guaranteed use and hydrogen offtake. Vice versa, this also applies to the import terminal [82].

Now that the import strategy has been selected, the next step is to determine the delivery time as it is an essential value for the send-out scenario. The delivery time depends on the location where the green hydrogen is produced and the amount of LH_2 ships dedicated to delivering to the import terminal. The green hydrogen will be imported from areas with a surplus of green energy, like North Africa, the Middle East and closer: Portugal [5]. The shipping times are determined with data from MarineTraffic and Maersk; in addition, the loading and unloading time of the ship is assumed to be one day [85], [86]. The shipping times are presented in the table and graph below, which are respectively 4, 5, 9, 11 and 23 days.

$(L)H_2$ production	Retour shipping time	Shipping time; 1 ship	Shipping time; 2 ships
Portugal	10 days	9 days	4 days
N-Africa	12 days	11 days	5 days
Middle-East	24 days	23 days	11 days

(a) Table of the shipping time

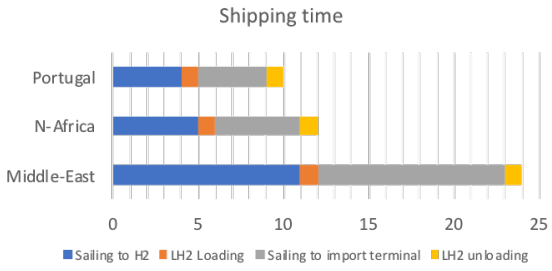

(b) Graph of the shipping time

Figure 18: Shipping time of the various scenarios

Storage capacity
Two LNG storage tanks are available for conversion to LH_2 storage, both with a capacity of 57.250 m^3. Retrofitting for LH_2 usage will be a significant investment, so converting just one tank is also an option.

For design purposes, it is assumed that the retrofitted tank has a storage capacity of 50.000 m^3. In this way, possible capacity losses of storage volume due to enhanced insulation are taken into account, and the fact that not all stored LH_2 can be pumped out of the tank due to the $NPSH_R$ of the pump [87].

Send-out functions
Considering the LH_2 terminal is connected to the hydrogen grid, two possible send-out functions are possible for the terminal. One function is a baseload supply; the other is called the Peakshaver function. A combination of both functions is also an option.

With the baseload function, hydrogen is supplied to the grid with a constant send-out volume every hour of the day. This baseload is purchased by companies in the industry that have a continuous hydrogen demand.

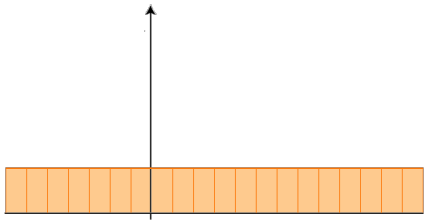

Figure 19: Baseload send-out function.

With the Peakshaver function, the terminal does not deliver a constant volume but an output capacity that can be quickly scaled up and down. In this way, the terminal provides one-sided flexibility to the grid, which means it can supply hydrogen to the grid when required. Offering flexibility is valuable for the hydrogen grid, for example, to absorb the fluctuating hydrogen production from wind energy in the Netherlands. This function is well suited for the LH_2 terminal because the regasification process can be easily adjusted enabling fast ramping up and down of the send-out capacity. This process takes more time and is complicated for hydrogen recovery from other H_2 carriers (e.g. NH_3 and LOHC) and blue hydrogen production [88], [89].

The fluctuating hydrogen production from wind energy can be compensated in various ways. One option is that the terminal is responsible for absorbing all fluctuations due to decreasing wind energy. In this case, a considerable storage capacity is required because it frequently happens that there is little wind for longer periods [90]. As a result, the terminal's storage capacity must be sufficient to guarantee the ability to cover the low hydrogen production of wind energy for days on end. However, if it is windy for a while, the terminal does not have to supply hydrogen to the grid, meaning the tanks remain full. This poses a problem for the LH_2 import because, as described earlier, it is assumed that the LH_2 import will happen via a dedicated supply chain. So, when in windy periods the terminal has not transmitted hydrogen to the grid for a while, the LH_2 production facility and the ship cannot dispose of the LH_2. For these reasons and after further evaluation, it has been determined that covering all fluctuations due to wind energy is not suited for the proposed LH_2 terminal in this research.

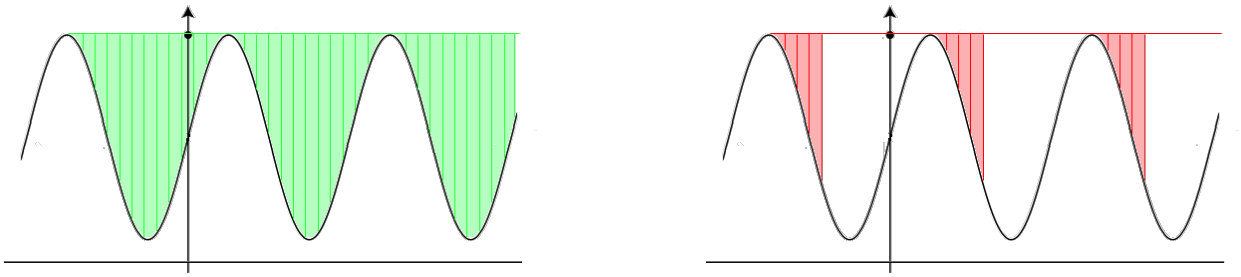

(a) Total Peakshaver function

(b) Short-Peakshaver function

Figure 20: Simplified illustration of the Peakshaver function to the hydrogen grid

Another option is that the terminal only absorbs the large fluctuations for a certain period of time in order to create time for other hydrogen producers to increase their production capacity. In this case, the terminal will compensate for the first few hours when there is less wind. This option does provide flexibility to the grid without the LH_2 terminal requiring a considerable amount of storage capacity. This type of peak shaving is called the short-Peakshaver function. A combination of this short-Peakshaver function with a baseload function has been analysed in more detail in the next section.

4.3.2 Analysing send-out scenarios (Send-out capacity)

In this section, the different send-out scenarios are evaluated by determining the possible send-out capacity. The evaluated send-out scenarios are 1. the baseload function and 2. a combination of short-Peakshaver and baseload function.

Since it is assumed that the import will happen via dedicated delivery, the size of the import volume is affected by two factors: the location of the LH_2 production and the number of ships used. Furthermore, it is assumed that the ships carry as much LH_2 per shipment as the terminal's available storage capacity. This means that the tanks at the terminal are considered almost empty when the LH_2 ships arrive with new cargo.

The intention is that 6 GW of electrolysers powered by wind energy will be operational in the Netherlands by 2030 [10], [33]. They have an efficiency of about 70% (LHV) [20], hence delivering 4.2 GW when there is sufficient wind. It is assumed that the Peakshaver function has to compensate for 50% of this energy in case of little/no wind, thus requiring a Peakshaver send-out capacity of 2,1 GW (LHV).

In this research, the higher heating value (HHV) is considered for the energy send-out to the grid. However, the maximum Peakshaver capacity of 2,1 GW has been defined for the LHV of hydrogen. For the HHV, this maximum energy supply of the Peakshaver function to the grid is equal to approximately 2,48 GW.

Baseload scenario
During the baseload scenario, the terminal has a constant send-out capacity. The send-out capacity is determined in such a way that the tank(s) are almost empty as soon as the LH_2 ship has returned with hydrogen. As stated before, the storage capacity of one retrofitted LH_2 tank is equal to 50.000 m^3.

The baseload scenario is evaluated and depends on the difference in shipping time and the number of available storage tanks (one or two). The baseload capacity for the different scenarios is shown in the table below. As expected, the maximum baseload capacity is reached with a short sailing time and when using two tanks.

Table 6: Baseload send-out capacity for the various scenarios (considering the HHV).

Baseload	1 storage tank		2 storage tanks	
Shipping time	Send-out rate [kg/s]	Energy supply [MW]	Send-out rate [kg/s]	Energy supply [MW]
4 days	10,3	1461	20,5	2909
5 days	8,2	1163	16,4	2327
9 days	4,6	653	9,1	1291
11 days	3,7	525	7,5	1064
23 days	1,8	255	3,6	511

Combination of short-Peakshaver and baseload

In this scenario, the terminal operates as a Peakshaver and has a baseload function as well. As described earlier, the short-Peakshaver function only covers large drops in wind energy for a certain period of time. In this way, the LH_2 terminal is used to its full potential as the easily adjustable regasification process is utilised. To accommodate both functions, the LH_2 terminal has to have enough storage and send-out capacity. To determine these for this scenario, the required capacity for the short-Peakshaver process has first to be defined. After that, it is possible to calculate the baseload capacity.

This short-Peakshaver function is only necessary when a significant drop in offshore wind energy takes place. By defining how often the Peakshaver function is needed, it is possible to determine how much storage capacity is required. It has been decided that the Peakshaver must come into action when the wind energy drops by more than 40% compared to the maximum wind energy, and also with an average wind energy decrease of at least 12%/hour. Taking the offshore wind energy of 2015 as basis, the short-Peakshaver function would be needed 55 times to absorb all offshore wind drops that year [90]. Thereafter, it is calculated how often it can happen during the shipping time (i.e. when the ship is absent) because the terminal must absorb the peak descents during that time. An overview of the percentage how often the short-Peakshaver function is needed during the shipping times to the different destinations can be found in the table.

Table 7: This table presents the percentage of the amount of times the short-Peakshaver function is needed during the shipping time. Considering the wind data from 2015 [90].

Number of times the PS function is required during shipping	**0**	**1**	**2**	**3**	**4**	**5**	**6**	**7**
4 days	51%	37%	5%	0%	0%	0%	0%	0%
5 days	43%	41%	9%	7%	0%	0%	0%	0%
9 days	28%	21%	33%	18%	0%	0%	0%	0%
11 days	13%	31%	38%	9%	9%	0%	0%	0%
23 days	0%	7%	20%	13%	33%	20%	7%	0%

As expected, the Peakshaver function is needed less often in case of shorter delivery times. For the delivery time of 4 and 5 days, it has been determined that the terminal must be able to operate as Peakshaver at least three times during that time. For the delivery time of 9 or 11 days, it is four times. And finally, for the LH_2 import from the Middle East, when it takes 23 days, the terminal should be capable of operating five times as a Peakshaver.

The final step to defining the Peakshaver function's storage capacity is to estimate the amount of LH_2 needed to perform the Peakshaver function once. This is done by calculating the average wind energy drop from the 55 times the reduction is significant. The average drop is equal to 70% compared to the maximum wind energy, with an average decrease period of 4 hours and 40 minutes. Assuming the decrease in wind energy is constant, the send-out capacity has to be equal to 35% of the maximum Peakshaver capacity (2,48 GW) over 4 hours and 40 minutes. Nevertheless, to ensure that the terminal has reserved enough LH_2 storage for the Peakshaver function, it has been determined that the storage volume to cover one significant drop should

allow the terminal to deliver a send-out capacity of 70% for 4 hours and 40 minutes (storage volume equal to 3.000 m^3 of LH_2). Or else it can provide a maximum send-out capacity of 2,48 GW for a period of 3 hours and 20 minutes. The required storage volume for the Peakshaver function is shown in table 8.

Now the storage volume for the Peakshaver function is known, the baseload capacity can be determined. Besides the storage volume for the Peakshaver part, the baseload depends on two other factors: the total storage capacity and the shipping time. The total storage capacity is influenced by the number of tanks put into use (1 or 2). The shipping time, as explained earlier, is affected by the LH_2 production location and the number of ships in use. Assuming the remaining stored LH_2 is supplied as a baseload, the send-out capacity for this function can be determined. The values for the baseload application are shown in table 8.

Table 8: Presents the possible send-out scenarios for the various cases, considering both the short-Peakshaver function and the baseload function.

	Peakshaver function		**Baseload**, 1 storage tank			**Baseload**, 2 storage tanks		
Shipping time	**Times PS function required [#]**	**Storage volume [m^3]**	**Storage volume [m^3]**	**Send-out [kg/s]**	**Send-out [MW]**	**Storage volume [m^3]**	**Send-out [kg/s]**	**Send-out [MW]**
4 days	3	9.000	41.000	8,42	1193	91.000	18,67	2649
5 days	3	9.000	41.000	6,73	955	91.000	14,93	2118
9 days	4	12.000	38.000	3,46	490	81.000	8,02	1140
11 days	4	12.000	38.000	2,83	402	81.000	6,56	931
23 days	5	15.000	35.000	1,25	177	85.000	3,03	430

4.3.3 Selected send-out scenario

In this report, a terminal with a combined short-Peakshaver and baseload application is analysed in more detail. This scenario has been selected because the advantage of an LH_2 terminal is exploited, namely the possibility to provide one-sided flexibility to the grid. This without causing problems for the LH_2 supply chain because the terminal can always receive LH_2 when the ship arrives as it also has the baseload function.

The selected location where the hydrogen will be imported is Portugal. Furthermore, it is assumed that only one LH_2 ship will be deployed to deliver to the LH_2 terminal. The send-out case, which will be evaluated in this report, is shown in table 9. As can be seen, the baseload capacity differs from the number of tanks in use.

Table 9: Presents the selected send-out capacity of the proposed LH_2 terminal.

	Peakshaver function				**Baseload**, 1 storage tank			**Baseload**, 2 storage tank		
Shipping time	**Times function required [#]**	**Storage [m^3]**	**Send-out [kg/s]**	**Send-out [MW]**	**Storage [m^3]**	**Send-out [kg/s]**	**Send-out [MW]**	**Storage [m^3]**	**Send-out [kg/s]**	**Send-out [MW]**
9 days	4	12.000	17,5	2480	38.000	3,46	**490**	81.000	8,02	**1140**

The send-out capacity of 490 MW is comparable to planned hydrogen projects in the Netherlands around 2025 [91]. The 1140 MW is on the high side but not inconceivable, especially if hydrogen for Germany is also imported via the port of Rotterdam. In addition, as the HyNetherlands project aims to scale up their electrolysers to a capacity of around 750 MW to 1 GW from 2027, this assumed send-out capacity is not at all out of proportion [92].

Process installation

The send-out scenario influences the process equipment. The regasification equipment must be able to handle the minimum and maximum send-out capacity with the meeting the following requirements:

- Minimum send-out capacity: Baseload (see table baseload)
- Maximum send-out capacity: Baseload + Peakshaver function (2,48 GW)
- The send-out capacity must be adjustable between the minimum and maximum value.

5 Ship unloading and LH_2 pipes

To receive the liquid hydrogen at the terminal, the LH_2 must be transported from the ship's cargo tank to the onshore storage tank. In this chapter, this unloading process is described. Thereafter, the designs of the LH_2 pipelines at the terminal are defined.

5.1 Unloading process

The terminal receives LH_2 from maritime vessels unloading their cargo; this is called the unloading process. The unloading process can be separated into three stages: recirculation, depressurization, and unloading [93]. The recirculation stage is operational, when there is no LH_2 vessel moored and available for unloading. During this stage the lines need to be kept cold since they are not in use. A small amount of LH_2 from the tank circulates continuously through the unloading pipelines. As shown in figure 21, a separate recirculation line is connected from the LP-pump to the unloading pipe [94].

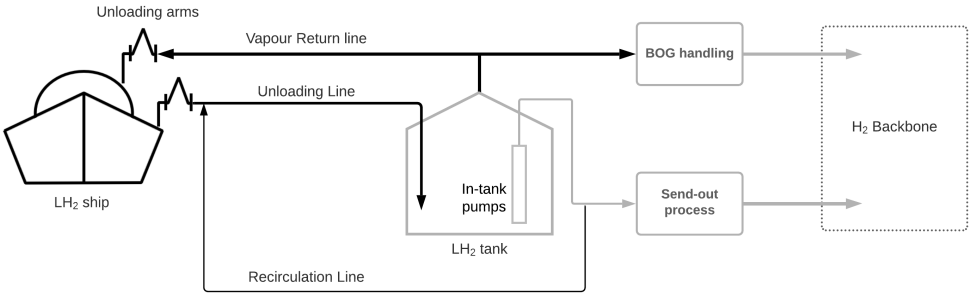

Figure 21: Schematic overview of unloading pipelines, redrawn from [94]

The depressurization stage is necessary to reduce the pressure inside the unloading pipes to create suitable conditions for the unloading stage [93]. During the recirculation stage, the pressure inside the unloading pipes is higher to minimize the BOG formation [93]. For the unloading stage, the pressure needs to be decreased as much as possible to prevent a significant pressure difference between the unloading pipe and the storage tanks. Importantly, the pressure inside the storage tank and most maritime vessels is just above atmospheric conditions [95]. The final step of the depressurization stage is to equalize the pressure between the onshore storage tank and the unloading pipeline by opening the unloading valve [93]. Before the unloading stage can start, the unloading arms at the jetty need to be purged as well [96].

As everything is ready to start the unloading stage, the LH_2 can be pumped to the storage tank by the LH_2 pumps at the ship [94]. For the LNG case, the discharge rate increases in approximately 1,25 hour from 200 m^3/h to the full speed unloading capacity of 12.000 m^3/h [96]. During this process, vapour is sent back to the ship to replace the discharged volume in order to maintain the operating pressure in the cargo tank and to avoid vacuum conditions [97]. The unloading stage of an average LNG carrier takes around 12 hours. However, due to other activities before and after unloading, a ship usually stays at the port for 24 hours [97].

For the design of the LH_2 terminal, it is assumed that the unloading phase of the LH_2 vessel also takes 12 hours. Therefore, the unloading capacity depends on the number of storage tanks that are utilized. In case only one tank is employed for LH_2 storage, the unload capacity is equal to 5.000 m^3/h. When using both tanks, the unloading capacity is 10.000 m^3/h.

5.2 Jetty

The LH_2 ships moor at the jetty for unloading. Unloading arms are installed on the jetty to transport the LH_2 from the ship to shore, as shown in figure 21. The capacity of the unloading arms for LNG use varies from 4.000 to 6.000 m^3/h [97]. Two or three unloading arms are installed at the jetty, depending on the ship's capacity and the terminal's storage capacity. In addition, one vapour return arm and a spare arm are installed at the jetty [97]. For safety measures, a special unloading and mooring PLC will control the unloading process and stop it automatically when unsafe conditions are detected [94].

The conventional unloading arms for LNG applications cannot be used for LH_2 because of safety concerns [98]. As will be discussed later in this chapter, the LH_2 pipelines must be vacuum insulated to prevent the formation of liquid oxygen. For this reason, the unloading arms also need to have vacuum insulated pipes and connections. The first LH_2 unloading arm has recently been developed by a collaboration of several Japanese companies [98]. This arm has a double-walled vacuum insulation structure, with a specially designed swivel joint that does not compromise the vacuum insulation [98]. Furthermore, the arm is equipped with an emergency release system (ERS) for safety measures [98].

5.3 BOG generation during unloading process

During the unloading process, the generation of boil-off gas (BOG) at an LNG terminal is about 8 to 10 times more than the BOG formation of the storage tanks [99]. The main sources generating BOG during the unloading process are depicted in table 10. Defining the additional BOG formation during unloading is necessary to determine the maximum BOG flow to be handled at the terminal.

BOG generated during unloading process
Vapour return to ship's tanks
Heat transferred to the LH_2 by the ship's pumps
Heat leak into the LH_2 through the pipes and equipment
Higher ship's operating pressure than the LH_2 storage tank
Cooling down the ship's manifold and unloading arms prior to unloading

Table 10: Main factors affecting the quantity of BOG released during the ship unloading process [100]

The main reason for the significant increase in BOG release is the displaced vapour volume from the storage tank to the ship, as the liquid level in the storage tank increases and in the cargo tank decreases [100]. The vapour return must supply an equal amount of volume to the cargo tank as the unloading capacity, which can be as high as 12.000 m^3/h [96]. The pressure and temperature difference between the storage tanks and the cargo tank influence the actual flow rate of the return line [96], [100]. The BOG can be sent back by vapour return blowers. However, if the pressure between the storage tank and the cargo tank is sufficient, no blower is required to return the vapour [96]. For the LH_2 terminal, this is desired, as the compressor/blower cannot operate at temperatures below -170°C.

Another source strongly influencing the BOG increase is the pumping of LH_2 from ship to storage tank. For the LNG case, it can be assumed that almost all the pumping energy is converted into heat adsorbed by the LNG due to friction and turbulence [100], [101]. Furthermore, heat is also entering the cryogenic liquid due to heat leakage into the unloading pipeline. As the cryogenic liquid is supplied to the storage tank, the absorbed heat needs to be removed, which results in significant BOG generation. The length of the unloading pipeline affects the actual heat ingress. This is also the case for the generated heat due to pumping [100], since more pumping energy is needed to transport the cryogenic liquid over a greater distance.

There are also other factors that influence the quantity of BOG, as is shown in table 10. For example, one factor is the pressure difference between cargo tank and storage tank. If the operating pressure in the cargo tank is higher than in the storage tank, the temperature of the LH_2 in the cargo tank will also be higher. A small amount of BOG is formed to decrease the temperature of LH_2 to the desired conditions of the storage tank [100]. However, vice versa, if the storage tank has a higher operating pressure, the BOG generation decreases [96]. Furthermore, before the unloading stage can start, the unloading arms and equipment at the LH_2 ship need to be cooled down, which also generates BOG [100]. Generally, the higher the operating pressure of the storage tank, the lower the BOG formation during unloading [96].

As mentioned, defining the additional BOG formation during unloading is necessary to estimate the maximum BOG flow to be handled at the terminal. Since the largest additional BOG generation occurs during full-speed unloading, this part will be analysed. It is assumed that the vapour return flow does not require treatment and is equal to the unloaded liquid volume flow. So, for this reason, only the pump energy and the heat leakage in the pipeline form BOG. The additional BOG generation due to unloading has been calculated in section 12.1.

5.4 LH_2 pipelines at the terminal

At the terminal, pipelines are necessary to transport LH_2 or hydrogen gas. The temperature, pressure and volume flow of the transported substance influence the requirements of the pipe. As discussed in section 3.1.1, the LH_2 pipes must be vacuum insulated to prevent the formation of liquid oxygen at the piping surface [98]. All pipes transporting hydrogen below the boiling point of oxygen must be vacuum insulated for safety precautions. For this reason, reusing the existing LNG pipes is not possible.

In collaboration with Demaco Holland B.V. and taking into account EN13480 design standards, the pipelines for the LH_2 terminal have been designed [102]. For the LH_2 pipes, stainless steel 316L is used, and the vacuum insulation conditions of the pipe are higher than 10^{-3} mbar [102]. For the LH_2 pipes, a schedule number of 10S is sufficient to handle the pressures at the terminal, but for safety concerns, a schedule number of 40S has been selected. The schedule number of the pipe is a dimensionless number related to the wall thickness of the pipe [103].

To determine the desired diameter of the pipeline, the volume flow and the erosion velocity is of interest. When a substance is transported through a pipe, the surface of the pipe will erode. The erosion rate will increase with a higher flow velocity. For this reason, an erosion velocity is defined to set a limited velocity before erosion will be a concern [104]. However, as the density of hydrogen is relatively low, the erosion velocity can be high and therefore it is not a restricting condition for the design of the pipe. The diameters variate between 6 to 32 inch, depending on the volume flow. However, there are no commercially available valves for LH_2 pipes greater than 10 inches in diameter [105]. These valves must be designed by reputable suppliers, which makes LH_2 piping significantly more expensive.

6 LH_2 storage

At the import terminal, large-scale LH_2 storage is required. Since the two well-insulated LNG tanks at the LNG-PS site are available, the goal is to reuse them as they are the most expensive part of the installation [106]. The two LNG storage tanks, each with a capacity of 57.250 m^3, are described in more detail in chapter 2. For clarity reasons, a schematic overview of the double-containment LNG tank is shown in figure 22. To evaluate the possibilities for reuse of the current LNG storage tank, first, the differences in physical and chemical properties that affect storage are determined. Thereafter, the state of the art of LH_2 storage tanks and options for retrofitting the existing tanks are discussed. Finally, two types of retrofit solutions are selected, and their BOR is calculated. Of note, this study does not take into account the decommissioning and additional safety requirements.

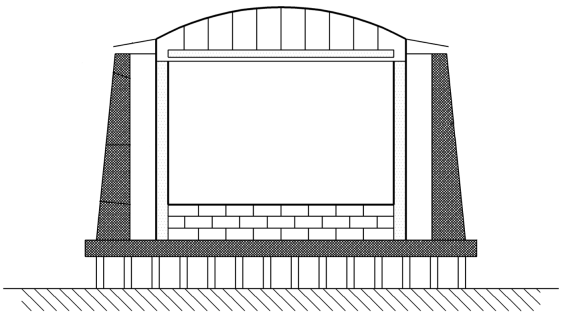

Figure 22: Schematic figure of the current double-containment LNG tank design [107].

6.1 Differences between LH_2 and LNG storage

Storing LH_2 instead of LNG is more complicated, mainly due to two property differences: the lower temperature and the easier evaporation ability of LH_2 [6]. For this reason, adjustments have to be made in order to store LH_2 in the current LNG tanks.

The operating pressure of a large-scale cryogenic tank is most often just above atmospheric conditions [108]. Hence, the storage temperature of LH_2 has to be at -253°C, which is significantly lower than the -162°C for LNG storage. However, the inner tank material is made of a nickel-steel that cannot withstand temperatures below -195°C [109]. For this reason, another layer of material must be applied to the inside of the LNG tank before it is able to store LH_2. Furthermore, due to the low temperature, it is also possible to have liquid oxygen formation, as discussed in section 3.1.1. Therefore, adding an additional layer inside the tank, creating a double-walled insulation, could be a solution to deal with this problem.

The boil-off rate is also influenced by the differences in characteristics between LH_2 and LNG; when storing LH_2 in the current tanks, the BOR will be significantly larger. This is mainly since LH_2 evaporates easily, caused by the low volumetric heat of vaporisation [110]. As shown in table 1, the heat of vaporisation of LH_2 is 31,4 kJ/L; for LNG, this value is considerably larger: 226 kJ/L [19]. As a result, external heat of 31,4 kJ entering the storage tank causes one litre of hydrogen boil-off gas. Whereas for LNG storage tanks, the heat leakage into the tank can be around seven times higher before one litre evaporates. As the goal is to minimize the amounts of BOG, additional insulation is required to achieve similar BOR as the current LNG storage tanks. In addition, considering the larger temperature difference, the insulation degree must be ten times higher to reach similar BOR [74].

The density of LH_2 is notably lower than LNG, as discussed in chapter 3. For this reason, the weight of the stored new liquid is not an issue for the structure of the existing tank. As a matter of fact, it gives possibilities to apply additional insulation in the tank from the inside. This is possible because when the tank is 100% filled

with LH_2, the stored weight is almost 25,000 tons less than allowed (designed liquid density is 500 kg/m^3) [111].

As stated above, the stored mass inside the tank is no constraint for LH_2 storage. Therefore, the tank can be utilized for 100% with LH_2. However, storing LNG results in a higher amount of stored energy than with LH_2 due to the fact that the HHV per volume of LNG is larger. Considering the higher heating value of LNG at 23,6 MJ/L, the total energy stored in the tanks is equal to 2700 TJ [39]. The volumetric energy density of LH_2 is more than two times lower, i.e., 10,05 MJ/L for the HHV, resulting in a total amount of stored energy equal to 1150 TJ [39].

6.2 LH_2 storage techniques

In order to store LH_2, an enhanced insulation method must be selected. Therefore, the existing LH_2 storage technique is discussed, and options to retrofit the current LNG tanks are analysed.

When looking for insulation methods, the state of the art for LH_2 tanks is of interest. The insulation requirement for LH_2 tanks is achieved most often with a vacuum insulation method. This method is commonly used at double-walled spherical tanks, but tanks with this design are not able to store large capacities [108], [112]. Currently, the largest LH_2 storage tank is in use by NASA and stores around 3.800 m^3 of liquid hydrogen [108]. The designs for double-walled spherical tanks go up to a maximum capacity of around 50.000 m^3 [66]. For capacities above 50.000 m^3, cylindrical tanks have to be used. Kawasaki Heavy Industries is designing cylindrical LH_2 storage tanks up to 200.000 m^3, and they aim to insulate the LH_2 tank in such a way that the boil-off rate is equal to that of LNG tanks. They are aiming to complete the research within a few years [113].

For retrofitting the LNG tank, other options are also investigated. From the evaluation in the previous section, it is concluded that the current LNG tanks are not yet suited for storing LH_2. Because the temperature of LH_2 is below the operating window of the material used inside the tank, and the insulation degree of the LNG tank is not sufficient for the LH_2 application. For this reason, an additional insulation layer needs to be applied inside the tank. This insulation layer must obviously increase the insulation ability of the tank, and be capable of withstanding temperatures as low as -253°C. Furthermore, the thickness of the insulation layer should be as thin as possible to leave as much space as possible for storage. For this topic, a trade-off can be made regarding the insulation degree and the thickness of the insulation material.

To be capable of withstanding the low temperatures of LH_2, an inner tank has to be added into the LNG tank. This inner tank will be made of metal; however, metals for cryogenic service (especially for LH_2) are limited. Structural metals that can handle LH_2 include some austenitic stainless steels, aluminium alloys and iron-nickel alloys [109], [114]. Other steel and nickel alloys, like the current material used in the LNG tank, are not suited for LH_2 storage [109], because those materials are susceptible to temperature and hydrogen embrittlement. The effect of lower temperatures can be seen in figure 23, where the fracture resistance of austenitic stainless steels and aluminium alloys are relatively insensitive to cryogenic temperatures [115]. However, the other steels and steel-nickel alloy do show significant degradation at low temperatures. The austenitic stainless steels utilised for LH_2 application are 304L and 316L [109], [116]. For the aluminium alloys, there are more options available; one of them is the 2219 [117].

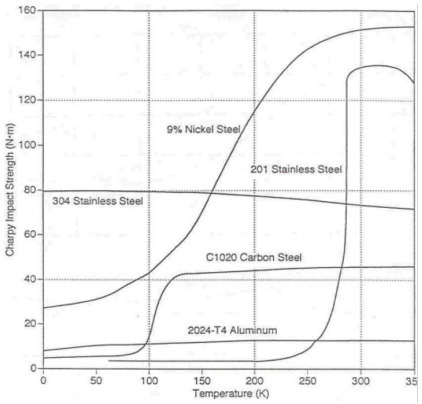

Figure 23: Charpy impact strength (fracture resistance) as a function of temperature for various materials [115]

Besides the inner tank, an additional insulation layer is necessary because the thermal conductivity of the metal structures are relatively high. Desired insulation materials have a low thermal conductivity, which results in a small heat flux value. There are multiple solutions to accomplish this low thermal conductivity. An option is to create a perlite vacuum insulation layer between the new applied inner tank and the old LNG tank surface. This type of insulation material is already widely utilised for LH_2 storage, for example, by Kawasaki [66]. The thermal conductivity can be 0,0015 W/m*K for a perlite powder at high vacuum conditions (10^{-3} torr) and a density of 100 kg/m^3 [118]. Another promising material that can be applied at vacuum conditions is glass microspheres (or bubbles). At similar vacuum conditions and a density of 70 kg/m^3, the thermal conductivity of glass microspheres can reach a value as low as 0,0005 W/m*K [118]. Nevertheless, implementing a vacuum condition between these two tanks is quite complicated. And it is unknown if the current nickel-steel inner tank is capable of handling vacuum conditions; therefore, it requires additional research.

Furthermore, research is being done into new types of insulation methods for LH_2 application. Such insulation methods are based on multi-layer insulation materials. In a study carried out by Zheng et al., two composite insulation systems are examined, all consisting of spray-on foam insulation (SOFI) and variating multi-layer insulation material, as is shown in figure 24a [119]. And for those two multi-layer configurations, the thermal conductivity for vacuum within the multi-layer material (as is shown in I and II, of figure 24a) as well as discharged hydrogen boil-off gas (III and IV, of figure 24a) was tested [119]. The proposed insulation systems have a 35,3 mm SOFI thickness, and the multi-layer material consists of 45 layers. The heat flux of the configurations under different vacuum degrees is shown in figure 24b. Another similar study regarding a multi-layer insulation system, consisting of a 45 layer MHTB and a 35 mm SOFI, has a heat flux of 0,22 W/m^2 at high vacuum conditions [120]. Altogether, the multi-layer insulation systems can achieve a minimal heat flux with a small thickness of the material, which is promising. However, this type of insulation is mainly used for aerospace application and is an expensive solution [121].

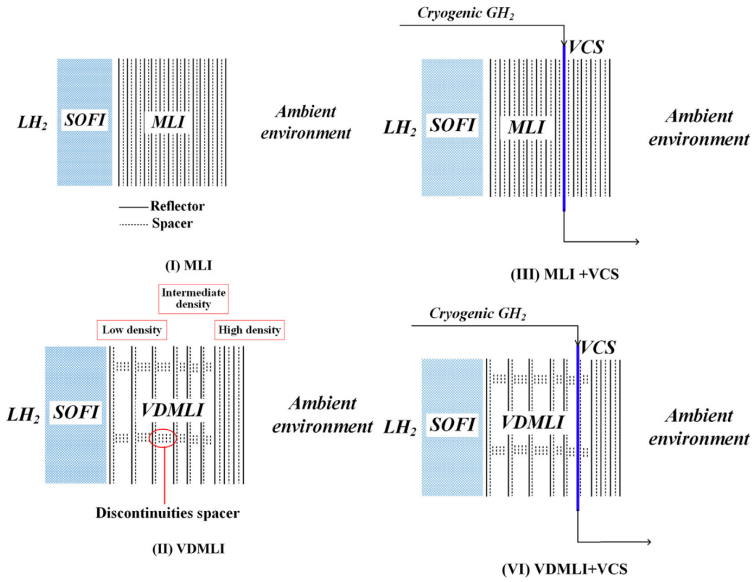

(a) Schematic of insulation system for LH_2 tank.

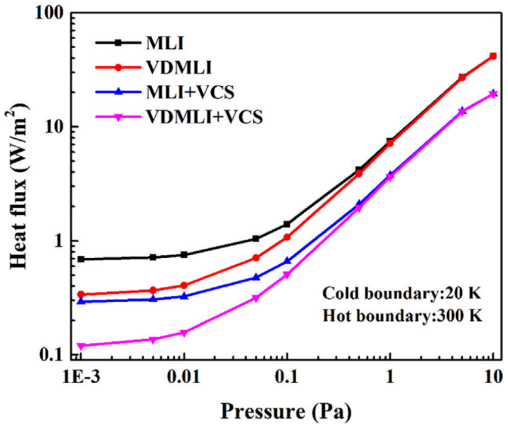

(b) Heat flux through insulation system under different vacuum degree.

Figure 24: Insulation technique for LH_2 storage, proposed by Zheng et al. [119].

Another solution is to use a membrane insulation system, which is often implemented at LNG cargo ships. Such a membrane insulation system is a containment and insulation system, which is directly supported by the ship's hull structure, as shown in figure 25 [122]. Since it can be applied directly to the hull of a ship, it may also be possible to attach this insulation technique directly to the inner wall of the LNG tank. In this way, the nickel steel tank acts as the ship's hull and provides support to handle the hydraulic pressure, which is significantly lower than for LNG. By applying this extra tank and insulation layer, the risk of liquid oxygen forming is covered, provided the roof is also properly insulated and hydrogen-tight. For these reasons, this technique offers opportunities for retrofitting the current LNG tank.

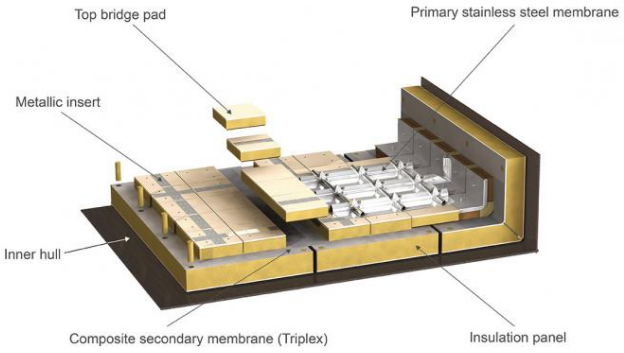

(a) Construction of the Mark III insulation panel.

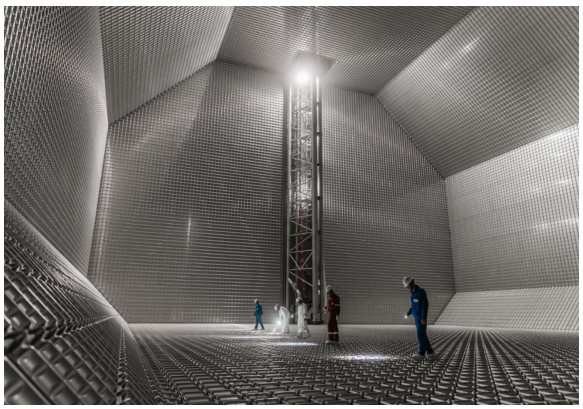

(b) The inside looking of the GTT Mark III tank

Figure 25: Mark III insulation technology, design by GTT [122].

The leading company developing membrane insulation systems is Gaztransport Technigaz (GTT) [122]. They have multiple designs, some of which are already suitable for the low temperatures of LH_2 as their primary membrane is made of stainless steel 304L [114]. The most promising is the Mark III technique, which is a modular system that can accommodate any shapes and capacities of tanks and is also used for onshore

storage [122]. As shown in figure 25a, it is composed of a primary corrugated stainless steel 304L membrane, positioned on top of prefabricated insulation panels, including a complete secondary membrane made of composite material [122]. Their newest and best insulating Mark III Flex+ technique has a total thickness of 480 mm, which can archive a BOR of 0,07%/day for large scale LNG storage [122]. Implementing this insulation degree in addition to the existing insulation could provide sufficient insulation for LH_2 storage.

6.3 The selected retrofit solutions

Although multiple solutions are possible to retrofit the LNG storage tank, in this research, only the vacuum insulation technique and the membrane insulation system Mark III are considered. The material selection and insulation methods are analysed in this study, but safety regulations, which is an essential part, were not considered. It is assumed that the proposed solutions meet the safety requirements for large-scale LH_2 storage.

The vacuum insulation technique has been chosen because it is widely used for LH_2 storage, and it is feasible for large-scale storage in the near future, according to Kawasaki [113]. Furthermore, the insulation degree of such a tank is significant. Therefore, to evaluate the benefits of a low BOR, it is essential to select this design. The downside of this solution is that the current insulation tank in the concrete construction must be removed to implement the new vacuum insulated tank, as shown in figure 26. This means that only the concrete structure can be reused, which entails high costs.

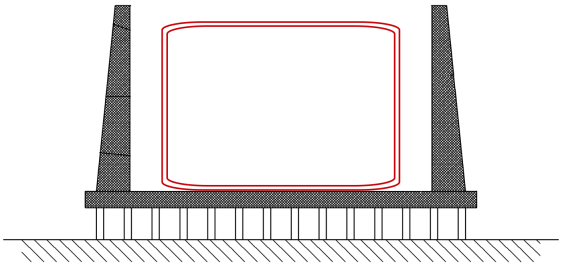

Figure 26: Schematic figure of the retrofitted cylindrical double-walled vacuum tank design.

For the new vacuum tank, it is assumed that a cylindrical double-walled vacuum design is used with a capacity of 50.000 m^3. The concrete structure can easily support this new, double walled vacuum tank since the old inner tank is removed and the stored mass is 25.000 tons less since the LH_2 density is lower. Furthermore, the corresponding heat flux for this type of insulation is approximately 1 W/m^2 [66]. Knowing the heat flux and the surface area of the tank, the heat flow Q can be determined with equation 2. Equation 9 is used to calculate the BOR of the tank, which results in a BOR of around 0,043%/day, which is lower than the current BOR of the LNG storage tank.

$$Q = q * A \qquad [W] \tag{2}$$

The membrane Mark III insulation technique has been selected as a retrofit solution because the entire LNG storage tank can be reused, creating a cheap solution. A disadvantage of this system is the relatively low insulation degree compared to the vacuum tank, which results in a higher BOR. However, since the terminal is assumed to have a baseload send-out to the grid, a higher BOR can be processed.

Applying this insulation technique is possible because it is calculated that the inner tank can carry the weight of the membrane insulation system since the stored mass of LH_2 is almost 25.000 tons lower. In figure 27, a schematic overview shows the added Mark III insulation technique. The storage capacity after retrofitting the LNG tank is assumed to be 50.000 m^3 as well.

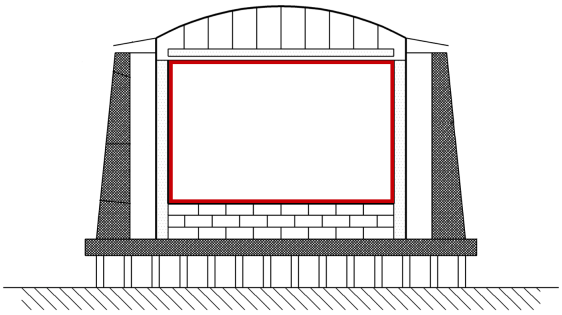

Figure 27: Schematic figure of the retrofitted membrane Mark III tank design. The additional Mark III insulation technology is indicated in red.

Calculations have been performed to determine the BOR of the converted LNG storage tank with membrane insulation. These calculations are performed in the same way as for the old LNG tank design [111]. First, the U-values for the different planes (wall, bottom and roof) are defined with equation 3. Then the heat flow Q can be determined, and finally, with equation 9, the BOR of the tank.

$$U = 1/\left(\frac{t_1}{k_1} + \frac{t_2}{k_2} + \frac{t_i}{k_i}\right) \qquad \left[\frac{W}{m^2 * K}\right] \tag{3}$$

$$Q = U * A * \Delta T \qquad [W] \tag{4}$$

Where t and k represent the thickness and thermal conductivity of the insulation material, respectively, the subscripts refer to the different materials used in each plane. Furthermore, A defines the surface area of the tank, and ΔT is the temperature difference between LH_2 and the outside wall. Since all these values are known, it is possible to determine the BOR for the retrofitted tank, which is 0,31%/day. In comparison, if no additional insulation layer is added to the storage tank, the BOR would be 0,45%/day. So implementing this technique reduces the BOG by more than 30%, and it makes the tank suited to handle extremely low temperatures. However, as mentioned before, additional research is required before implementing this solution is feasible.

Altogether, the vacuum insulated tank results in a significantly lower BOR than the Mark III technique. A higher BOR of the tank is unwanted as it affects the efficiency of the LH_2 terminal. However, applying the Mark III technique is assumed to be a considerably cheaper solution because the current tank can be reused, which is only partly the case with the vacuum tank. In chapter 8, the influence of the different BORs on the process efficiency of the terminal is analysed. These results make it possible to determine which type of tank is best suited for the proposed LH_2 terminal.

7 LH_2 pump process

Pumping the LH_2 to the desired pressure of the H_2 grid is the first step within the regasification processes. Two types of LH_2 pumps will be used for this process, similar to the current process at the LNG-PS. The first pump is employed to pump the LH_2 out of the storage tank. This will be done with a submerged pump inside the tank which delivers a slight pressure increase. After that, the second pump (high-pressure pump) will be used to pump the LH_2 to the desired grip pressure (50 bar). As the send-out capacity has been determined before, the required flow throughput of the LH_2 pumps is known.

This chapter first discusses the complexity of LH_2 pumps, followed by solutions to solve these problems. Thereafter, the state of the art of LH_2 pumps is analysed. With knowledge of the state of the art and in collaboration with Nikkiso Cryo Inc., a suitable pumping process is determined for the LH_2 terminal. Finally, the calculation methods of the pumps are explained.

7.1 LH_2 pumping complexities

The LH_2 pumping process is seen as a difficult task, not only due to the physical and chemical properties of LH_2 but also because of the process conditions of the LH_2 terminal [27]. The process conditions of LH_2 pumping require both high flow and respectively high pressure. Although the desired pressure of 50 bar does not seem so high, the corresponding pressure head is significant due to the low density of hydrogen.

Reusing the current centrifugal LNG pumps is not possible because some of the physical and chemical properties that influence the pumping process differ too much. The main properties that affect this process are the lower temperature and density of LH_2. First of all, the lower temperature of LH_2 affects the material choice of the pump. This material must be capable of withstanding extremely low temperatures without becoming brittle [17]. Furthermore, the extremely cold temperatures in the pump must be maintained to keep the hydrogen in a liquid state at all times; any evaporated hydrogen will cause damaging cavitation in the pump [17]. Therefore, the thermal insulation at the outside and even inside the pump is considered a complicated aspect of designing the LH_2 pump [123].

The low-density of LH_2 results in a low available Net Positive Suction Head ($NPSH_A$), meaning the difference between the saturated vapour pressure and the liquid pressure is small [124]. This low $NPSH_A$ causes cavitation to occur more easily during LH_2 pumping [112]. Since the density of LNG is significantly larger, this value is less of a concern for the LNG pumps. The effect of the NPSH is especially relevant for centrifugal pumps as this type of pump is most vulnerable to cavitation damage [112], [87].

Another effect of the low density is the necessary high pressure head of the pump. As can be concluded from formula 5, the head for LH_2 will be significantly higher than for LNG, considering the same pressure. This is caused by the specific gravity (SG) of LH_2 which is notably smaller than that of LNG, namely 0,0709 and 0,554, respectively [19].

$$P = head * g * SG \quad [Pa] \tag{5}$$

P	Pressure [Pa]
$head$	Pressure head [m]
g	0,00981; gravitational acceleration
SG	Specific gravity [-]

The higher required head for LH_2 pumping influences the centrifugal pumping process significantly. The theoretical head (or Euler head) delivered by the impeller of a centrifugal pump is calculated with equation

6 [125]. As can be seen, the density is not a component of the equation, meaning the theoretical head of a pump is independent of the fluid type. In other words, if the LH_2 pump has a similar geometry as the LNG pump, the delivered head would be the same. However, the pressure increase of the LH_2 pump would be significantly less.

$$head = \frac{1}{g}(U_2 V_{w2} - U_1 V_{w1}) \quad [m] \tag{6}$$

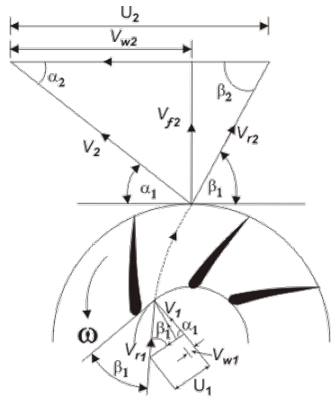

Figure 28: Velocity triangles for centrifugal pump Impeller [125].

7.2 How to overcome those difficulties

As mentioned, the LH_2 evaporates relatively easily, so a small amount of heat leakage into the pump could already cause severe issues for the pump [87]. Therefore, the HP pump should be vacuum insulated to minimize heat leakage. For the submerged pump, heat leakage from the surrounding is not a concern because it is located inside the tank. In addition, heat is also generated in the pump due to friction and by the electromotor, which is often implemented inside the pump [126]. According to Cryostar, handling the internal heat is one of the major bottlenecks in designing an LH_2 pump [123]. To remove this heat, most of it can be sent along with the fluid [126]. Furthermore, some heat can be dissipated by boil-off gas.

The $NPSH_A$ of LH_2 is low, which could lead to cavitation; however, there are options to increase this value. Furthermore, it is also possible to decrease the required NPSH of the pump itself. The $NPSH_R$ is a characteristic of the pump, which describes the minimum NPSH the fluid must have before entering the pump; otherwise, cavitation will occur. In other words, to avoid cavitation, the following must apply $NPSH_A \geq NPSH_R$ [124].

Several ways to prevent cavitation in the pump are given below [124], [87]. For clarification, the equation of the $NPSH_A$ is provided first, with accompanying figure.

$$NPSH_A = P_{suction} - P_{saturation} = P_a + P_{st} - h_f - P_{sat} \quad [m] \tag{7}$$

$NPSH_A$	Net positive suction head available
P_a	Absolute pressure on the surface of the liquid
P_{st}	Pressure due to elevation between the liquid surface and pump suction
h_f	Head losses in the pump suction piping
P_{sat}	Saturation pressure of the liquid being pumped

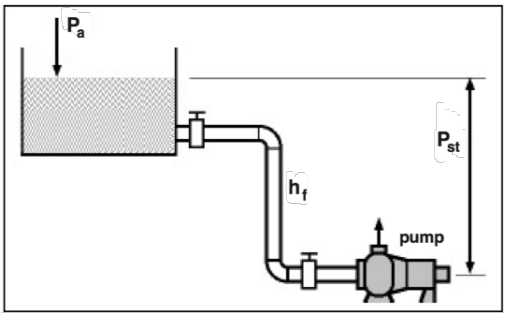

Figure 29: An image to clarify equation 7

Increase $NPSH_A$

- Increase the pressure at the suction of the pump. In the case of the submerged pump, this can be done by raising the liquid level in the tank.
- Decrease the temperature of the liquid which is pumped. In this way, the saturation pressure is decreased.
- Decrease head losses in the pump suction piping. This can be done by increasing the pipe's diameter, reducing the number of valves and elbows in the pipeline, and decreasing the pipe length. This aspect could be an interesting solution for the HP pump.

Reducing the $NPSH_R$ of the pump

- The $NPSH_R$ increases significantly as the flow rate through the pump increases. So reducing the flow rate results in lower $NPSH_R$.
- Reducing the rotational speed of the impeller results in lower $NPSH_R$. However, a certain flow rate is necessary for the system, so limited adjustments are possible. Or else, parallel pumps are necessary to decrease the flow rate through the pump.

For the LH_2 pump to reach a higher pressure head, the rotational speed can be increased, as can be concluded from equation 6. However, as stated above, a higher rotational speed will lead to a higher $NPSH_R$, which is not desired. Therefore, multiple-stage pumps and/or pumps in series are required to reach a high head.

7.3 Currently available pumps

Two types of LH_2 pumps are currently available for commercial use, i.e. a centrifugal and a reciprocating pump [127]. The current centrifugal LH_2 pump can reach a relatively high throughput capacity of 600 m^3/h [128]. However, the pressure ratio of these pumps is low as the centrifugal pumps have difficulties increasing the pressure due to the low density of LH_2. For this reason, the centrifugal LH_2 pumps are mainly used to pump LH_2 out of a storage tank [112]. Companies such as Cryostar and Nikkiso Cryo Inc. are doing research into centrifugal LH_2 pumps. Cryostar has made submerged LH_2 pumps commercially available. As explained, they can have a relatively large throughput, however the pressure ratio of the 600 m^3/h pump is below 2 bar [128]. The performance chart of those pumps is shown in Appendix C.1.

The reciprocating pump, on the other hand, is capable of handling large pressure ratio's. These types of pump can increase the LH_2 pressure up to 900 bar [127], because the effect of the NPSH is less of a problem. Nevertheless, the maximum throughput of the reciprocating pump is currently too small for the LH_2 terminal application, namely 120 kg/h H_2 (1,7 m^3/h) [17]. Hence, thousands of reciprocating pumps would be necessary to compress the large volume flow up to 50 bar. Cryostar mentioned that they are capable of reaching a max throughput of 41 m^3/h for the process conditions of the terminal, with their triplex pump design [123]. Nevertheless, this is still not close to the wanted throughput of the terminal.

7.4 Selected LH_2 pumps

Although no LH_2 pump can be found in the literature for the requirements of an LH_2 terminal, it turned out that Nikkiso Cryo Inc. was able to design it. In collaboration with Nikkiso Cryo Inc., LH_2 pumps have been designed for the specific process conditions of the LH_2 terminal proposed in this report. The selected LH_2 pumps are very similar to the currently used type of pumps for the LNG process but have been made suitable for LH_2.

To pump the LH_2 out of the tank, a vertical, submerged, removable in-tank pump is designed. This is a centrifugal pump, similar to the submerged type of pumps used for the LNG process, as is shown in figure 30. This submerged pump can increase the pressure to around 5 bar, resulting in a head of approximately 720 m. Furthermore, the $NPSH_R$ of the pump is given, which is a relatively small value due to a special inducer. The inducer is specifically designed to prevent cavitation and is derived from aerospace technologies used to pump LH_2 in rocket engines [126]. Considering $NPSH_R$ and the guideline for NPSH margin, ANSI/HI 9.6.1, the minimum LH_2 level inside the tank can be determined [129]. This minimum LH_2 level is between 2 and 3,5 meter depending on the throughput of the pump. Furthermore, the pump is removable, which is beneficial for maintenance purposes.

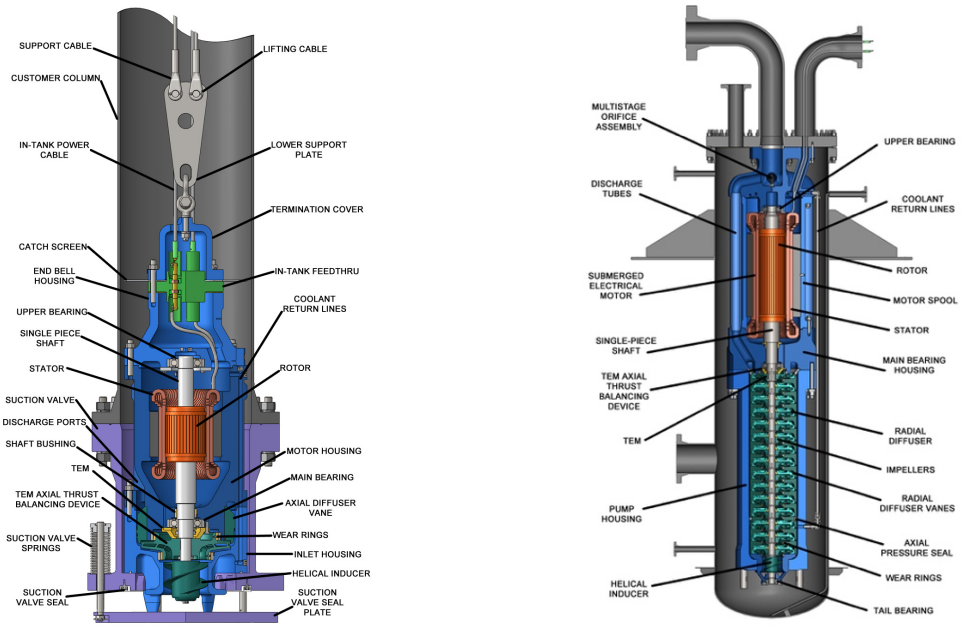

(a) Submerged pump

(b) Pot mounted pump

Figure 30: Centrifugal pumps employed for LNG application but similar designs will be used for LH_2 treatment [130]

For the high-pressure pump, a vertical, submerged pot mounted type of pump is utilized. Again, it is a centrifugal pump and has a similar design as an LNG HP pump which is shown in figure 30. As mentioned before, increasing the pressure of LH_2 is difficult for a centrifugal pump because of the low density of LH_2. For this reason, three pumps in series are required to achieve the desired pressure of 50 bar. For the LNG pumping process, only one pump was sufficient to increase the pressure up to 80 bar. Furthermore, the pot mounted pumps are vacuum insulated for thermodynamic reasons and to prevent liquid oxygen formation.

The three HP pumps in series are identical, and each pump has a pressure increase of around 16,5 bar. At the first HP pump in succession, the critical pressure of hydrogen, 13,3 bar, is exceeded. However, the fluid does not become supercritical during the pumping process because the temperature does not reach the criti-

cal value of -240°C. When the pressure of the HP pumps is above the critical value, it is impossible to have a gas-liquid equilibrium. For this reason, extracting boil-off gas out of the pump is not an option. Therefore, all generated heat is sent along with the fluid [126].

Both centrifugal pumps are driven by an electric motor, which is submerged in the LH_2 as well. A power cable from the outside is connected to the motor to deliver the energy. The set-up of the LH_2 pumping process at the terminal is shown in the figure below. As explained, one submerged pump is needed to pump the hydrogen out of the tank. Thereafter, three HP pumps in series are required to pump the LH_2 to the desired pressure of 50 bar.

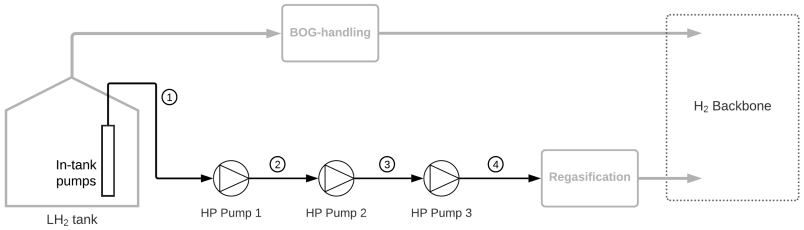

Figure 31: An overview of the pumping process on the terminal

Nikkiso Cryo Inc. delivered data sheets and expected performance curves of the two different type of pumps. The performance curves give insight into the $NPSH_R$, pump efficiency and pressure head for different flow rates. These data can be used to calculate the required power input and also for determining the necessary LH_2 level in the tank. However, since these data are confidential, this study assumes an isentropic efficiency of 67% for both pumps. These efficiencies are in line with the highest efficiencies of the LH_2 pumps. Nonetheless, for actual centrifugal pumps the flow rate influences the efficiency, as is shown in figure 32. For this reason, selecting suitable LH_2 pumps depends on the requires send-out capacity of the terminal as well.

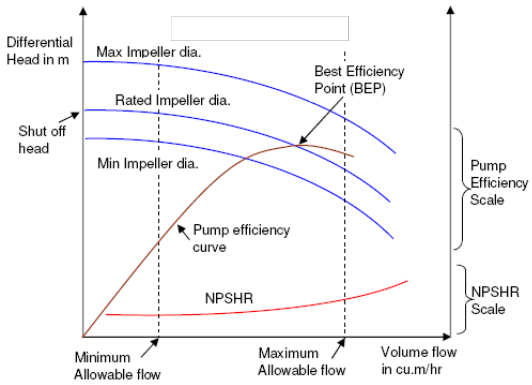

Figure 32: Example of a performance curve of a centrifugal pump [131]

7.5 Pump calculations

The formula used to calculate the power of the pump is shown in equation 8 [132]. In this way, the electrical power required by the electric motor of the pump is calculated, neglecting the mechanical losses. As mentioned above, the isentropic efficiency for both LH_2 pumps is defined at 67%.

$$P_{pump} = \frac{\dot{V} * H * SG}{367,46 * \eta} \qquad [kW] \tag{8}$$

P_{pump}	Power input pump [kW]
$\dot{V}$	Flow rate [m^3/h]
H	Differential head [m]
η	Isentropic pump efficiency (less than 1)
SG	Specific gravity [-]

With the value for the $NPSH_R$ of the submerged pump, it is possible to determine the minimum LH_2 level in the tank before cavitation occurs during pumping. Furthermore, it is ensured that the margin between the $NPSH_A$ and the $NPSH_R$ for all pumps complies with the standard specified in ANSI/HI 9.6.1 [129].

8 BOG processing

When processing cryogenic liquids such as LH_2, boil-off gas (BOG) formation will always occur [100]. The BOG has to be removed to prevent pressure increase inside the system and because BOG could damage the process equipment [100]. Handling the BOG has a major impact on energy consumption and the safe operation of the terminal [96]. How to process the BOG is defined in this chapter. At first, the BOG formation of the different processes is determined. Subsequently, insight is provided into the hydrogen-BOG compression by defining the complexity and the equipment for the process. After that, other methods to handle the BOG are explained. And finally, a selection is made of various BOG processing solutions, which will be analysed within this research.

8.1 BOG formation

Hydrogen in the liquid phase is obviously below its boiling point, just like every liquid. Because the boiling point of hydrogen is extremely low, it is difficult to maintain these temperatures at all time. When the temperature is above the boiling point, the LH_2 will evaporate and lead to BOG. Several sources at the receiving terminal result in BOG generation [100], [133]. As discussed in the previous chapters, external heat leakage into the storage tanks and the procedures for unloading tankers at the terminal are processes generating BOG. Also, heat entering the pipelines is a source producing BOG. In addition, the process equipment must be kept cold even when not in use in order to prevent the material from contracting and expanding due to temperature changes. Most LNG terminals use an LNG recirculation line from the tank to cool the equipment and pipes. Finally, the recirculated LNG is flashed into the tank resulting in significant BOG [133].

An in-depth look is given at the different BOG sources. Considering the terminal, the effect of each source is described, and the BOG calculation method is determined. First, however, the physical and chemical properties of LH_2 that influence BOG formation are discussed. Due to the extremely low temperature of LH_2, there is a significant temperature difference with its surrounding. This large temperature difference results in more heat transfer assuming similar insulation [134]. As discussed in chapter 3, the enthalpy of evaporation of LH_2 is significantly smaller than for LNG, namely 31,4 kJ/L and 226 kJ/L, respectively [19]. Hence, a minor heat ingress can already lead to a considerable BOG formation. Altogether, hydrogen BOG occurs more easily than when processing LNG. As BOG is unwanted, enhanced insulation measurements are desired.

The BOG generation inside the tank is already explained in chapter 6. With equation 9, the boil-off rate (BOR) of the tank can be determined in percentage volume per day [135].

$$BOR = \frac{Q * 24 * 3600 * 10^{-3}}{V * \rho * H_{vap}} * 100 \qquad \left[\frac{\%}{day}\right] \tag{9}$$

Where ρ is the density of the stored liquid, $Hvap$ is the enthalpy of evaporation per mass, and V is the volume of the tank. Q is the heat flow into the tank, which is influenced by the insulation degree of the tank. As can be concluded from the formula, a smaller enthalpy of evaporation causes more BOG.

During pumping, electrical power is converted into kinetic energy by increasing the velocity or pressure of the fluid leaving the pump. Some of the energy is lost due to pump deficiency, which creates heat and could result in BOG generation. However, as explained in section 7.4, the HP pumps operate in the critical pressure regime of hydrogen. Therefore, BOG generation is impossible for these pumps, so the heat will be sent along with the fluid [126]. Since the HP pumps are used for the regasification process, it is possible to send the heat along with the liquid because it evaporates anyway. Nevertheless, in case pumps are used to transport LH_2 from the ship to the LH_2 tank, during unloading, the generated heat has to be removed, which results in significant BOG production [95]. As stated in section 5.3, all energy used for the LH_2 ship pumps is completely converted into heat.

In the pipelines, some BOG formation is possible. As the LH_2 pipes are vacuum insulated, the heat flux is low [102]. For this reason, the heat will be sent along with the fluid when a flow is going through the pipes. For the send-out pipes, it can be assumed that the heat ingress will not lead to BOG formation at the terminal since the slightly heated LH_2 will be evaporated anyway. However, for the unloading pipes, the heat ingress will lead to BOG formation because the LH_2 from these pipes is transported to the storage tank. As discussed in chapter 5, this heat is removed by BOG generation in the tank. If there is no flow through the pipes, the generated BOG can be removed since the pipes are slightly inclined. To estimate the BOG generation in pipes, equation 10 is used [136].

$$\dot{m}_{piping} = 3600 \frac{k_p * A_p}{H_{vap}} \quad \left[\frac{kg}{h}\right] \tag{10}$$

$\dot{m}_{piping}$	Piping generated BOG [kg/h]
k_p	Average heat flux [kW/m^2]
A_p	Piping surface area [m^2]
H_{vap}	Enthalpy of evaporation per mass [kJ/kg]

Furthermore, the BOG generated while filling the storage tank by unloading maritime vessels is discussed in chapter 5. This process leads to a peak in the BOG formation [137]. So when designing the terminal, it should definitely be taken into account. During normal send-out operations, when no unloading is taking place, the BOG is mainly formed due to heat leakage to the storage tanks and the unloading pipelines. The generated BOG at the terminal is defined in section 12.1. Since the terminal is assuming a baseload send-out, the (peak) BOG can be delivered to the grid.

8.2 H_2 BOG compressor process

8.2.1 Complexity

The hydrogen compressor at the receiving terminal is employed to compress the hydrogen boil-off gas. Since it is boil-off gas, the temperature of the hydrogen gas, which must be compressed, is very low. The low temperature has several consequences for the H_2 compressor, such as material selection and insulation requirements [27]. Another factor is the hydrogen density at these low temperatures. The density of hydrogen BOG will be relatively high compared to hydrogen at ambient temperatures, which is beneficial for the required power of the compressor. However, at these low temperatures, the density changes significantly with a slight temperature change, as shown in figure 33. This phenomenon complicates H_2 compression at these low temperatures [138].

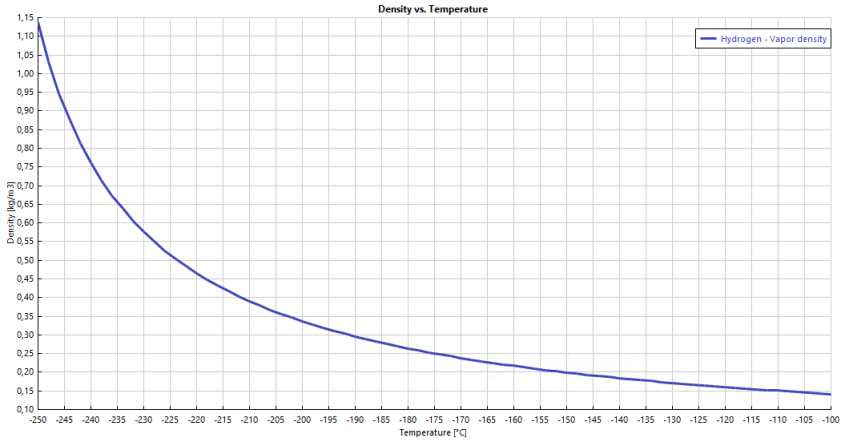

Figure 33: Hydrogen vapor: Density vs. Temperature @ 1,01325 bar. Computed with Aspen plus, using REFPROP [139].

The rapidly changing density at low temperatures influences the design and calculations of the compressor process. For example, if hydrogen enters the compressor at -252°C instead of -250°C, the density is, respectively, 1,27 kg/m^3 and 1,14 kg/m^3. This implies a difference of more than 10% in volume flow, considering the same mass flow. For this reason, it is essential to precisely determine the temperature of the hydrogen BOG entering the compressor. Furthermore, this changing density also has an influence on the compressor process itself. This is because during compression, the temperature of the gas increases inside the cylinders or impellers of the compressor. Determining how much the temperature rises during compression is an important value to define, but this is complicated [138]. Therefore, the behaviour of the hydrogen gas during compression at these low temperatures is difficult to predict [138].

In addition, some unique problems arise in hydrogen compression because of its properties. One of them is that hydrogen easily migrates through small spaces because it is the lightest gas of all gases, and it has a lower viscosity than NG [23]. For that reason, special seals and tolerance standards need to be established for the compressor [23]. Another issue that arises is hydrogen embrittlement, which occurs at elevated pressure and temperature [23]. However, the temperature of the hydrogen BOG that will be compressed is very low, so for the material selection, some additional studies have to be done on this topic. Altogether, hydrogen (BOG) is seen as a difficult gas to compress due to its physical properties.

This fact is also reflected in the relatively high work required for compression at ambient temperatures, as is shown in figure 34 [140]. This is mainly due to the lower density of hydrogen. Since hydrogen BOG density is considerably higher, the energy consumption for BOG compression will -luckily- be less.

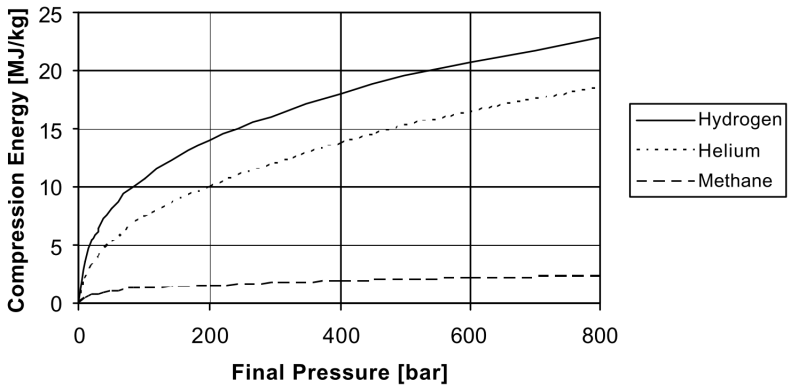

Figure 34: Adiabatic compression work for methane, helium and hydrogen [24].

8.2.2 Compressor equipment

Hydrogen compression is a hot topic, as it is one of the most critical issues for the hydrogen industry [141]. It is widely accepted that there is a strong desire for changes in efficiency, reliability and durability of H_2 compressors and cost savings. For this reason, a lot of research is done into different types of hydrogen compressors [140], [142], [143]. However, most of it is done for hydrogen gas transport through pipelines instead of BOG compressors. For gas transport through pipelines, two types of compressors can be distinguished: a centrifugal and a multiple-stage reciprocating compressor [56]. These compressors are both capable of reaching high throughput and the required moderate compression ratio, which is also desired for the BOG compressors [17].

Nevertheless, the centrifugal compressors for hydrogen transport through pipelines are not yet employed because hydrogen is the lightest gas of all gases [23]. The small molar weight influences the necessary rotational speed of the compressor. To reach the same compression ratio as an NG compressor, the rotational speed of the hydrogen compressor have to be 1,74 times larger [57], [144]. The materials of the NG compressors are not capable of reaching this rotational speed because the stress inside the rotating material becomes too

high, which eventually results in fractures to the rotor [27], [145]. A lot of material research is done to select the correct material to compress hydrogen with a centrifugal compressor, but they are not yet commercially operational.

On the other hand, the multi-stage reciprocating compressor is already employed for hydrogen gas transport through pipelines. That is possible because, for this type of compressor, the working gas is of no importance [57]. However, the side effect is the compressor's poor reliability because it uses piston heads for compression [17]. The linear movement of the components causes the components to wear (e.g. valves, rider bands, piston rings) [23]. Therefore, a lot of maintenance is required resulting in much downtime. To overcome downtime and make sure the boil-off gas can always be compressed, spare installations are necessary [68]. In short, the multi-stage reciprocating compressor is operational, but they require high maintenance and capital cost. Nevertheless, this type of compressor is currently used at the LNG-PS and at many LNG terminals to process the boil-off gas [146].

8.2.3 Selected compressors

In the literature, no information was found on hydrogen BOG compression, considering the capacity of the LH_2 terminal. Therefore, two renowned cryogenic compressor manufacturers have been approached to determine the possibility of compressing hydrogen at extremely low temperatures. Disappointingly, both companies are currently unable to compress hydrogen at temperatures below -170°C [138], [147]. This temperature limit is due to the fact that their equipment is designed for LNG applications. The materials used in the compressor are not tested at lower temperatures [138]. Extensive research is needed to determine whether hydrogen compression at lower temperatures is possible with regard to material selection and the hydrogen density problem previously explained [138].

For hydrogen compression at -170°C, the company Burckhardt Compression was able to design compressors suited for the proposed LH_2 terminal in this report. The BOG is compressed to the desired pressure of the grid, with two types of reciprocating compressors in series. The first low-pressure compressor is a two-stage vertical labyrinth compressor design, illustrated in figure 35. This type of compressor is suitable for operation at cryogenic temperatures, as it does not require any seals or lubrication [148]. The maximum pressure increase of the first pump is around 8 bar, with a maximum capacity of about 1700 kg/h [147].

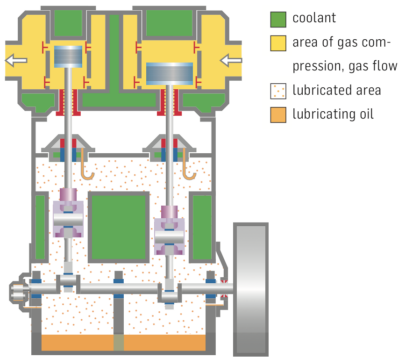

Figure 35: A schematic illustration of the labyrinth compressor [148]

The discharge pressure of the labyrinth compressor is around -50°C, depending on the pressure ratio. Thus, the temperature of hydrogen entering the second compressor does not cause any problem with regard to lubrication and seal limitation. The design of the HP-compressor is a Comprehensive API 618 type of compressor [149]. This compressor is capable of increasing the pressure up to 60 bar in three stages. The volume flow capacity is significantly larger, so one compressor of this type will be sufficient to handle all BOG. With special

adjustments of the cylinder valves during compression, the flow capacity of the compressor can be regulated [150]. Furthermore, intermitted cooling with air is added between the stages to increase the efficiency of the compressor.

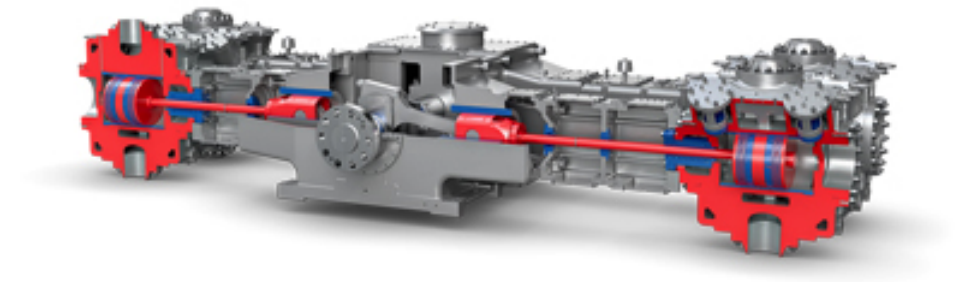

Figure 36: A schematic illustration of the comprehensive HP compressor [149].

The compressors designed by Burckhardt are used in the simulation of the terminal. However, it is also important to investigate the benefits of using hydrogen BOG compressors that can handle extremely low temperatures because compression at lower temperatures results in a higher energy efficiency of the process. In addition, when compressing at extremely low temperatures, the BOG can potentially be recondensed. Both factors could significantly increase the efficiency of the send-out process of the terminal.

The hydrogen BOG compressors that can handle extremely low temperatures are referred to in this report as “cold” compressors. Since these compressors are not yet available, assumptions for efficiency have to be made. The low- as well as the high-pressure compressor operate at cryogenic temperatures. Therefore, a vertical labyrinth type compressor is required. For both cold compressors (LP and HP), an isentropic efficiency is assumed that is comparable to the efficiency of the labyrinth compressor designed by Burckhardt.

8.3 Different ways of BOG processing

Conventional LNG terminals supply the BOG directly to the grid with compressors. However, as compression is an energy consuming process and requires more work than pumping a liquid [95], different options might be preferable. Nowadays, most LNG terminals use a BOG recondenser to improve the efficiency of the BOG handling process [151]. In this section, three solutions for processing the hydrogen BOG are briefly described. More information can be found in Appendix F.

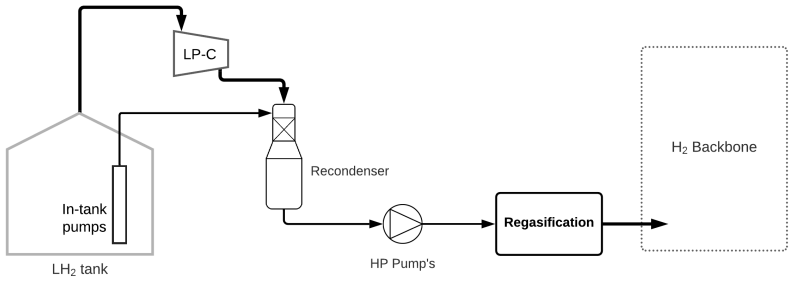

Figure 37: Process flow diagram of the BOG recondenser process.

The first solution to process hydrogen BOG in a more efficient way is by employing a recondenser. As illustrated in the figure above, the BOG flow and the LH_2 flow are compressed with a small amount before both streams enter the recondenser. This pressure increase is necessary to create subcooled LH_2; most recondensers operate between 6 and 10 barg [152]. The subcooled LH_2 is brought in contact with the BOG, and liquefies the BOG. Depending on the temperature and pressure of both streams, a ratio between those streams can be determined in order to have a total liquid stream leaving the condenser. The liquid stream leaving the BOG condenser can then be processed as a liquid stream, as is shown in figure 37. The benefit of handling the BOG flow in this manner is that hydrogen compression is minimized. For an LNG terminal, it is estimated that processing of BOG with a recondenser instead of an HP compressor results in a 30-60% more energy efficient process [96].

As mentioned earlier, employing a recondenser is only an option when hydrogen compression at extremely low temperatures is possible (around -250°C). With the currently available hydrogen compressors operating at -170°C, the outlet temperature of the LP-compressor is too high. The BOG outlet temperature, in that case, is already at -50°C with a six bar pressure increase [147]. Another disadvantage is the fact that the recondenser requires an LH_2 flow; otherwise, recondensing is not possible. For this reason, most BOG recondensers are applied at terminals with a continuous send-out to the grid [152].

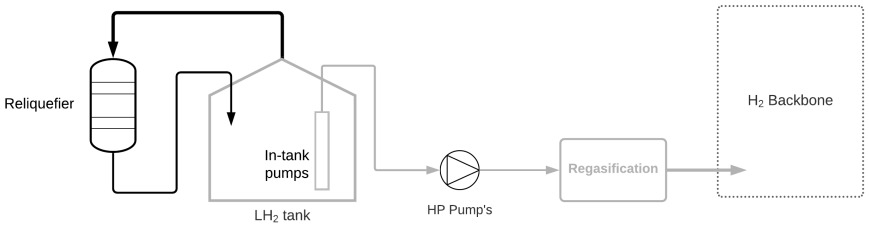

Figure 38: Process flow diagram of the actively reliquefaction process of the BOG.

Actively reliquefy the generated hydrogen BOG. The benefit of handling the BOG in this way is that the terminal is capable of having no send-out to the grid. Furthermore, the hydrogen BOG is already extremely

cold and in the high para-concentration. Therefore, reliquefaction consumes significantly less energy than the liquefaction process. Nevertheless, the energy input to reliquefy is still significant. According to Lee et al., an energy input of around 9,6% of the LHV of hydrogen is required [110]. Another disadvantage is the additional equipment and extra Helium cycle needed for processing the BOG flow in this way.

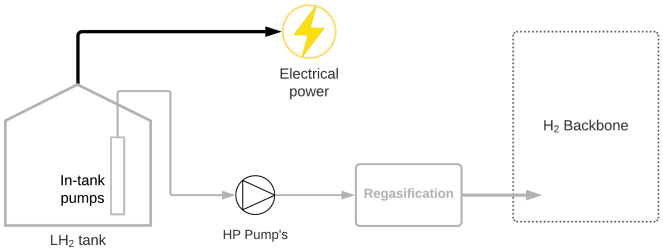

Figure 39: Process flow diagram of the Electrical utilization process of the hydrogen BOG.

The utilisation of the boil-off gas into electricity can be done in two ways, using a fuel cell or a hydrogen gas turbine. The gas turbines are not yet capable of operating at 100% hydrogen input. Therefore the combustion fuel has to be mixed, for example in a mix of hydrogen, with natural gas; however, this will lead to CO_2 emission. A lot of research is done to overcome these problems by multiple companies. For example, Mitsubishi aims to achieve this 100% hydrogen combustion technology by 2025 [153], and Siemens in 2023 [154].

The efficiency and the power produced by a fuel cell depend on several factors, including the fuel cell type, size, temperature at which it operates, the pressure at which gases are supplied and if pure oxygen or air is used [155]. Therefore, the hydrogen BOG must be processed before entering a fuel cell. An example of the hydrogen boil-off utilisation into electricity with the use of a fuel cell and a heat recovery system is done by Marandi et al., which is shown in Appendix F.5. Marandi et al. analysed a system with a PEM fuel cell and two Organic Rankine Cycles operating as heat recovery system [156]. The total energy efficiency of the BOG utilization is defined at 58% [156]. More details regarding this cycle can be found in Appendix F.5. The downside of such a system is the additional equipment and processes needed at the terminal, which require extra space at the terminal site as well as a significant investment cost. Instead, just using a fuel cell is likely to be more cost-efficient.

8.4 BOG Handling options

As discussed in the previous section, many solutions are possible to handle the hydrogen BOG flow. In this report, a selection of three types of BOG handling are discussed: . Normal BOG handling, Cold BOG handling, and BOG recondenser process. Normal BOG handling processes the hydrogen BOG with the compressors designed by Burckhardt, as discussed in section 8.2.3. The LP-compressors operates from -170°C; therefore, the process requires a HEX in front of the compressor. For Cold BOG handling, it is assumed that compressors are capable of handling BOG at any temperature. So no additional heat transfer is needed before the BOG enters the LP compressor. For this process, a HEX is required after the compression process. Lastly, the BOG recondenser process will be analysed, as discussed in the previous section. Since a continuous send-out is considered at the terminal, a recondenser process is promising. Process flow diagrams of the different BOG handling options are showed in Appendix F.

These three options have selected because, in this way, the benefit of compression at extremely low temperatures can be defined. This result is of interest for a future LH_2 terminal and could encourage compressor manufacturers to develop H_2 BOG compressors.

8.5 Calculation method

In order to analyse the most suitable BOG processing method, it is necessary to define the energy consumption of the different techniques. To do so, the required power for the compressors and pumps must be determined. The desired BOG/LH_2 ratio of the recondenser is an essential value for these calculations.

The calculations for the pumps is already defined in section 7.5. For the pumps, performance curves are used to determine the power. For the designed compressors by Burckhardt, operating conditions regarding the inlet and outlet flows are given for the different cylinder stages. In addition, the shaft power for these stages is provided.

With the inlet and outlet conditions of the cylinders, the isentropic efficiency can be calculated with equation 11 [157]. As mentioned before, it is assumed that the isentropic efficiency for the "cold" compressors operating at extremely low temperatures is similar to the efficiency of the Labyrinth compressor designed by Burckhardt.

$$\eta_{is} = T_s[(P_d/P_s)^{(k-1)/k} - 1]/(T_d - T_s) \quad [\%] \tag{11}$$

Where η_{is} is the isentropic efficiency, the subscripts s and d respectively represent the suction and discharge flows of the compressor (or cylinder), with P equal to the pressure and T is the temperature in °R (Rankine). Lastly, k is the ratio of the specific heats (Cp/Cv).

As the isentropic efficiency of the compressors is known, it is possible to determine the power, which can be calculated with the following equations [68]:

$$\eta_{is} = \frac{\Delta h_s}{\Delta h_{tot}} = \frac{h_{4s} - h_1}{h_4 - h_1} \quad [\%] \tag{12}$$

$$P_{comp} = \dot{m} * (h_4 - h_1) \quad [kW] \tag{13}$$

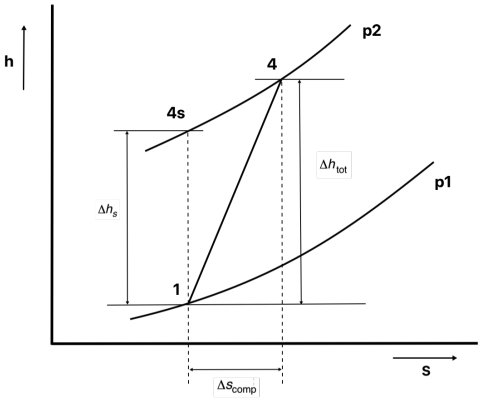

Figure 40: Enthalpy-entropy graph of compression

Where Δh_s is the enthalpy change of the isentropic compression, i.e. compression without losses. The Δh_{tot} is the enthalpy change of the real compression with losses, as is shown in figure 40

To determine the required BOG/LH_2 ratio of the recondenser to ensure that the outlet flow is completely in the liquid phase, the following equation is used:

$$[c * h_{BOG} + (1 - c) * h_{LH_2}] < (h_{sat} - z) \quad \left[\frac{kJ}{kg}\right] \tag{14}$$

$$c = \frac{\dot{m_{BOG}}}{\dot{m_{BOG}} + \dot{m_{LH_2}}} * 100 \quad [\%] \tag{15}$$

where h is equal to the specific enthalpy, with subscripts BOG and LH_2 referring to the inlet flows, and subscripts sat describes the saturated liquid enthalpy of hydrogen. c represents the percentage BOG mass flow into the condenser, and z is a correction factor. This correction factor z is needed because a liquid that is exactly at its saturation point has no available NPSH [124]. Since the HP pump requires some $NPSH_A$ to be able to pump the liquid, the enthalpy value of the outlet LH_2 flow must be below the h_{sat} value. This value can be calculated as the $NPSH_R$ of the HP pump is known.

9 LH_2 regasification process

Besides utilizing pumps and compressors to reach the desired pressure, a heat exchanger (HEX) is employed to increase the temperature of hydrogen to meet the Backbone requirements. As stated before in chapter 4, the minimum temperature of the hydrogen supplied to the grid must be 5°C.

In this chapter, the LH_2 regasification process is analysed by first comparing the process with LNG and defining conventional techniques used for the LNG regasification process. Then the para- to ortho-hydrogen conversion is discussed. The regasification equipment for LH_2 application is defined. Finally, the calculation methods are explained.

9.1 Comparisons with regasification of LNG

The regasification process is typical for the LNG industry. However, that is not yet the case for LH_2 regasification, but they appear to have many similarities [61]. The main difference between the LNG and LH_2 evaporation process is the lower temperature of LH_2. The temperature of LH_2 entering the HEX is around 90 degrees lower than for the LNG case. Therefore, the temperature increase during the process is bigger. This also affects the enthalpy difference, so more heat transfer is needed during the LH_2 evaporation process [158]. Furthermore, the material must be capable of handling the lower temperatures. The material cannot become brittle and must be able to withstand a larger temperature gradient [22]. Another difference is the expansion ratio. For hydrogen, this ratio is almost 850 as compared to the expansion ratio around 600 of natural gas [39].

Multiple regasification technologies are available for LNG application. Since the LNG regasification is a similar process to the LH_2, these technologies are analysed. Regarding the location of the LNG-PS, the two most conventional methods are either a "combustion heat vaporizer" or an "open rack vaporizer" (ORV) [25]. There are also technologies with ambient air as a heat source, but in the Netherlands, where it can be cold, it is not suitable [25].Moreover, using air as the heat source is not an option since liquid oxygen formation can occur, which is hazardous [159].

Currently, at the LNG-PS, a combustion heat vaporizer is employed. This technology, as its name suggests, uses heat from LNG combustion for heat transfer. As shown in figure 42, a hot water bath heated by the submerged combustion burner vaporizes the LNG in the submerged tube bundle [160]. The emitted exhaust gasses of the burner are fed into the water bath to increase the heat transfer by creating some flow and extra heat [25]. This type of vaporizer is used at the LNG-PS because it can rapidly fluctuate the evaporation process, which is desired for the current purpose of the Peakshaver [22]. However, a drawback of this process is that it partly consumes the gaseous product for heat transfer, resulting in relatively low efficiency. For LNG application, it consumes approximately 1,5 – 2% of the LHV of LNG [25]. Reusing the current combustion heat vaporizer for the LH_2 regasification process is impossible, as explained before in chapter 3.

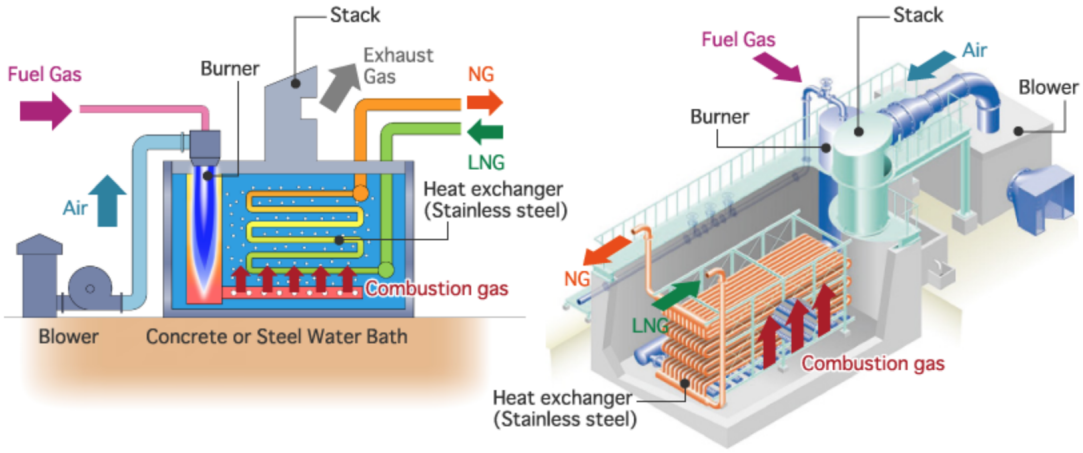

Figure 41: Principle of a heat combustion vaporizer [160].

The other common technology for the LNG regasification process is the Open Rack Vaporizer, where seawater instead of combustion heat is used as the heat source. In the Open Rack Vaporizer, seawater flows on the surface of panels with many heat exchanger tubes to vaporize the internal LNG, as is shown in figure 42 [25]. The advantage of this method is the higher efficiency, as it does not consume the gaseous product also resulting in lower operational costs. Furthermore, this type of equipment is easy to operate and maintain [160]. For this reason, it is the most used heat exchanger for LNG evaporation worldwide; as many as 95% of the LNG terminals utilize this technology [25].

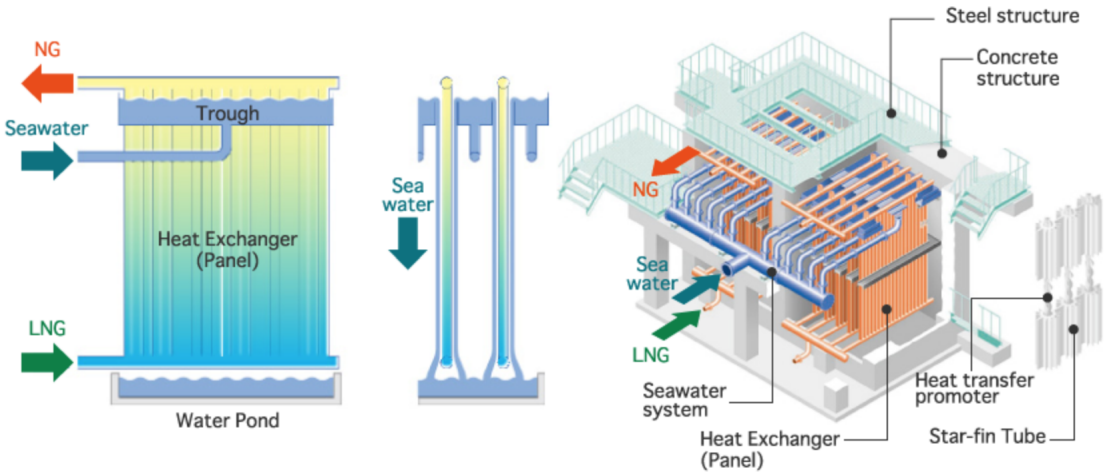

Figure 42: Principle of an Open Rack Vaporizer with seawater as heat source [160].

A disadvantage of the ORV is the ice formation of seawater at the outside of the tubes, which causes a lower thermal conductivity. The lower part of the tubes is subjected to ice formation, as this is the location where the cryogenic fluid enters the vaporizer. To minimize the ice formation, the Super-ORV has been designed, which has a double pipe structure at the lower part of the tubes, as can be seen in figure 43. Due to the enhanced heat transfer, the regasification capacity per heat transfer tube is three times higher than the conventional design [161]. Furthermore, this regasification process requires less seawater. Importantly, utilizing seawater at a temperature as low as 2°C is possible for LNG evaporation [162], [163]. For the LH_2 regasification process, the use of this design is promising as temperatures are even lower than LNG, meaning ice formation is a bigger concern, which is avoided when using the Super ORV. Besides limiting the ice formation, the temperature

gradient within the material of the tubes will be lower. For these reasons, employing a Super-ORV is the desired ORV for LH_2 application.

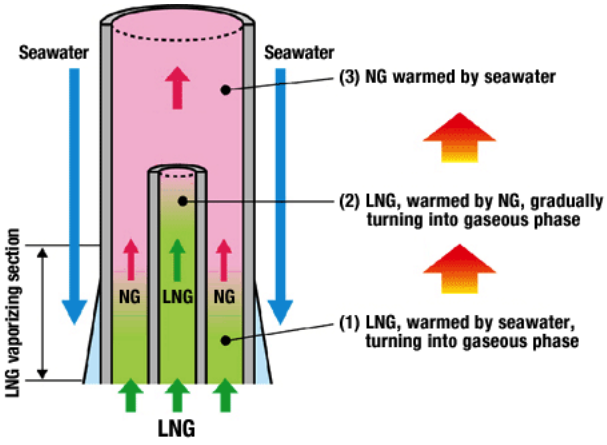

Figure 43: Tube design of the Super-ORV [161]

9.2 Para – ortho conversion during regasification

As described in section 3.2, the para to ortho conversion does not occur during the regasification process without adding a catalyst [61]. If no catalyst is added, a high concentration para-hydrogen, at least 98%, is delivered to the hydrogen grid. As explained in section 3.2, supplying the para-hydrogen instead of "normal" hydrogen to the grid has its advantages and disadvantages. In this section, a trade-off is made to determine if utilizing a catalyst during evaporation is desired. First, the pros and cons defined in section 3.2 are summed up. After that, these points are analysed to determine a solution.

The advantages and disadvantages of supplying para-hydrogen to the grid and not accommodating the para to ortho conversion during regasification are the following:

+ The regasification process is less complicated as no catalytic reaction is required.
+ The energy consumption is lower because no endothermic conversion reaction takes place.
− The temperature of hydrogen gas in the grid can potentially drop below 0°C. Since the endothermic conversion absorbs heat from the surrounding, the temperature of the hydrogen gas will decrease.
− The supplied energy content to the hydrogen grid is slightly lower. This is because the energy state of the para-hydrogen is lower than that of the ortho-hydrogen.

9.2.1 Temperature drop issue

The main reason to add a catalyst during the hydrogen liquefaction process is to prevent the exothermic conversion reaction from happening inside the LH_2 storage tank. Because the heat released by the exothermic conversion could, in the worst-case, lead to 65% of the LH_2 volume to evaporate [59]. However, the question is whether the heat absorbed by the endothermic para to ortho conversion resulting in the temperature drop is a reason to add a catalyst to the regasification process. The send-out temperature of the hydrogen to the grid is determined at 5°C because the temperature of gases in underground pipes must be above 0°C due to safety regulations [57]. Considering the enthalpy of conversion, 523 kJ/kg, the hydrogen of 5°C could potentially drop to -31,5°C due to the total endothermic conversion. However, this is only possible when no additional heat transfer takes place, which is not the case in the underground H_2 pipelines.

It is determined that the endothermic conversion will not cause the temperature of hydrogen in the grid to drop below 0°C. This is because the heat flux into the pipe is significantly higher than the heat absorbed by the conversion reaction. The maximum heat adsorption over time is deduced from figure 14, which is -0,00122 kJ/s*kg, assuming the conversion rate of para to ortho and ortho to para is equal [62]. This is a relatively small value since the conversion rate is very low [59]. For example, it takes more than three hours to lower the temperature by one degree. The heat flux of an underground natural gas pipe is around 60 W/m^2 [164]. Besides heat entering the pipelines through heat transfer with the soil, also the negative Joule-Thompson coefficient of hydrogen will add some heat. As explained in section 3.1.7, the temperature of hydrogen will rise as the pressure in the grid decreases, which is equal to 0,035°C/bar [57]. Al in all, it can be assumed that the temperature decrease due to the endothermic conversion is not an issue.

9.2.2 Energy supply difference

As explained in section[**?**], para-hydrogen has a negative effect on the energy content of the hydrogen gas. So, if the terminal delivers para-hydrogen to the grid, the energy supply is lower. The maximum difference is 0,37% of the HHV of hydrogen, taking into account the conversion enthalpy (523 kJ/kg) from para-hydrogen (99,8%) to "normal" hydrogen [63]. This difference in energy content seems small, but given the terminal's considerable send-out capacity, it is still a factor to take into account. Looking at the baseload functions, in the worst case the energy content delivered to the grid is 1,8 MW and 4,2 MW lower for a send-out of 490 MW and 1140 MW, respectively.

The maximum energy difference is 0,37% of the HHV of hydrogen. However, over time this difference decreases as the spin isomer composition converts to a higher ortho-hydrogen concentration. For this reason, the time it takes before the end-user consumes the hydrogen, affects the actual difference in energy content. By defining the conversion rate with figure 14, an estimate is made of the difference in energy content over time [62]. Results are detailed in the table below. Note that for the conversion rate, it is assumed that the rate from ortho to para is comparable to para to ortho.

Table 11: Difference in energy content of the para-hydrogen compared to "normal" hydrogen over time.

Time after send-out	**0 h**	**1 h**	**2 h**	**4 h**	**8 h**	**16 h**	**24 h**	**48 h**	**180 h**
Energy difference, % HHV	0,37%	0,37%	0,36%	0,36%	0,35%	0,32%	0,31%	0,26%	0,15%
Enthalpy difference [kJ/kg]	523	518,6	514,3	505,7	490,7	457,9	433,7	370,9	209,2
Lower energy send-out [kW] (for baseloadcase 1, 490 MW)	1809	1797	1780	1751	1697	1585	1502	1282	722
Lower energy send-out [kW] (for baseload case 2, 1140 MW)	4186	4157	4118	4051	3926	3667	3475	2966	1670

It can be concluded from table 11 that the energy content difference of the supplied hydrogen remains more or less the same for a considerable time, which is again a result of the low conversion rate of the spin isomers. Another study determined the half-life of the conversion reaction at 4,87 days, which results in an even slower reaction [165]. As the energy difference remains similar for a significant amount of time, it can be assumed that the para-hydrogen send-out has still a lower energy content when consumed by the end-users. For this reason, adding a catalyst might be a desired addition to the regasification process.

9.2.3 Additional heat required during the regasification process

The heat input required for the LH_2 regasification process at the terminal (at 50 bar, with desired output temperature of 5°C) is equal to 3619 kJ/kg. However, the required heat input increases if a catalyst is added to

ensure the endothermic conversion occurs. The extra heat is equal to the enthalpy of conversion, 523 kJ/kg. So to accommodate the catalytic conversion reaction, the regasification process requires 14,5% additional heat input. Note that since seawater is used as a heat source, the actual energy input is significantly lower.

9.2.4 Catalytic reaction/ reactors

Next to this additionally needed 14,5% heat input; the process equipment and philosophy are also affected by adding a catalyst. The equipment must be able to accommodate the catalytic reaction. Multiple factors can influence the design of the evaporator, such as the catalytic conversion rate and the type of catalyst. The philosophy of the regasification process can also be affected by the catalytic conversion rate. For example, the ability to quickly adapt the terminal's send-out capacity is compromised when the catalytic conversion rate is low. Below different catalytic conversion processes are analysed. However, in the literature, most information can be found about the opposite isomeric conversion (ortho to para) as it is a relevant topic for the liquefaction process. Since most catalytic reactions work in two directions [166], analysing these opposite conversions is still appropriate.

To achieve the conversion, a magnetic field gradient is necessary to allow the spin isomer to flip [167]. The hydrogen molecule itself has a small magnetic moment. However, a stronger magnetic moment will result in a significant increase of the reaction rate. Therefore, a magnetic catalyst is used, which facilitates the magnetic gradient. Metal oxides are suitable catalysts because the oxygen molecule has a large magnetic moment which is about 2000 times that of hydrogen [64].

An example of a commonly used catalyst is Ionex®-Type O-P Catalyst (Fe2O3), with an average price of $100 per kg [165]. This catalyst is used primarily during liquefaction, but it is also implemented for para to ortho conversion [168]. According to the manufacturer, the catalyst will achieve a 46,5% or higher concentration of para hydrogen during the liquefaction process, assuming 25% para-hydrogen is fed to the process [169]. However, before these rates can be achieved, the catalyst must be reactivated for 16 hours with a dry hydrogen flow at 160 °C [169]. Another commercially used catalyst is the OXISORB® catalyst, which consists of chromium(II) oxide (CrO) attached to a silica carrier [170]. To regenerate this catalyst, again a hot flow of dry hydrogen at 200 – 500°C is required [64].

In conceptual and existing hydrogen liquefaction plants, two types of catalytic reactors are used, namely the "Continuous conversion catalyst-packed heat exchangers" and the "Adiabatic batch conversion beds" [171]. During the liquefaction process, multiple reactors are connected in series to reach the desired para concentration [171]. In Germany, a liquefaction plant uses four adiabatic reactors in series to reach a para-hydrogen concentration of 95% [172]. For the para to ortho conversion, which is desired at the LH_2 terminal, it is assumed that similar types of reactors can be used. However, besides the fact that multiple reactors are required, also the pressure drop in the mentioned reactors can be significant [173]. To create a smaller pressure drop in the packed bed reactors, a monolith structure can be used; nevertheless, these structures are costly [173]. If the pressure drop is significant, adding a compressor after the catalytic reactor is necessary to reach the requirements of the grid. Implementing a hydrogen compressor after the regasification process is unwanted because hydrogen compression requires a lot of power [24]. To handle a pressure drop of around 14 bar requires more energy than the energy difference of para and ortho hydrogen. And when using the adiabatic reactor, an additional HEX is needed as the temperature of the hydrogen drops during the endothermic conversion.

9.2.5 Conclusion

Although, the energy content of supplied para-hydrogen to the grid is a bit smaller than "normal" hydrogen, namely 0,44% at worst, accommodating the para to ortho conversion at the terminal seems to be too complicated, costly and energy-consuming to be competitive. It is complex because many additional processes are

necessary, which also affect the terminal's flexibility. A significant number of catalytic reactors is needed to guarantee 100% supply to the grid. And additional heating equipment is needed for the reactivation process of the catalyst. Regarding the energy consumption, some extra energy input is needed for the heat transfer, as the endothermic conversion takes place. However, energy consumption for the para to ortho conversion is a real issue if the catalytic bed reactor has a significant pressure drop. Meaning additional hydrogen compression is required. So as long as there are no requirements for the hydrogen grid, it is assumed that converting the para to ortho hydrogen at the terminal is undesirable.

9.3 Potential LH_2 regasification processes at the terminal

For the regasification process at the proposed LH_2 terminal, a Super-ORV with seawater as the heat source is assumed to be the best option. As explained before, this type of vaporizer is also favourable for LNG terminals as it is easy to operate and maintain. It is possible to quickly adjust the evaporation capacity needed for the flexible send-out of the terminal. Furthermore, the energy consumption is low because only the seawater pumps require power. Lastly, for the lower temperatures of LH_2, the enhanced heat transfer of the Super-ORV design is desired.

Currently, there are no Super-ORV designs capable of LH_2 regasification. This is mainly because the operating temperatures of the ORV are designed for LNG application. As described in chapter 3, the lower temperature of LH_2 entering the vaporizer results in a larger temperature gradient in the material, which could lead to additional stresses in the HEX material. For this reason, a material study has to be carried out to determine which material is suited for the Super-ORV. Currently, aluminium alloys are employed as tube material. A factor of interest is the decreasing thermal conductivity of the aluminium alloy at lower temperatures [174]. However, this is out of the scope of this research. Therefore, it is assumed that the vaporizer's material can withstand the larger temperature gradient and has sufficient thermal conductivity.

When using a Super-ORV heat exchanger, seawater is cooled during the evaporation process. Due to environmental regulations, the seawater temperature should not drop more than 5°, which limits the capacity of the evaporator. However, if seawater is heated before entering the Super-ORV, the temperature drop may be greater.

Instead of cooling seawater there are also options to utilize the cold exergy of the LH_2. The liquefaction process of hydrogen requires around 20% of the HHV of hydrogen [26]. By utilizing the cold exergy during the evaporation process, some of the energy used for liquefaction can be recovered. There are multiple ways to use cold exergy during the evaporation process, which is discussed in chapter 10.

9.4 Calculation

For the LH_2 terminal design, it is important to determine how many Super-ORVs are needed for the different send-out cases. In this section, the calculations for the heat transfer and the assumptions of the Super-ORV are described. Thereafter, the evaporation capacity of one Super-ORV is defined with a corresponding cost estimation.

From data of an LNG ORV, it can be assumed that there is no heat transfer with the surrounding [175]. So, the heat transfer only takes place between the heat source and heat sink: seawater and (liquid) hydrogen respectively. In addition, the Super-ORV is presumed to be an isobaric process. With these assumptions and considering the counter-current design of the Super-ORV, the energy balance of the vaporizer is as follows:

$$\dot{m}_p * (h_2 - h_1) + \dot{m}_s * (h_4 - h_3) = 0 \quad [kW] \tag{16}$$

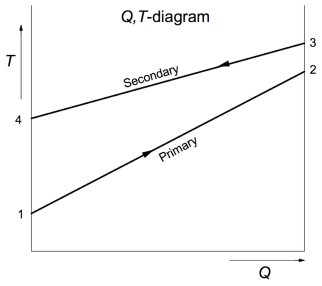

Figure 44: Q,T-diagram of a counter current flow

Where $\dot{m}$ is the mass flow, and the subscript p is the primary flow, in this case the LH_2. The subscript s is the secondary flow, as is shown in figure 44, in this case the seawater. The h is the specific enthalpy with the subscripts used in the same way as shown in figure 44. Therefore subscript 2 refers to the primary flow output and subscript 1 to the primary flow input. Subscripts 3 and 4 are the specific enthalpy of the seawater of respectively the input and output. The energy balance is equal to zero since there is no heat transfer with the surrounding.

The enthalpy difference of the hydrogen flow stays constant due to the fact that the input and output temperatures remain similar. The hydrogen input temperature is around -245°C, and the desired send-out temperature is defined at 5°C. For seawater, the temperature cannot drop more than 5°C due to environmental regulations, as mentioned before. This means that the enthalpy difference of seawater also remains about the same. However, in winter, when the sea temperature is low in the Netherlands, it happens that the temperature drop of 5°C is no longer possible. In that case, the heat transfer decreases resulting in less vaporization capacity of the Super-ORV [163]. On the other hand, when the temperature drop of seawater can exceed 5°C, the evaporation capacity will increase.

The maximum vaporization capacity of one Super-ORV has to be defined to determine the total number of vaporizers necessary for the regasification process. Since there are no Super-ORVs available for LH_2 regasification, an estimate is made using data from LNG equipment. The maximum vaporization capacity for LNG ORV is typically around 300 t-LNG/h (83,3 kg/s), with a maximum seawater mass flow of 7000 t-seawater/h [162], [175]. Assuming the seawater mass flow is similar for the LH_2 Super-ORV, the max vaporization capacity can be determined. As explained above, the seawater temperature drop influences the vaporization capacity. For this reason, different vaporization capacities have been defined for various seawater temperatures drops and flows. The results of the vaporization capacity with corresponding seawater flow and temperature is shown in figure 45. The seawater mass flow ranges from 2500 to 7000 t/h because the ORV has a limitation on the minimum seawater mass flow to ensure sufficient heat transfer [175]. For the LH_2 flow, there are no restrictions on the minimum flow [175].

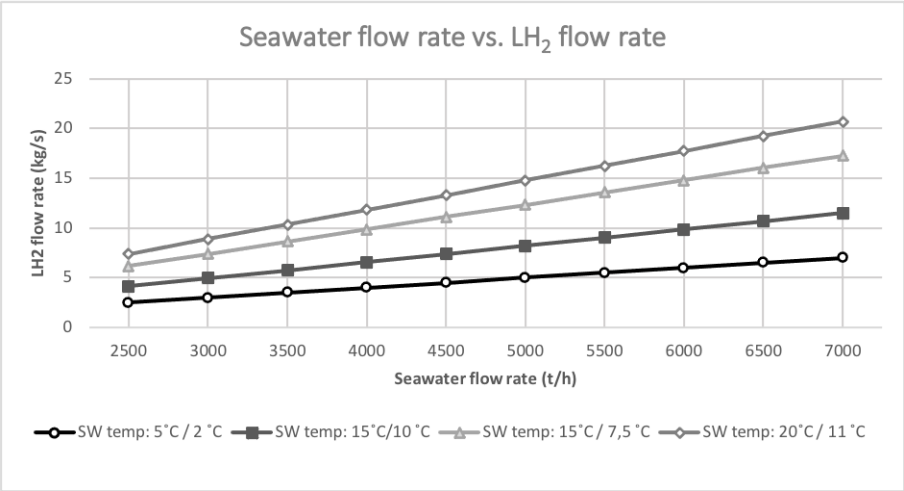

Figure 45: Seawater flow rate vs. LH_2 flow rate, for various seawater in-and outlet temperatures.

From figure 45, it can be concluded that the maximum vaporization capacity of a Super-ORV for LH_2 regasification is significantly smaller compared to LNG. When vaporizing LNG, the maximum vaporization capacity is around 83 kg/s, and for LH_2, it is only 21 kg/s. This is mainly due to the lower temperature of LH_2, resulting in a larger enthalpy difference. Nevertheless, these capacities are sufficient for the requirements of the LH_2 terminal.

In addition, figure 45 shows that the seawater temperature drop of the Super-ORV significantly influences the vaporization capacity, as expected. Therefore using waste heat from nearby plants to heat the seawater flow could be desired, as this provides the opportunity to have a more significant seawater temperature drop in the Super-ORV

The energy input for the vaporization is equal to the energy consumption of the seawater pump. This pump increases the pressure to 3 bar, sufficient to supply the seawater to the Super-ORV. The isentropic efficiency of the pump is assumed to be 0,75%. The required work for the seawater pump can be calculated with equation 17.

$$P_{SW-pump} = \dot{m} * (h_2 - h_1) \quad [kW] \tag{17}$$

10 Cryogenic exergy utilization

During the hydrogen liquefaction process, a lot of energy is consumed to decrease the temperature of hydrogen. This liquefaction process requires around 20% of the HHV of hydrogen [26]. Recovering some of this energy during the regasification process would be beneficial. Nonetheless, the previously described conventional regasification technologies in chapter 9 do not use the cold exergy. In this chapter, the cold exergy of LH_2 is determined and compared with LNG. Furthermore, potential options to utilize the cold exergy are explained, and results are given regarding the most promising power cycles to recover the thermal exergy.

10.1 Exergetic potential

To understand the potential cold energy, the exergy value of a fluid is first explained. Exergy is a thermodynamic value that shows the maximum amount of work that a subsystem can deliver as it approaches thermodynamic equilibrium with its surroundings by a reversible process [176]. Meaning, the exergy of a substance increases in case the thermodynamic state of the substance moves further away from the thermodynamic equilibrium of the surroundings. The exergy content can be divided into several types. However, for cryogenic fluid streams like LNG (and LH_2), only the physical and chemical parts are considered, as is shown in the equation 18 below [177].

$$E = E^{ph} + E^{ch} = \dot{m}(ex^{ph} + ex^{ch}) \quad [MJ] \tag{18}$$

Where $\dot{m}$ is the mass flow, and subscript *ch* and *ph* represent chemical and physical, respectively. The chemical exergy of LNG and LH_2 can be determined with equation 19.

$$ex^{ch} = \xi * LHV \quad [MJ/kg] \tag{19}$$

Where LHV is the lower heating value and ξ is the ratio of chemical exergy to LHV. For LH_2 and LNG, this ratio is respectively 0,985 and 1,06 [178]. Considering the LHV, the chemical exergy for LNG is then equal to 58,9 MJ/kg, and LH_2 equals 118,1 MJ/kg.

The physical exergy can be calculated by equation 20, and as this equation shows, it can be broken down into mechanical and thermal exergy [162]. The mechanical exergy (ex^M) describes the pressure component, and the thermal exergy (ex^T) is related to the low-temperature.

$$ex^{ph} = ex^T + ex^M \quad [MJ/kg] \tag{20}$$

$$ex^T = (h_{T,p_0} - h_{T_0,p_0}) - T_0(s_{T,p_0} - s_{T_0,p_0}) \quad [MJ/kg] \tag{21}$$

$$ex^T = (h_{T_0,p} - h_{T_0,p_0}) - T_0(s_{T_0,p} - s_{T_0,p_0}) \quad [MJ/kg] \tag{22}$$

Where h represent the specific enthalpy and s describes the specific entropy of the flow, subscript 0 represents the reference environment state. As can be deduced from equation 20, a higher regasification pressure gives a higher mechanical exergy value, which results in less thermal exergy available to utilize.

The chemical exergy and all components of the physical exergy are calculated and detailed in table 12. For the calculations, the surrounding conditions are set to 101,325 kPa and 298,15 K. The LH_2 (and LNG) entering the regasification process is defined at 50 bar with the corresponding temperature, assuming the cryogenic pump has a 75% isentropic efficiency.

Table 12: Exergy content of LNG and LH_2, at 50 bar and an isentropic efficiency of 75%. Determined with CoolProp [179] and Matlab [180]

	LH_2		LNG	
Exergy content	Exergy [kJ/kg]	Pct. [%]	Exergy [kJ/kg]	Pct. [%]
Chemical exergy	118.100	91,1	56.816	98,1
Physical exergy	11.536	8.9	1.088	1,9
- Thermal part	6.787	5,2	498,67	0,9
- Mechanical part	4.749	3,7	589,63	1,0

As can be seen, the percentage of physical exergy of LNG is less than 2% of the total exergy. According to Atienza-Márquez, this is one of the main reasons why the low-temperature exergy is rarely recovered during the LNG regasification process [162]. However, the physical exergy potential of LNG is not negligible and can be utilized in various applications. This is the reason why currently more investigation is done regarding this topic [162].

The thermal exergy of LH_2 has a significantly higher percentage than LNG, which can be explained by its much lower temperature. This makes utilizing the low-temperature exergy of LH_2 very promising to be economically competitive and is therefore evaluated in this research.

10.2 Methods to recover the thermal exergy

Conventional LNG regasification methods do not utilize the physical exergy. However, as indicated by Atienza-Márquez, the public opinion about recovering this exergy has changed [162]. This is reflected in the increasing amount of scientific research on this topic, which has increased significantly in the last few years [162]. There are multiple technologies and applications that can utilize the physical exergy. Nonetheless, in this report, only the component of the low-temperature exergy recovery is investigated. For the thermal recovery of LNG, various implementations at different temperature ranges are shown in figure 46. Similar applications are available during the LH_2 regasification process and potentially other options due to the lower temperature of LH_2.

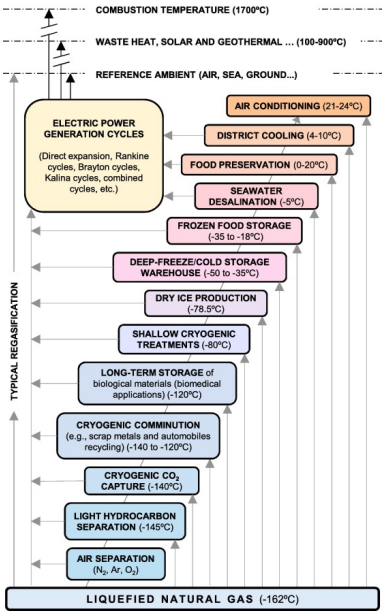

Figure 46: Temperature levels for several applications that can use the cold from LNG-regasification [181].

As can be seen, a large variety of applications are available to utilize the thermal exergy. However, evaluating all possibilities is too extensive for this research and out of scope. Therefore, some boundary conditions have been drawn up:

- Synergy with other plants is not considered.
- Potential hazardous processes are not evaluated.
- Only the thermal exergy of the baseload send-out function is recovered.

Many implementations are possible for synergy with nearby industrial plants, such as refrigeration and cryogenic CO_2 capturing and liquefaction [181]. Furthermore, cryogenic air separation could be very interesting and profitable in the harbour area, as there are a lot of chemical plants. However, determining the needs of other nearby plants is out of the scope of this research. The second boundary condition eliminates cryogenic air separation because the production of liquid oxygen at an LH_2 plant is a dangerous combination [159].

In addition, the send-out rate of the terminal also influences the choice of a suitable application. For the baseload send-out function, the LH_2 flow is constant, and so is the available thermal exergy. But in case the send-out rate of the terminal fluctuates, which happens during the Peakshaver function, the thermal exergy is also a varying value. As shown in figure 47, some techniques require constant send-out, and others can cope with fluctuating conditions [182]. But to exploit the thermal exergy peaks is challenging to accomplish. Taking into account that the Peakshaver function, which operates for a short amount of time delivering significant peaks, it is assumed that the fluctuated send-out rate of the LH_2 terminal is not available for thermal exergy utilization. Therefore, only the thermal exergy recovery of the baseload function is investigated in this research. The regasification process for the Peakshaver send-out will be covered with conventional equipment, which is capable of handling the rapidly changing send-out rates.

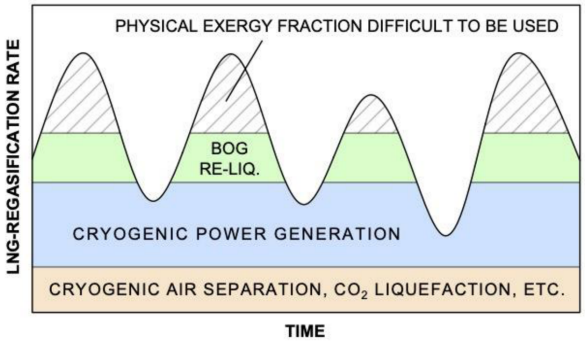

Figure 47: LNG demand variation and available fraction for some applications [162]

Two applications remain suitable for thermal exergy recovery, given the boundary conditions and the fact that only the thermal exergy of the baseload is available. The first one is electrical power production, which can be achieved by various cycles such as a Brayton cycle and Rankine cycle. The second option which will be discussed is liquid nitrogen production. As mentioned in chapter 2, the LIN storage tank at the terminal site remains operational. Currently, the LIN tank is filled by trucks, so producing LIN at the terminal site would be beneficial.

10.3 Cryogenic power generation

The thermal exergy can be converted into electrical power by using the low temperature of LH_2 as a heat sink in a thermodynamic cycle. A thermodynamic cycle can produce electrical power because the pressure increase requires less work than the turbine generates during expansion [97]. This is possible because the

working fluid (of the thermodynamic cycle) is cooled down before compression and heated up before expansion, illustrated in figure 50.

The heat sink can be used for the LNG case in a temperature range of -160°C till -20°C [183]. For LH_2, this heat sink temperature window is even wider as the pumped LH_2 entering the regasification process will be around -245 °C. This very low temperature also results in complexity because there is a risk that the working fluid will crystallize in the condenser. For this reason, only two working fluids are considered to operate in the lowest temperature domain, namely helium and nitrogen (as is shown in figure 48). Helium as a working fluid is selected because its boiling point is even lower than hydrogen, so crystallization cannot be an issue [19]. Nitrogen could potentially crystallize because its freezing point is at -210°C, whereas the LH_2 entering the condenser is around -245°C [19]. However, in a study conducted to determine feasible working fluids for LNG exergy recovery, a maximum temperature difference was defined between the cold flow and the freezing point of the working fluid to avoid crystallization in the condenser [184]. Since the temperature difference of the LH_2 entering the condenser and the freezing point of N2 is within the range defined in this study by Atienza-Márquez et al. [184], it is assumed that crystallization will not be a problem provided the condenser is appropriately designed [185].

In order to recover maximum thermal exergy, two power cycles in series are considered. The first power cycle operates in the lowest temperature regime of the LH_2 heat sink. The second cycle is employed to operate in the intermediate temperature range, as is shown in figure 48. As mentioned, for the first cycle, nitrogen or helium is used. The working fluid for the second power cycle is either methane or ethylene. These last two working fluids have been selected based on the existing knowledge of thermal exergy recovery from LNG, as the intermediate temperature range (T_5 till T_6) is comparable at this stage [162], [186].

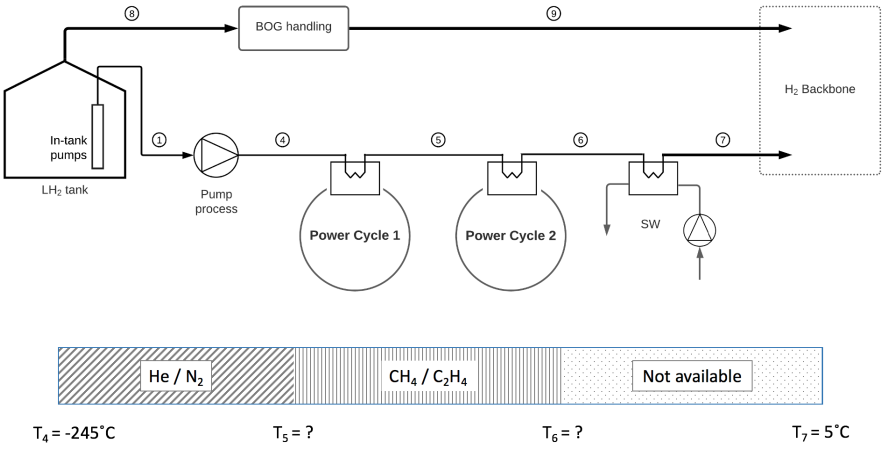

Figure 48: Schematic overview of the two power cycles in series.*cold temperature range (T_4-T_5), intermediate temperature range (T_5-T_6) [162].

The working fluid, methane, is selected because this fluid is most suited to recover the thermal exergy of LNG from -160°C to -130°C, according to Atienza-Márquez [162]. The T-s graph of the proposed methane RC is illustrated in figure 49, which has a higher and lower pressure of 105,3 and 7,5 bar, respectively. The thermal efficiency of this cycle is 30,2% [162]. Another study conducted by Ferreiro García et al., showed that a methane RC could also recover the thermal exergy at a higher temperature window of the thermal exergy of LNG [187]. This is possible because the working fluid operates at higher pressures (191 and 40 bar for the higher and lower pressures, respectively), which results in the opportunity to use the thermal exergy of LNG from -122 till -75°C [187]. However, as can be concluded from figure 49, the higher pressure domain has a negative effect on the thermal efficiency as it is only 20%.

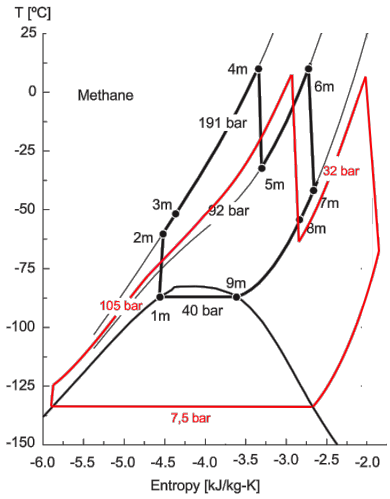

Figure 49: T-s diagrams of the RCs operating with methane. In back the RC proposed by García et al. [187], in red the RC of Atienza-Márquez [162].

Lastly, ethylene has been selected to investigate as a working fluid for the second power cycle. Considering the boiling point of ethylene, it would be possible to utilize a larger temperature window of the hydrogen heat sink. Meaning the temperature of T_6, illustrated in figure 48, could be higher. This is beneficial because, in this way, more thermal exergy of the LH_2 flow is utilized.

Table 13: Thermophysical properties, environmental data and safety group of candidate fluids [184], [188]

Fluid	**Type**	**T_{fr} [°C]**	**NBP [°C]**	**T_c [°C]**	**P_c [kPa]**	**GWP**	**Safety group**
Helium	I.C.	-271,38	-268,93	-267,95	288	-	A1
Nitrogen	I.C.	-210	-195,8	-146,95	3400	-	A1
Methane	I.C.	-182,46	-161,48	-82,59	4599,2	23	A3
Ethylene	HC	-169,16	-103,77	9,2	5041,8	<20	A3

Two different types of thermodynamic power cycles are investigated to recover the thermal exergy, namely a (closed) Brayton-cycle (BC) and a cryogenic Rankine-cycle (RC). The closed BC is required when helium is the working fluid because a BC is suitable for a working fluid that remains in a gaseous state throughout the cycle, which is the case with helium [189]. For the other proposed working fluids, an RC is needed. In the RC, the working fluid is liquified in the condenser, making it possible to use a pump instead of a compressor to increase the pressure [190]. Employing a pump instead of a compressor is preferable, in most cases, as pumping requires relatively less power to increase the pressure, as can be concluded from the corresponding T-s diagrams shown in 50.

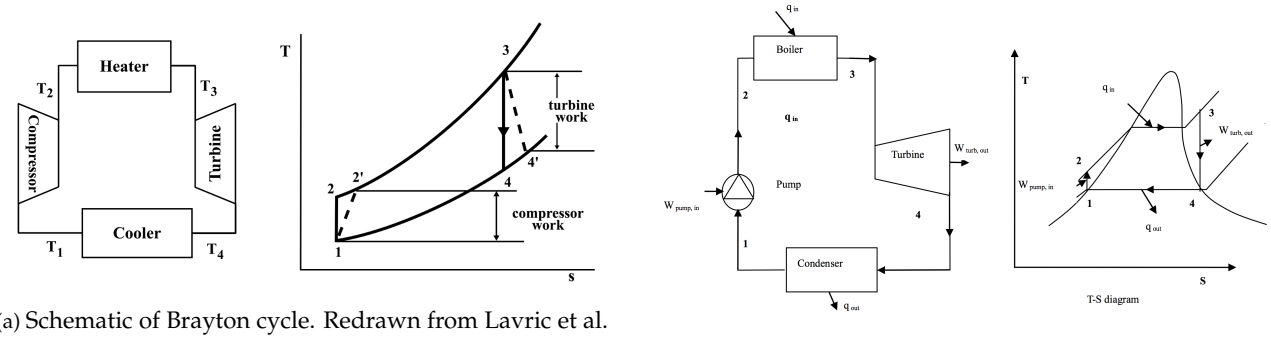

(a) Schematic of Brayton cycle. Redrawn from Lavric et al. [191].

(b) Schematic of Rankine cycle [146].

Figure 50: Schematic overview of the proposed power cycles.

Seawater is selected as a heat source for the proposed power cycles because seawater requires no synergy with other plants. As seawater is at ambient conditions, it is impossible to fully utilize the cold exergy because there must be a temperature difference between the heat source and heat sink—the more significant the temperature difference, the higher the thermal efficiency [97]. Therefore, the cold exergy of LH_2 near ambient conditions is not available to utilize, as shown in figure 48. If the heat source had higher temperatures, it would be possible to convert this part into electrical power as well.

Since seawater is the heat source, working fluids with a relatively high normal boiling point, such as propane, are not eligible because it provides a low thermal efficiency [184]. These working fluids are feasible if the temperature of the heat source would be higher. Also, due to environmental aspects, some working fluids are not suitable to employ, such as R14 [184].

10.4 Liquid nitrogen (LIN) Production

Specifically for this proposed LH_2 terminal, the production of LIN is a valuable addition as the plant must continue to store and use LIN for other purposes. Nowadays, the LIN is delivered by trucks, however, the LIN can also be produced at the terminal site by utilizing the cold exergy of LH_2.

Cryogenic air separation is the most efficient way to produce LIN, but during this process liquid oxygen is also formed [192]. The formation of liquid oxygen at an LH_2 terminal is hazardous, which makes cryogenic air separation an unwanted process. Luckily, there are multiple other air separation technologies available to extract nitrogen from the air, such as adsorption, membrane or chemical processes [193]. These processes produce oxygen-enriched air, but unlike the cryogenic air separation, these processes can take place further away from the hydrogen equipment. In order to prevent oxygen-enriched air from coming into contact with hydrogen equipment, the air separator must be placed at a certain distance. In view of the AIGA 067/10, it has been determined that the terminal has sufficient space to build an air separator on-site (Argent et al., n.d.).

The most common process to extract nitrogen out of the air is pressure swing adsorption (PSA), which is considered in this report as well [193], [194]. The PSA process is illustrated in figure 51 and can generate high purity nitrogen, up to only 1 ppm of oxygen contamination [195]. The generated nitrogen gas can be delivered at 4 till 9 barg [195].

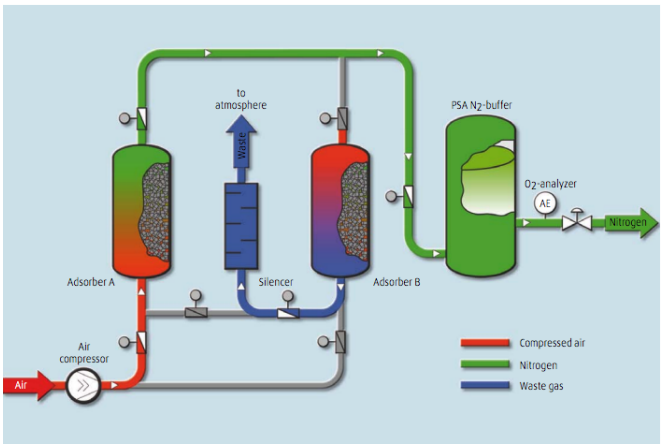

Figure 51: Pressure Swing Adsorption Design for nitrogen generation [195].

After the PSA, the produced nitrogen is fed into a condenser, where the cold exergy of LH_2 is used to liquefy the nitrogen. Because the LIN demand is not constant and the required LIN production is relatively small, there is room for other processes to utilize the thermal exergy of LH_2. So this process can be combined with the power cycles explained before.

10.5 Regasification configuration set-ups

In this section, the configurations of the different power cycles are described with associated assumptions and operating parameters. As is mentioned in section 10.3, it is assumed that two power cycles in series are recovering the thermal exergy. The first power cycle is either a helium BC or a nitrogen RC, as they utilize the lowest temperature range of the LH_2 thermal exergy. The second power cycle, which converts the intermediate temperature of LH_2 into electrical power (T_5 till T_6 of figure 48) is a methane or ethylene RC. The liquid nitrogen production is defined as an extension of the nitrogen RC.

The closed Brayton Cycle, with helium as working fluid, is shown in figure 52. As helium remains gaseous throughout the cycle, a compressor is employed to increase the pressure. Ideally, this compression takes place at very low temperatures [97]. However, similar to hydrogen compression, it is very complicated to compress helium at extremely low temperatures. In literature, the lowest operating temperature for a helium compressor is around -190°C, with a maximum pressure ratio of eight [196]. Therefore, a constraint on the temperature of helium entering the compressor has been defined. This constraint has significant effects on the efficiency of the power cycle and the required mass flow of the working fluid. The hydrogen outlet temperature is specified at -194°C. This temperature is well suited in combination with a second power cycle in series because a significant amount of cold exergy is conserved, and the potential issue of crystallization of the working fluid for the second cycle is eliminated. Two turbines and seawater HEXs are employed to improve the efficiency of the BC.

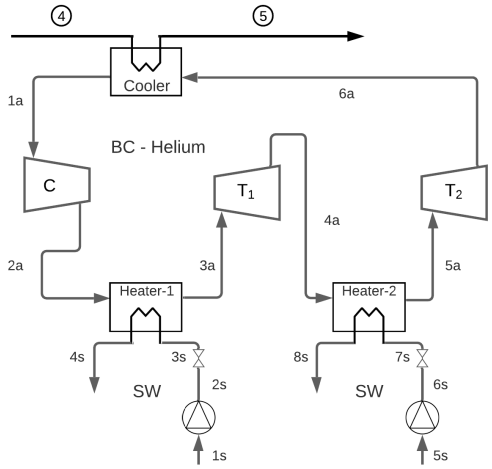

Figure 52: Overview of the proposed configuration of the Brayton cycle, with helium as the working fluid.

Next, the cryogenic Rankine cycles are described. All three RCs have a different working fluid, but the system configuration is similar, which is depicted in figure 53. In the RC, two turbines are employed to expand the working fluid. Besides the higher efficiency of the RC, using two turbines is also necessary to make sure that the working fluid remains in the vapour phase, because during expansion, the temperature of the working fluid decreases significantly. Furthermore, some general constraints are defined for the condenser to ensure condensation occurs without the issue of crystallization. These constraints regarding the condenser are in line with the conditions specified in the study conducted by Atienza-Márquez et al., which investigated feasible working fluids to recover the thermal exergy of LNG [184].

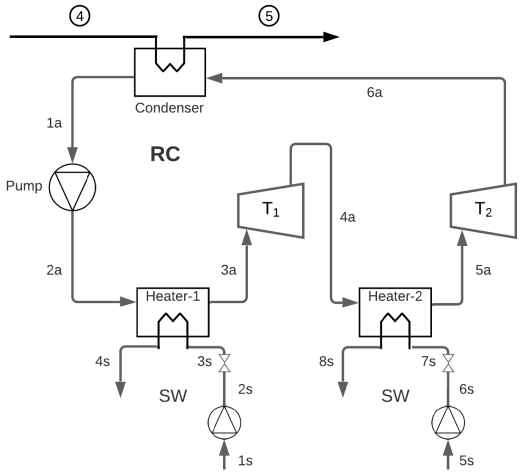

Figure 53: Overview of the proposed configuration of the Rankine cycle, with nitrogen as the working fluid.

- The condensing temperature of the working fluid (1a) has to be at least 5°C lower than the temperature of the hydrogen exiting the condenser (2) in order to ensure condensation in the condenser takes place.
- The temperature difference between the freezing point of the working fluid and the LH_2 exiting the condenser (5) cannot be higher than 35°C to prevent the working fluid from crystallizing in the condenser.

- The critical temperature must be larger than the condensing temperature. Otherwise, condensation is not possible inside the condenser.

Knowing the constraints for the condenser, the nitrogen RC can be discussed. For the nitrogen RC, utilizing the current process equipment of the LNG-PS is possible, such as the liquid nitrogen (LIN) pumps. For this reason, a maximum pressure increase of the LIN pump in the RC is defined at 81 bar, which is similar to the existing LIN pumps. Besides the general RC, also a nitrogen RC with a recuperator heat exchanger has been investigated, as shown in figure 54. This recuperator HEX improves the heat usage within the cycle resulting in higher efficiencies. Furthermore, an enhanced nitrogen RC can produce LIN by attaching a PSA to the cycle. Results of this configuration producing 0,5 kg/s LIN, are presented in Appendix E.2. However, for clarity reasons, it is not further evaluated in this chapter.

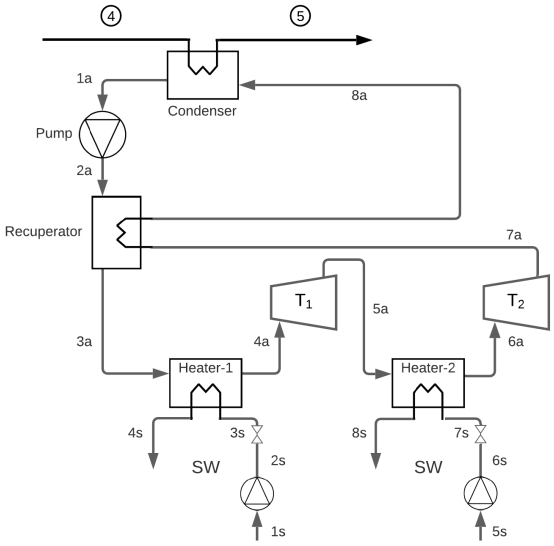

Figure 54: Overview of the proposed configuration of the nitrogen Rankine cycle, with recuperator.

The cycles available to operate as the second power cycle in series are the methane and ethylene RCs. The configuration of these RCs is similar and is shown in figure 53. Like the nitrogen RC, there are also possibilities to reuse current LNG equipment for the methane RC. For this reason, the maximum pressure increase of the methane pump is set at 81 bar.

10.6 Modelling and calculating performance cryogenic power cycles

The power cycles are modelled in order to determine the performance characteristics of those cycles and to define the net power production. The aim of these calculations is to define the most efficient power cycle considering the given constraints. As explained in section 11.1, the calculations are carried out with the simulation software Aspen Plus [197]. The following assumptions have been made in the power cycle models, which is partially derived from the study conducted by Atienza-Márquez et al. [184]:

General

- The process is at steady-state, as only the thermal exergy of the baseload send-out is recovered.
- Potential and kinetic exergy are not taken into account.
- Pressure and thermal losses are neglected.

Cooler/Condenser

- Hydrogen outlet temperature 1st cycle (stream 5), -194°C.
- The working fluid leaving the condenser is assumed to be at a saturated liquid state, meaning the vapour fraction is zero.
- Hydrogen outlet temperature 2nd cycle (stream 6), T_{1a} – 5°C. Meaning the hydrogen outlet temperature is five degrees lower than the boiling point of the working fluid to ensure condensation. (This is also the case for the nitrogen cycle).

SW Heater

- The composition of seawater is assumed as regular water.
- Seawater inlet/outlet temperature is defined at 14°C / 9°C.
- Operating pressure seawater stream, 3 bar.
- Outlet temperature working fluid, 5°C.

Compressor/pump/turbines

- The isentropic efficiency of the compressor, pump and turbine: 78%, 75% and 85%, respectively.
- Minimum inlet temperature helium compressor is set at -190°C.
- Mechanical and electrical losses are not considered.
- The seawater pump increases the pressure up to 6 bar.

Recuperator

- The minimum temperature approach within a recuperator HEX is 15°C.

The heat transfer rate of the heat exchangers of the power cycles is calculated with equation 24, using the energy balance.

$$Q = \dot{m}_i(h_{i,in} - h_{i,out}) = \dot{m}_j(h_{j,out} - h_{j,in}) \qquad [kW] \tag{23}$$

The next step is to determine the energy production of the power cycle. The compressors and pumps consume power, and the turbines generate power. The heat exchangers do not consume energy, besides seawater having to be pumped to the HEX. The additional power for seawater pumping is added in the equations. The equations to determine the net power production of the power cycle are shown below:

$$P_{net} = \sum P_{turbine} - \sum P_{compressor} - \sum P_{pump} \qquad [kW] \tag{24}$$

A general performance characteristic of a power cycle is thermal efficiency. Equation 25 is used to calculate this value.

$$\eta_{th} = \frac{P_{net}}{Q_{in}} \qquad [\%] \tag{25}$$

Q_{in} is equal to the heat transfer in the heat sink, which is the heat transfer of the hydrogen flow to the cycle's working fluid.

In addition to the efficiency parameter, also performance indicators regarding the working fluids are defined. The first indicator is the specific energy produced per tonne regasified LH_2, $P_{net}/\dot{m}_{LH_2}$. The second value of interest is the required mass flow rate of the working fluid, as it gives insight into the size of the power cycle system. For this the following performance value is defined, $\dot{m}_{WF}/P_{net}$.

Another performance indicator of interest is the overall net power production of the cycles in relationship with the hydrogen energy supplied to the grid. As only the baseload send-out is taken into account, the energy supply to the grid is either 490 MW or 1140 MW. This value gives an indication of the energy production compared to the energy send-out to the grid.

$$\eta_{eff} = \frac{P_{net}}{\dot{m}_{H_2} * HHV} \qquad [\%] \tag{26}$$

Above the performances of the individual power cycles are evaluated. However, to define the overall power generation during the regasification process and to give insight into the overall performance of the power cycles, equation 27 is used. The most efficient power cycle configuration can be defined with this value, considering the first and second cycle.

$$P_{net,tot} = P_{net,RC1} + P_{net,RC2} \qquad [kW] \tag{27}$$

The defined performance characteristics are influenced by the system configuration of the power cycle. Especially the pressure ratios of the power cycle have a significant effect on these performance values. Sensitivity studies are carried out with the simulation programme Aspen Plus to determine the most efficient cycle configuration. The results of the most efficient cycles are discussed in the next section.

10.7 Results & discussion - Power cycles

In this section, the results regarding the cryogenic power cycles are presented and discussed. This is done by first evaluating the different power cycles separately. After that, various combinations of the two power cycles in series are defined.

The tables present the results of the power cycle characteristics. These results are detailed for the most efficient cycle set-up obtained with the Aspen Plus optimization software [197]. Besides the cycle characteristics, more information regarding the thermodynamic data and HEXs can be found in the E. The results shown in this section are related to the 490 MW baseload send-out function of the terminal, which has an LH_2 mass flow of 3,46 kg/s. Since the calculated values are in a linear relationship with the send-out capacity, an easy comparison can be made for the other baseload case.

Given the baseload function, the temperature of the pumped LH_2 (50 bar) entering the cooling HEX of the first power cycle is around -245°C. The temperature of the hydrogen stream leaving the cooler depends on the employed power cycle.

The results of the Brayton cycle with helium as the working fluid, are shown in table 14. The thermal efficiency of 21% is relatively low which is mainly due to the minimum temperature limitation of the helium compressor [196]. Another striking value is the ideal pressure rise of the cycle, which is small compared to the other proposed cycles. This is due to the fact that during compression, the temperature of the working fluid increases significantly, which results in the fact that compression consumes more work in later stages. To reach higher pressures, intermittent cooling during the compression stage is recommended. This could potentially also increase the thermal efficiency of the cycle.

Table 14: Results of the helium Brayton cycle, where the LH_2 stream (mass flow 3,46 kg/s) is heated from -245°C to -194°C.

1st cycle - Helium BC	Q_{in}	P_{net}	η_{th}	$P_{net}/\dot{m}_{LH_2}$	$\dot{m}_{WF}/P_{net}$	Seawater	pump/turb1/turb2
Units	[kW]	[kW]	[%]	[kJ/kg]	[kg/MJ]	[kg/s]	[bar]
Helium	2871	604	21,0%	175	7,47	167,28	17/10/4

The Rankine cycle with nitrogen as a working fluid can reach high thermal efficiencies, up to 61,4% for the general RC configuration. And if a recuperator heat exchanger is employed, an even higher thermal efficiency can be achieved, namely 74,8%. Taking into account all performance values, the nitrogen cycle is favourable in every aspect over the helium BC, apart from the seawater consumption.

Table 15: Results of the nitrogen Rankine cycle, where the LH_2 stream (mass flow 3,46 kg/s) is heated from -245°C to -194°C.

1st cycle - Nitrogen RC	Q_{in}	P_{net}	η_{th}	$P_{net}/\dot{m}_{LH_2}$	$\dot{m}_{WF}/P_{net}$	Seawater	pump/turb1/turb2
Units	[kW]	[kW]	[%]	[kJ/kg]	[kg/MJ]	[kg/s]	[bar]
N2 - Rankine cycle	2871	1763	61,4	510	6,29	223	81/32/2
N2 - RC recuperator	2871	2147	74,8	621	6,29	241	81/34/2

The performance of the second power cycles is shown in table 16. As is depicted, methane as a working fluid results in higher thermal efficiency. Nevertheless, the ethylene RC produces more electrical power since it can consume more heat (Q_{in}). This is because the boiling point of ethylene is higher than that of methane, and therefore the temperature of the hydrogen leaving the condenser can be higher. Hydrogen exiting the second condenser is -157,5°C and -101°C for the methane and ethylene Rankine cycle respectively.

Although the net power production for the ethylene RC is considerably larger, it is assumed that the methane RC is the favourable cycle to deploy as the second power cycle at the proposed LH_2 terminal. This is since the equipment to accommodate the methane cycle can be significantly smaller. This can be seen from the working fluid performance value, $\dot{m}_{WF}/P_{net}$, which shows that the methane mass flow can be smaller than the ethylene flow. In addition, the results of the HEXs also prove that a significantly larger amount of equipment is required for the ethylene RC. The results of the HEXs used in the power cycles are shown in Appendix E. The smaller equipment size results in a lower CAPEX, which is desirable.

Table 16: Results of the 2nd power cycle in series. With the LH_2 mass flow equal to 3,46 kg/s.

2nd cycle - RC	Q_{in}	P_{net}	η_{th}	$P_{net}/\dot{m}_{LH_2}$	$\dot{m}_{WF}/P_{net}$	Seawater	pump/turb1/turb2
Units	[kW]	[kW]	[%]	[kJ/kg]	[kg/MJ]	[kg/s]	[bar]
Methane (-194 / -157,7°C)	1628	742	45,6	214	3,85	114	81/32/2
Ethylene (-194 / -101°C)	4155	1077	25,9	311	9,60	233	29/12,9/1,5

The next step is to determine the total net power production of the combined cycles in series. The results of the different combinations are presented in table 17. For the nitrogen RC, the cycle with a recuperator is used. As expected, the highest overall power is generated with the nitrogen and ethylene Rankine cycles in series. Nevertheless, the nitrogen and methane Rankine cycles in series perform also very well, with relatively low CAPEX for the methane cycle, as mentioned above. For this reason, the nitrogen-methane Rankine cycles in series are selected as the most suitable power cycles to recover the cold exergy at the LH_2 terminal.

Table 17: Overall results of the two power cycles employed in series to recover the thermal exergy. With the LH_2 mass flow equal to 3,46 kg/s.

Power-cycles	$P_{net,tot}$ **[kW]**	$\eta_{th,tot}$ **[%]**	ΔT **[°C]**	$P_{net,tot}/(HHV * \dot{m})$ [%]
Helium-methane	1346	29,9%	-245 / -157,7°C	0,27%
Helium-ethylene	1681	23,9%	-245 / -101 °C	0,35%
Nitrogen-methane	2889	64,2%	-245 / -157,7°C	0,59%
Nitrogen-ethylene	3224	45,9%	-245 / -101 °C	0,66%

As the power cycles generate a significant amount of energy, the LH_2 terminal can potentially be energy neutral or even energy positive (generate energy). In this study, only the thermal exergy of the baseload send-out function is assumed to be available for recovery. Nevertheless, as is shown in figure 47, the power cycles can also handle some flexibility. For the proposed terminal, this is explicitly the case because LIN is stored on the terminal site. This provides the opportunity to add extra nitrogen to the RC easily and quickly from the LIN tank, which makes it possible to adjust the RC to fluctuating send-out capacities.

Furthermore, an even larger amount of thermal exergy could be recovered when considering synergy with nearby plants. For example, utilizing waste heat could result in higher efficiencies of the power cycles, and potentially a third cycle in series would be an option. Another possibility to use more thermal exergy is to operate the power cycle in a higher pressure regime, as explained in section 10.3. This is not considered in this study, because reusing the current equipment was desired. Nevertheless, a higher pressure regime could increase the temperature window of the hydrogen heat sink (lower T_6). An example of a higher pressure regime (105,3 – 32 – 7,5 bar) of a methane RC is given in Appendix E.3.2. The efficiency of the cycle is lower (30,5%), but the net power production is higher, namely 803 kW instead of 742 kW.

10.8 Conclusion

The thermal exergy of LH_2 is high compared to LNG: 5.2% and 0.9% of the total exergy, respectively, as shown in table 46. Therefore, utilizing this cold exergy is desired and can have a considerable impact on the efficiency of the terminal and the overall hydrogen import chain. Indeed, having an energy positive hydrogen import terminal would be a great advantage over the other hydrogen import methods. However, currently, little research has been done on the utilization of the cold exergy of LH_2. Due to the lower temperatures, differences in recovery methods can be expected compared to the LNG case. For this reason, it is recommended to do further research on this topic.

In this chapter, thermal exergy recovery with the help of power cycles has been investigated. It is found that the nitrogen (recuperator) and methane Rankine cycles in series are the best solutions to recover the cold exergy of the LH_2 baseload stream. However, note that safety measurements, equipment selection and an enhanced cost evaluation are not considered, as it is beyond the scope of this research. In particular, the cost efficiency of the power cycles is an essential factor to determine the feasibility of recovering the cold exergy. In addition, synergy with other plants and enhanced power cycles, for example producing LIN, also require further research.

The results of the power cycles are used in the calculations to determine the desired terminal design in chapter 12. The results obtained in that chapter show that the LH_2 terminal is energy positive when using the power cycles.

11 Simulations description

The main purpose of this research is to design a suitable LH_2 terminal on the LNG-PS site. After analysing the separate process components of the LH_2 terminal in the previous chapters, the next step is to use this information in the simulations. These simulations are performed to gain insight into specific indication values of the terminal, such as the required process equipment and the efficiency of the LH_2 terminal. With these data, selecting the suitable LH_2 terminal design is possible.

This chapter describes the different terminal designs which are selected to be evaluated and the BOG generation sources. For accurate simulations and results, defining the basis of design and assumptions is very important. Furthermore, the selection values are described, and the used simulation software, Aspen Plus, is explained. Lastly, the various simulations that have been performed are explained.

11.1 Simulation software

Aspen Plus is the used simulation software to analyse the different terminal configurations [197]. This software is based on flowsheet simulation and is suited to quantitatively model a process plant [198]. Aspen Plus is selected because it enables optimisation of energy use and throughput of the terminal [199]. In addition, it has the most complete set of physical properties data, which is essential for simulating hydrogen at extremely low temperatures [199].

All process components in Aspen Plus need property calculations (equation of state) to generate results [200]. To generate accurate results, it is essential to select the correct property method—the low temperatures of hydrogen influences this selection. According to Azizabadi et al., some common equations of state used for liquid hydrogen production simulations do not generate reliable data at low temperatures, namely Peng-Robinson, SRK and BWRS [201]. On the other hand, the Modified-Benedict-Webb-Rubin (MBWR) equation of state performed very well at similar conditions of an LH_2 terminal [201].

In this research, REFPROP is selected as the property method, which uses MBWR as EOS [200]. REFPROP is developed by the National Institute of Standards and Technology (NIST) and is based on the most accurate pure fluid and mixture models currently available [200]. The various substances used at the different terminal configurations (hydrogen, nitrogen, methane and water) are all defined in REFPROP. Most importantly, it performs accurate calculations for hydrogen at temperatures from -259.19°C to 727°C and pressures up to 20.000 bar [200]. Therefore, REFPROP is a suitable property method for the LH_2 terminal simulation.

11.2 Assumptions prior to simulations

For accurate simulations and results, defining the basis of design and assumptions are very important, as stated before. The basis of design is described in chapter 4. The general assumptions used in the performed simulations are the following:

Simulation process

- Steady-state operation of systems.
- ASPEN Plus, with calculation method REFPROP.
- Pure hydrogen is assumed, without para-ortho conversion.
- Atmospheric conditions: 1,01325 bar; 25°C.

Pipelines (Chapter 5)

- All pipes transporting H_2 below -183°C are vacuum insulated.

- For the other pipes, the pressure drop and heat loss/gain is neglected.

Unloading (Chapter 5)

- The unloading capacity is 5.000 m^3/h and 10.000 m^3/h for the terminal configuration with one tank and two tanks, respectively.
- The developed head of the ship pump is 150 meters.

Storage tank (Chapter 6)

- Operating pressure 0,04 barg.
- Storage capacity 50.000 m^3/tank.
- BOR for vacuum insulated storage tank is 0,043%.
- BOR for membrane insulated storage tank is 0,31%.

LH_2 pumps (Chapter 7)

- The isentropic efficiency of the centrifugal submerged pump and HP pump is 67%.
- The $NPSH_R$ for the HP pumps is 2,5 meters.
- The maximum capacity of the submerged pump is 10,38 kg/s.
- The maximum capacity of the HP pump is 11,26 kg/s.

Compressors (Chapter 8)

- The isentropic efficiency of the LP labyrinth compressor is defined at 71%. The corresponding max. capacity is 0,47 kg/s.
- The HP compressor operating at higher temperatures, has intermitted cooling between the three compressor stages. The isentropic efficiency for stages one to three is 88%, 97%, and 97%. Between those stages, the hydrogen gas is cooled to 40°C. The corresponding max. capacity is 1,91 kg/s. This equipment is only used in the Basic-model.
- The isentropic efficiency of the LP and HP compressor operating at extremely low temperatures is defined at 71%. The corresponding max. capacity is 0,47 kg/s. (Similar to the LP labyrinth compressor).

Recondenser (Chapter 8)

- The LH_2 outlet stream must have an available NPSH that meets the requirements of the HP pumps.
- Pressure drop of 10 mbar.

Evaporator (ORV) (Chapter 9)

- Seawater is assumed to be normal water
- Due to environmental regulations, the seawater temperature difference cannot be higher than 5°C.
- The HEX used are counter-current, and the minimum pinch temperature difference is 5°C.
- The inlet and outlet temperature of seawater is defined at 15°C/10°C.
- The seawater pump has an isentropic efficiency of 75%.
- The maximum evaporation capacity is 7 kg/s H_2, in case seawater temperature is at its lowest (see figure 45)

Cryogenic power cycles (Chapter 10)

- A nitrogen and methane Rankine cycle are employed in series. With an overall thermal efficiency of 64,2% over the temperature range from -245°C till -157,7°C.
- Only the baseload function utilises the cold exergy.

11.3 Different terminal configuration

Four terminal designs are selected to be evaluated in this study to gain insight into a suitable LH_2 terminal design. The four different models are called: Basic-model, Cold-model, Recondenser-model and PC-model.

The Basic-model presents the terminal configuration with currently available process equipment, which is shown in figure 55. The compressors designed by Burckhardt are employed [148], [149]. For this reason, a HEX (heater) is necessary before the compressor as they are not capable of handling hydrogen below -170°C. In addition, after the BOG compression, a cooler is needed to meet the requirements of the grid. As explained in chapter 7, the used pumps are LH_2 dedicated and designed by Nikkiso Cryo Inc. These pumps are used in all four models.

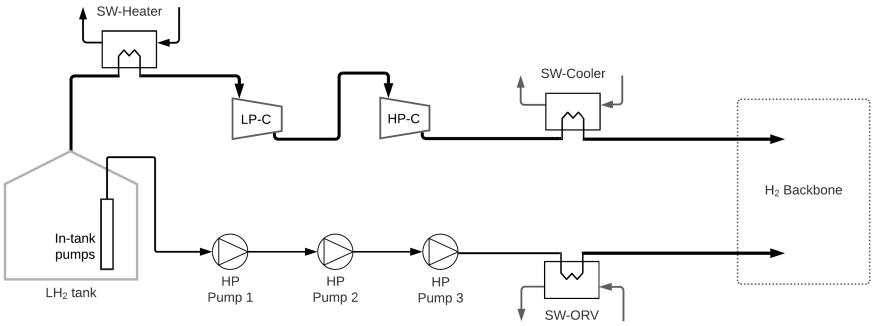

Figure 55: Schematic overview of the Basic-model set-up.

For the three other models, it is assumed that the compressors can handle extremely low temperatures. These compressors that can operate at temperatures as low as -252°C is directly the only difference between the Basic-model and the Cold-model. Analysing this terminal design is important to define the benefits of hydrogen BOG compression at low temperatures.

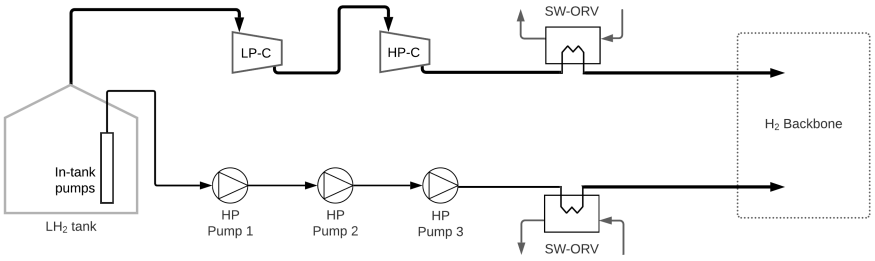

Figure 56: Schematic overview of the Cold-model set-up.

The Recondenser-model is shown in figure 57, and uses a recondenser to decrease the required energy for BOG compression, as is explained in section 8.3.

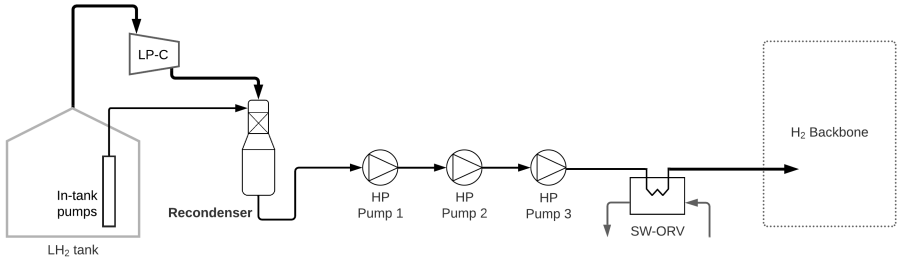

Figure 57: Schematic overview of the Recondenser-model set-up.

The final design, PC-model, employs two cryogenic power cycles to utilise the cold exergy of LH_2. As determined in chapter 10, the best-suited option for the two power cycles in series are the nitrogen and methane Rankine cycle. These two power cycles are considered in this model, as is shown in figure 58. Furthermore, it is assumed that only the cold exergy is recovered from the baseload send-out rate. So therefore, the bypass is added for the Peakshaver function of the terminal.

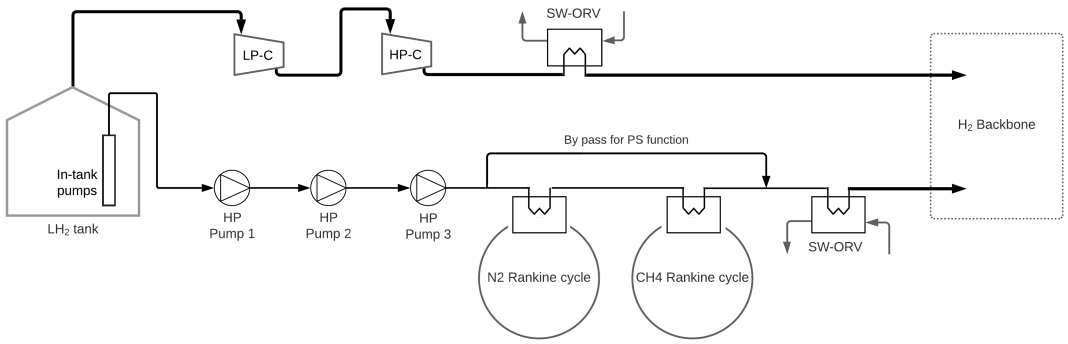

Figure 58: Schematic overview of the PC-model set-up.

11.4 BOG generation calculation

As seen from the different simulation models, processing the BOG is an essential part of the terminal design. Therefore, defining the amount of BOG generation is crucial. Table 18 lists the sources that generate the BOG, which have been defined in section 8.1. During unloading, the BOG generation increases significantly because of the LH_2 ship pump. It is assumed that all the pumping energy is converted to heat, and the delivered head of the ship pump is 150 meters.

Table 18: An overview of the assumed BOG sources at the LH_2 terminal, during normal and unloading procedures

Normal send-out operation	**Unloading opertion**
Heat leakage into the unload pipelines (Recirculation line)	Heat leakage into the unload pipelines (Recirculation line)
Heat leakage into the storage tank	Heat leakage into the storage tank
	Heat transferred to LH_2 by the ship's pumps

Two types of insulation techniques have been investigated for the storage tank as discussed in chapter 6, namely the Mark III membrane technology and vacuum insulation. Both methods result in different BORs of the tank. In addition, the number of storage tanks employed also affects the required unloading capacity and the heat ingress into the recirculation pipes.

As mentioned in section 5.3 and 8.1, the vapour return flow during the unloading process does not require treatment and therefore is not added as a BOG source. The heat leak into the non-operational LH_2 HP pumps is not considered. However, the send-out volume extracted from the storage tank is also not taken into account, which would result in less BOG.

11.5 Indication values

Similar indication values are obtained for all terminal configurations to allow comparison of the different designs. The parameters that have been used to analyse the configurations are:

- Overall net power balance
  - Send-out efficiency loss
  - Energy input per kilogram H_2 send-out
- Minimum send-out rate
- Seawater requirement
- Amount of process equipment needed

The **overall net power balance** describes the required power to supply hydrogen to the grid. This is a very important parameter to design an energy-efficient terminal. The process equipment that requires power are the BOG compressors, LH_2 pumps and seawater pumps. For the PC-model, where power cycles are employed, the working fluid pump and a turbine are added. The turbine generates power, which is why the turbine power has a minus sign. With equation 28, the overall net power is calculated.

In addition, the **send-out efficiency loss** and **energy input per kilogram H_2 send-out** have been added to clarify the results. These values make it possible to compare the different results of terminal designs at a glance with regard to energy consumption. To calculate the efficiency loss, equation 29 is used. The energy input per kilogram hydrogen supplied to the grid has been calculated with equation 30.

$$P_{net} = \sum P_{pump} + \sum P_{comp} - \sum P_{turb} \qquad [kW] \tag{28}$$

$$\eta_{loss} = \frac{P_{net}}{\dot{m}_{H_2} * HHV_{H_2}} * 100\% \qquad [\%] \tag{29}$$

$$E_{kg} = \frac{P_{net}}{\dot{m}_{H_2}} \qquad \left[\frac{kJ}{kg}\right] \tag{30}$$

Minimum send-out rate is an important indication for an import terminal. Although it is assumed that the terminal will supply a baseload to the grid, having a low minimum send-out is beneficial to provide enhanced send-out flexibility of the terminal. The minimum send-out capacity is influenced by the BOG formation and how this BOG is processed. As shown by equation 31, only when using the recondenser, the minimum mass flow is greater than the BOG flow.

$$\dot{m}_{min.send-out} = \dot{m}_{BOG} + \dot{m}_{LH_2-recondenser} \qquad \left[\frac{kg}{s}\right] \tag{31}$$

The **seawater requirement** describes the seawater mass flow consumed by the terminal during the send-out process. Depending on the configuration of the terminal, there is one or multiple seawater intakes.

$$\dot{m}_{SW} = \sum \dot{m}_{SW_i} \qquad \left[\frac{kg}{s}\right] \tag{32}$$

The **amount of process equipment needed** can give an indication regarding the costs and size of the terminal. These values are obtained for the baseload and the maximum send-out capacity of the terminal. To determine the amount of equipment, the maximum throughputs of the different process components are defined. The maximum capacities of the different devices are as follow:

- LH_2 submerged pump : 10,38 kg/s
- LH_2 HP pump: 11,26 kg/s
- LP Compressor: 0,472 kg/s
- HP Compressor (Cold): 0,472 kg/s
- HP Compressor (Burckhardt): 1,9 kg/s
- Open Rack Vaporizer (HEX): 7 kg/s (with seawater inlet of 5°C)

For the HP compressor capable of operating at extremely low temperatures, a vertical labyrinth compressor design is assumed, as it can operate at these low temperatures. Similar designs are used for the LP compressors; therefore, the capacity is supposed to be equal. For the Open Rack Vaporizer, the maximum LH_2 flow has been selected for the case when the seawater temperature is at its lowest (5°C), as defined in chapter 9. Equation 33 is used to calculate the amount of required equipment.

$$\#_{equipment} = \frac{\dot{m}_{(L)H_2}}{\dot{m}_{equipment}} \tag{33}$$

11.6 Simulation explanation

This section describes the different simulations that have been performed in this research. The first step to evaluate the different terminal configurations is to determine the various BOG flows. The generated BOG flow varies due to the terminal capacity, processes and the type of insulation technique used for the storage tank, as described in section 11.4. The results for the generated BOG can be found in section 12.1.

For clarity reasons, some choices have been made regarding the simulation scenarios that have been evaluated in this research. Since there are many simulation scenarios possible for all four terminal configurations, considering; the terminal size, tank insulation and unloading process.

To provide insight into the difference in terminal capacity (or terminal size), only the Basic-model is evaluated, as it is believed to provide sufficient information on this topic. The terminal capacity influences the send-out rate, as discussed in section 4.3. For the three other terminal configurations, only the second case for the send-out capacity of the terminals, so with two tanks, is considered. The send-out capacities defined in section 4.3 are depicted again in the table below.

Table 19: Send-out rate of the LH_2 terminal with regard to the terminal capacity

Scenario	Baseload	Peakshaver	Max. capacity	Units
Case 1 (1 tank)	3,46	17,5	20,96	[kg/s]
Case 2 (2 tanks)	8,02	17,5	25,52	[kg/s]

For all four terminal configurations, the simulations have been performed for the minimum send-out capacity, the baseload function and the maximum send-out capacity of the terminal. The maximum send-out capacity has been evaluated to define the required amount of process equipment at the terminal.

For the **minimum send-out capacity** of the terminal, three indication values are of interest, namely the "Send-out efficiency loss", "Energy input per kilogram" and "Minimum send-out rate". These values give insight into the BOG handling process since the minimum flow is related to the BOG flow.

For the **baseload function**, the "Overall net power balance", "Send-out efficiency loss", "Energy input per kilogram" and "Seawater requirement" are the desired indication values to obtain. The simulations have been performed for both cases regarding the insulation method of the storage tank to provide insight into the advantages of the different insulation technologies. Besides the indication values, the percentage of the required net power to process the BOG flow and LH_2 stream are presented. These percentages give additional information about the impact of the BOG process on the terminal.

Lastly, the **required amount of process equipment** at the terminal has been defined. Therefore the maximum send-out capacity, equal to the baseload and Peakshaver function, is evaluated to obtain the amount of additional equipment necessary to handle the Peakshaver function. The energy efficiency of this capacity is not determined, as it will be pretty similar to the baseload function. Furthermore, the required amount of equipment to handle the BOG flow during unloading procedures has been calculated. The unloading procedures are considered as this results in the maximum BOG flow.

12 Results & Discussion

This chapter is dedicated to presenting and discussing the obtained results from the simulations carried out in this research, beginning with the results for the generated BOG at the LH_2 terminal. After that, the results of the four terminal configurations are presented, with a summary of the key indication values shown in section 12.6. This chapter is concluded with a visual overview of the required power for the various process components, and general points of discussion.

12.1 Results BOG generation

The amount of BOG generation depends on multiple factors, namely the insulation method of the LH_2 storage tank, the assumed capacity of the terminal (number of tanks used) and the operation function of the terminal.

Regarding the insulation method of the storage tank, a vacuum and a membrane insulation are considered, as discussed in section 6.3. Both techniques have a different BOR, as is shown in table 20. The capacity of the terminal affects the number of tanks that are utilised, namely one or two. In addition, for the larger terminal capacity the unload pipes require a larger diameter, resulting in more BOG, as shown in table 21. Lastly, the operation functions of the terminal can be distinguished into two processes: the normal send-out operation and the unloading operation. As discussed in section 11.4, the difference is caused by the BOG formation created by the ship's LH_2 pump.

The BOG formation in the storage tank and the pipes are presented in table 20 and 21. The BOG generation due to the ship unloading is detailed in table 22.

Table 20: Presents the generated BOG of the two different insulation methods of the storage tank.

		1 tank		**2 tanks**	
Tank insulation	BOR [%/day]	mass flow [kg/s]	mass flow [kg/h]	mass flow [kg/s]	mass flow [kg/h]
Membrane insulation	0,310	0,127	458	0,254	917
Vacuum insulation	0,043	0,0176	63,5	0,0353	127

Table 21: Presents the overall BOG generation due to heat ingress into the unloading pipes.

Pipelines	Pipe	**Length** [m]	**Diameter** [inch]	**Heat loss** [W/m]	**Tot. heat leak** [kW]	**BOG** [kg/s]	**Tot. BOG** [kg/h]
1 tank	Unload line	672	24"	19,60	13,17	0,0297	
	Recirculation line	470	4"	3,30	1,55	0,0035	
					Overall:	**0,0332**	**120**
2 tanks	Unload line	814	32"	26,10	21,25	0,0479	
	Recirculation line	470	4"	3,30	1,55	0,0035	
					Overall:	**0,0514**	**185**

Table 22: BOG production due to LH_2 ship unloading. The isentropic efficiency of the LH_2 ship's pump is assumed to be 75%, and the delivered head is 150 m.

Unloading	Unload capacity [m^3/h]	Pump power [kW]	BOG [kg/s]	BOG [kg/h]
1 tank	5.000	192	0,434	1562
2 tanks	10.000	385	0,868	3125

12.1.1 Overall generated BOG for the different cases

In table 23, the total generated BOG for the different BOG cases is presented. As can be concluded from these results, the insulation method of the LH_2 storage tank significantly affects the BOG production during the normal send-out operations. During these operations, the vacuum insulated tank results in a BOG flow more than three times lower than the LH_2 terminal with a membrane insulated storage tank.

Table 23: The overall BOG production for the various terminal designs.

		Normal process		**Unloading process**	
Overall BOG	Type tank	Tot. BOG [kg/s]	Tot. BOG [kg/h]	Tot. BOG [kg/s]	Tot. BOG [kg/h]
1 Tank	Membrane	0,160	577	0,594	2139
	Vacuum	0,0508	183	0,485	1745
2 tanks	Membrane	0,306	1100	1,17	4225
	Vacuum	0,0866	312	0,955	3437

However, during the ship unloading process the BOG flow is less effected by the type of insulation technique used for the storage tanks because the BOG generation due to unloading is a very large factor. The generated BOG due to unloading procedures is around 75% or 90% of the overall BOG formation at the terminal with respectively membrane or vacuum insulated tanks. Therefore, the maximum BOG flow rate at the terminal is quite similar for both insulation methods of the storage tanks.

The larger terminal capacity results in a larger BOG flow. For the case with the membrane insulated tanks, the BOG flow is around two times as high for the larger capacity. However, when the tanks are vacuum insulated, the larger capacity has less effect on the BOG flow (during normal operations) because with this technique a large part of the BOG production is caused by heat ingress into the pipelines, which is influenced to a lesser extent by the terminal capacity as is depicted in table 21.

Altogether, it can be assumed that the vacuum designed tank improves the efficiency of the LH_2 terminal since less BOG has to be handled during normal operations. Nevertheless, the amount of BOG processing equipment will be comparable as the maximum BOG flow is in the same range. More details regarding these topics are being discussed in the following sections of this chapter.

12.2 Basic-model

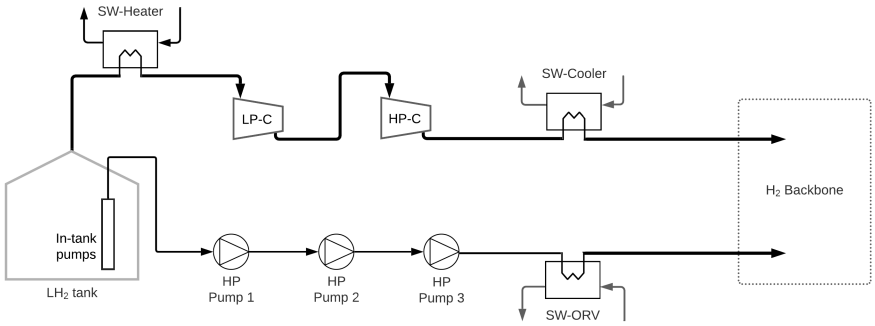

Figure 59: Schematic overview of the Basic-model set-up.

In this section, the results for the Basic-model configuration of the LH_2 terminal (illustrated in figure 59) has been evaluated. This has been done for the different terminal capacities and the two selected storage solutions determined in section 6.3. In the tables, the difference in terminal capacity is indicated for one and for two tanks and the insulation method of the storage tank is referred to as the membrane or vacuum technique. The corresponding mass flows for the different scenarios are presented in the table below. In Appendix G, the Aspen model with corresponding thermodynamic data of each stream is presented.

Table 24: Present the defined mass-flows for the terminal

Overall BOG	Type tank	BOG flow (a) [kg/s]	LH_2 flow (b) [kg/s]	Baseload (a+b) [kg/s]	Peakshaver (c) [kg/s]	Max. send-out (a+b+c) [kg/s]
1 Tank	Membrane	0,160	3,3	3,46	17,5	20,96
	Vacuum	0,0508	3,41	3,46	17,5	20,96
2 tanks	Membrane	0,306	7,71	8,02	17,5	25,52
	Vacuum	0,0866	7,93	8,02	17,5	25,52

12.2.1 Minimum send-out - Basic-model

At first, the minimum flow of the Basic-model has been evaluated. As can be seen from the set-up of this terminal (figure 59), the minimum flow is equal to the BOG flow.

In table 25, the desired indication values of the minimum flow are presented. The send-out efficiency loss shows that 3,1% of the HHV of the hydrogen BOG flow is needed in electrical power to process the BOG. In addition, the required energy input for handling one kilogram of hydrogen BOG is presented. These two indication values are similar for each BOG rate. Lastly, as stated above, the minimum flow is equal to the BOG flow.

As defined in section 12.1, the BOG flow rate is affected by multiple factors. Therefore, the minimum flow rate and power required to process the BOG varies. The different BOG flow rates are presented in table 23.

Table 25: The general results of processing the minimum flow (BOG) with the Basic-model

Basic-model	η_{loss} [%]	E_{kg} [kJ/kg]	Minimum flow
Minimum flow process	3,1	4360	BOG

12.2.2 Baseload - Basic-model

For the baseload case, not only the BOG flow is processed but also the LH_2 stream, as can be concluded from table 24. Processing the LH_2 stream requires only 0,13% of the HHV of the supplied hydrogen to the grid. Therefore, the energy consumption to process one kilogram of LH_2 is significantly less compared to processing the BOG flow, namely more than 24 times less. The more significant energy input for processing the BOG flow can be explained by the fact that pumping a liquid takes much less energy than compressing a gas.

The desired indication values for the baseload function are presented in table 26. The corresponding mass flows are presented in table 24.

Table 26: The process results for handling the baseload function with the Basic-model terminal

Basic-model: baseload		η_{loss} [%]	E_{kg} [kJ/kg]	P_{net} [kg/s]	Perc. power for BOG flow [%]	Perc. power for LH_2 flow [%]	$\dot{m}_{SW}$ [kg/s]
1 Tank	Membrane	0,26	372	1289	54%	46%	570
	Vacuum	0,17	241	833	27%	73%	581
2 tanks	Membrane	0,24	339	2716	49%	51%	1327
	Vacuum	0,16	224	1800	21%	79%	1352

The overall net power for the terminal employing membrane insulated tanks is considerably larger compared to the vacuum insulated tanks. This results from the larger BOG flow, which requires significantly more energy, as mentioned above. For this terminal configuration with membrane insulation technology, around half of all energy is used to process the BOG flow. However, the BOG mass flow is only 4% of the total hydrogen delivered to the grid.

Regarding the terminal capacity, it can be seen that the overall efficiency loss is slightly higher for the smaller terminal design, which is a result of the relatively higher BOG flow in comparison with the LH_2 flow. Therefore, a higher percentage of the total required power is needed to process the BOG flow.

12.2.3 Required amount of process equipment - Basic-model

In this section the required amount of process equipment to handle the BOG flow and the LH_2 stream are presented.

To be able to handle the BOG flow at the terminal at any time, the maximum BOG flow is considered, which is the BOG flow during unloading procedures. As mentioned before in section 12.1, during unloading procedures the overall BOG flow is less affected by the insulation method of the storage tank. After evaluation, it appears that the insulation method of the storage tank does not influence the required amount of equipment to handle the BOG flow. The amount of equipment to process the BOG flow are presented in table 27.

Table 27: The required equipment to process the BOG flow, considering the Basic-model.

Equipment BOG flow	LP-comp. [#]	HP-comp. [#]	Heater [#]	Cooler [#]
1 tank	2	1	1	1
2 tanks	3	1	1	1

The process equipment to handle the LH_2 stream are depicted in table 28. As can be seen, the required amount of equipment changes with the send-out function. Therefore, to accommodate a Peakshaver function at the terminal, considerably more process equipment is required. The large number of required HP pumps is partly due to the fact that these pumps must have three in series to achieve the desired pressure output. For the submerged pumps, adding an additional tank also requires an extra submerged pump. Note that backup

equipment is not taken into account. However, to guarantee the send-out capacity at any time, this should be considered when building the LH_2 terminal.

Table 28: The required equipment to handle either the baseload function or the maximum send-out capacity considering the Basic-model.

Equipment	**Baseload capacity**			**Max. send-out capacity**		
LH_2 stream	Sub. pump [#]	HP pump [#]	ORV [#]	Sub. pump [#]	HP pump [#]	ORV [#]
1 tank	1	3	1	3	6	3
2 tanks	2	3	2	4	9	4

12.3 Cold-model

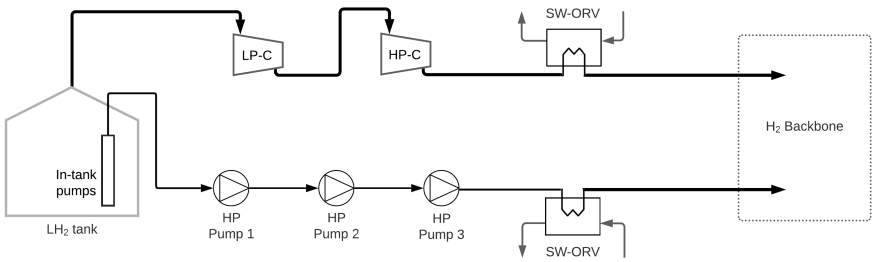

Figure 60: Schematic overview of the Cold-model set-up.

This model assumes that the compressors can compress the BOG flow at extremely low temperatures. Therefore, the results for processing BOG flow will be different compared to the Basic-model. The LH_2 flow is handled in a similar way as is done in the Basic-model, meaning the general results for processing the LH_2 will be the same. However, since handling the BOG flow consumes a significant amount of the total energy during baseload send-out, the difference in BOG processing will influence the terminal's overall efficiency. These results are presented in this section.

12.3.1 Minimum send-out - Cold-model

Like the Basic-model, the minimum flow of the Cold-model configuration is equal to the BOG flow. The different BOG flow rates are presented in table 23.

The results for processing the hydrogen BOG stream with compressors that can handle extremely low temperatures are shown in table 29. With this configuration, the energy input to manage the BOG flow is significantly lower than the Basic-model, about 3,6 times. This can be explained by the fact that compression at lower temperatures requires less power [68].

Table 29: The general results of processing the minimum flow (BOG) with the Cold-model

Cold-model	η_{loss} [%]	E_{kg} [kJ/kg]	Minimum flow
Minimum flow process	0,86	1220	BOG

12.3.2 Baseload - Cold-model

The processing of the LH_2 flow is done in the same way as in the Basic-model. Nonetheless, due to the more efficient BOG treatment, the overall net power requirements are considerably lower, as is depicted in table 30. This is also shown by the fact that the BOG process consumes around 21% (table 30) of all necessary power, instead of 49% for the Basic-model configuration with membrane insulation technology (table 26). Furthermore, the seawater requirement is about the same as for the Basic-model.

Table 30: The process results for handling the baseload function at the Cold-model terminal

Cold-model: baseload		η_{loss} [%]	E_{kg} [kJ/kg]	P_{net} [kg/s]	Perc. power for BOG flow [%]	Perc. power for LH_2 flow [%]	$\dot{m}_{SW}$ [kg/s]
2 tanks	Membrane	0,15	219	1757	21%	79%	1338
	Vacuum	0,13	191	1532	7%	93%	1354

12.3.3 Required amount of process equipment - Cold-model

The required amount of equipment to process the LH_2 flow is similar to the Basic-model since the LH_2 flow is treated similarly. These results can be found in table 28.

However, there are more HP compressors required to process the BOG flow during the unload procedures. This is because these HP compressors operating at extremely low temperatures are assumed to have the same throughput capacity as the LP compressors. But in addition, no extra HEXs are needed to handle the BOG because the ORV can be used for both the liquid and the BOG flow. Altogether, the efficiency of this terminal design is better compared to the Basic-model and does not require more equipment.

Table 31: The required equipment to process the BOG flow, considering the Cold-model.

Equipment BOG flow	LP-comp. [#]	HP-comp. [#]
2 tanks	3	3

12.4 Recondenser-model

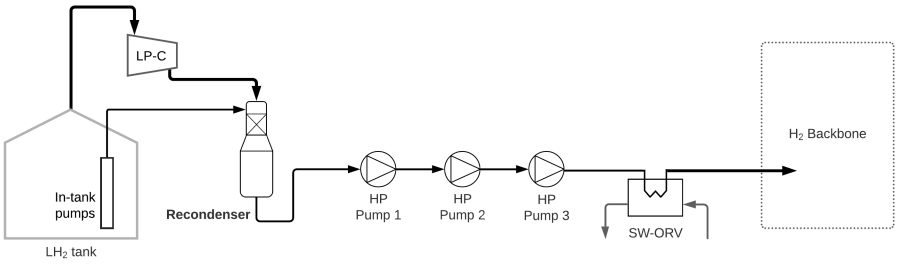

Figure 61: Schematic overview of the Recondenser-model set-up.

In this configuration, a recondenser is used to minimize energy consumption for BOG treatment. As shown in figure 61, the HP compressor can be eliminated when utilizing the recondenser. This is beneficial because the HP compressor requires approximately 75% of the total power to compress the hydrogen BOG to the desired pressure.

As discussed in section 8.3, the recondenser can operate at different pressures. The operating pressure of the recondenser affects the minimum flow and the efficiency of the send-out process. However, for the results of the minimum flow presented in this section, the highest operating pressure of the recondenser is considered as this leads to the lowest minimum flow. And for the baseload function, the lowest operating pressure of the recondenser is used as this provides the highest energy efficiencies. The operating pressure of the recondenser ranges from 4 to 8 bar as these are the pressure ranges of the submerged pump and LP compressor. More information and results regarding the operating pressure of the recondenser can be found in Appendix G.1.3.

12.4.1 Minimum send-out - Recondenser-model

Using a recondenser affects the minimum flow capacity of the terminal because the recondenser requires LH_2 input to condensate the hydrogen BOG. Therefore, the minimum flow is not equal to only the BOG flow.

In table 32, the indication values of the minimum flow are presented with the recondenser operating at 8 bar. As can be seen, utilizing the recondenser decreases the send-out efficiency losses significantly. However, as mentioned above, the minimum send-out capacity of the terminal increases compared to the two previously discussed configurations. To condensate the hydrogen BOG, the recondenser requires a mixing LH_2/BOG ratio of 5,3. Therefore, the minimum flow is equal to 6,3 times the BOG flow.

Table 32: The general results of processing the minimum flow with the Recondenser-model

Recondenser-model	η_{loss} [%]	E_{kg} [kJ/kg]	Minimum flow
Minimum flow process	0,18	260	6,3 * BOG

12.4.2 Baseload - Recondenser-model

Table 33 presents the results for the baseload send-out with the recondenser operating at 4 bar. The results show that the total efficiency loss is comparable to the processing of the LH_2 stream separately, namely 0.13%. Furthermore, since the BOG treatment consumes less energy, a greater BOG flow, as in the membrane case, has a significantly smaller effect on the overall net power requirement. For this reason, when the terminal is assumed to have a baseload send-out capacity, like the proposed terminal, the insulation degree of the tank has limited influence on the terminal efficiency if a recondenser is employed. Finally, the amount of seawater consumption is comparable to the other terminal configurations.

The percentages of the total power required for the BOG and LH_2 stream treatment are not shown since the BOG flow is merged within the LH_2 stream.

Table 33: The process results for handling the baseload function at the Recondenser-model terminal

Recondenser: baseload		η_{loss} [%]	E_{kg} [kW]	P_{net} [kg/s]	Perc. power for BOG flow [%]	Perc. power for LH_2 flow [%]	$\dot{m}_{SW}$ [kg/s]
2 tanks	Membrane	0,13	186	1490	7%	93%	1351
	Vacuum	0,13	178	1428	2%	98%	1359

12.4.3 Required amount of process equipment - Recondenser-model

Since the BOG flow is merged with the LH_2 flow, no process equipment is dedicated explicitly for the BOG stream except the LP compressors. Compared to the other configurations, the Cold-model requires multiple additional HP compressors and the Basic-model also requires extra HEXs to process the BOG flow; this design only requires an additional recondenser.

Table 34: The required equipment to process the BOG flow, considering the Recondenser-model.

Equipment BOG flow	LP-comp. [#]	Recondenser [#]
2 tanks	3	1

The amount of process equipment necessary to handle the Baseload capacity and the maximum send-out capacity are detailed in table 35. For each process component that is also used in the Cold-model and the Basic-model (submerged pump, HP pumps and the ORV), the required quantity is comparable.

Table 35: The required equipment to handle either the baseload function or the maximum send-out capacity considering the Recondenser-model.

Equipment	**Baseload capacity**			**Max. send-out capacity**		
LH_2 stream	Sub. pump [#]	HP pump [#]	ORV [#]	Sub. pump [#]	HP pump [#]	ORV [#]
2 tanks	2	3	2	4	9	4

Altogether, the efficiency of this terminal design is even better than the Cold-model and does not require more equipment. However, the minimum send-out capacity is considerably higher. Nevertheless, as a baseload send-out rate is assumed for the proposed terminal, this is not an issue.

12.5 PC-model (Power cycle)

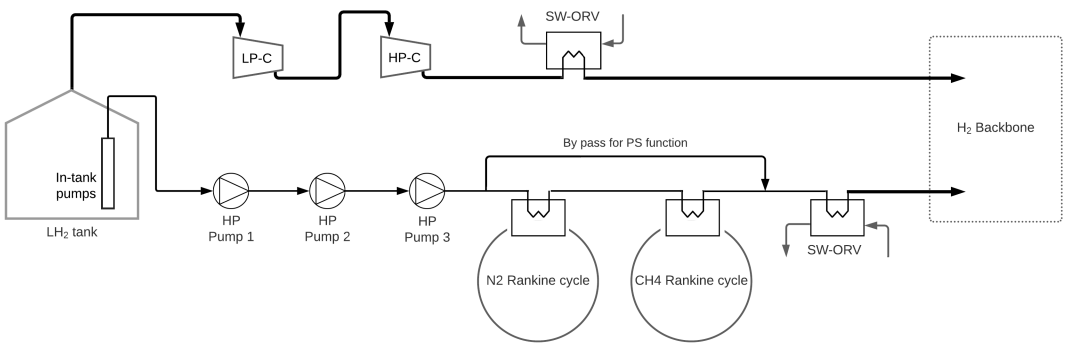

Figure 62: Schematic overview of the PC-model set-up.

The results for the terminal employing power cycles to recover the cold exergy of the LH_2 stream are presented in this section. In chapter 10, the two best-suited power cycles in series to convert the cold exergy into mechanical power are already determined, namely the nitrogen and methane Rankine cycles. An overview of the results obtained for these cycles can be found in table 17 at section 10.7.

12.5.1 Minimum send-out - PC-model

For this configuration, it is assumed that the minimum send-out capacity is comparable to the baseload function because the power cycles require a constant cooling source. This cooling source is the LH_2 flow, as discussed in chapter 10. Besides the LH_2 stream, the BOG is processed in the same way as in the Cold-model, so the results for processing the BOG flow can be found in section 12.3.1.

12.5.2 Baseload - PC-model

The power cycles only recover the cryogenic exergy of the baseload send-out capacity since a constant LH_2 flow is desired for these cycles. The overall thermal efficiency for both cycles in series has already been determined, and is 64,2% over the temperature range from -245°C till -157,7°C. Knowing the terminal's baseload capacity and the corresponding LH_2 mass flow (see table 24), the overall net generated power can be determined. In addition, the seawater pumps connected to the ORVs require less power because less seawater is needed since the hydrogen flow is already heated up to -157,7°C instead of the -245°C at which it usually enters the vaporizer. Note that the additional seawater pumps needed for the Rankine cycles are taken into account with the overall thermal efficiency of these cycles.

The overall results for the baseload capacity, i.e. the processing of the BOG flow is also taken into account, are shown in table 36. These results show that the cold exergy recovery is larger than the power input to process the baseload flow. This means that the send-out process generates energy instead of consuming it while supplying hydrogen at a baseload rate to the grid. So, the benefits of employing power cycles are significant in terms of the energy efficiency of the terminal, which is desirable in view of environmental regulations.

The terminal with vacuum designed tanks has a greater total energy production due to the fact that less energy input is required since the BOG flow is smaller. In addition, it generates slightly more power because the LH_2 flow is larger. The total seawater consumption for this configuration is a bit higher compared to the other terminal designs. Nevertheless, the required amount of ORV will be less as the hydrogen entering the vaporizer is already at -157°C.

Table 36: The process results for handling the baseload function at the PC-model terminal. (Negative signs indicate power production instead of consuming.

PC-model: baseload		η_{loss} [%]	E_{kg} [kJ/kg]	P_{net} [kW]	Power input [kW]	Generated power [kW]	$\dot{m}_{SW}$ [kg/s]
2 tanks	Membrane	-0,42	-599	-4800	1564	-6364	1390
	Vacuum	-0,46	-650	-5212	1333	-6545	1407

12.5.3 Required amount of process equipment - PC-model

The amount of equipment required for this configuration is higher than the other configurations due to the added power cycles. However, since the BOG flow is processed similarly as in the Cold-model, the amount of process equipment to handle the BOG flow will be similar and can be found in table 31.

As mentioned before, the power cycles are only employed to recover the baseload capacity. So, therefore, the amount of equipment for the power cycles is not affected by the send-out function. The required amount of equipment for the nitrogen and methane Rankine cycle is shown in table 37.

Table 37: The required amount of equipment to handle the nitrogen and methane Rankine cycle.

	WF pump	**Turbine**	**SW HEX**	**Condenser**	**Recuperator**
Nitrogen RC	1	2	2	1	1
Methane RC	1	2	2	1	0

In addition to the power cycles, the other equipment needed to process the hydrogen is shown in table 38. From these results, it can be concluded that the terminal requires only one ORV for the baseload send-out capacity due to the higher inlet temperature of the hydrogen. Due to this higher inlet temperature, the maximum hydrogen throughput of the ORV increases to 11 kg/s instead of 7 kg/s. Nevertheless, the maximum send-out capacity requires a comparable amount of ORVs to handle the hydrogen throughput as for the other configurations.

Table 38: The required equipment to handle either the baseload function or the maximum send-out capacity considering the PC-model.

Equipment	**Baseload capacity**			**Max. send-out capacity**		
LH_2 stream	Sub. pump [#]	HP pump [#]	ORV [#]	Sub. pump [#]	HP pump [#]	ORV [#]
2 tanks	2	3	1	4	9	4

12.6 Summary results

This section presents an overview of the key indication values presented and discussed for the various LH_2 terminal configurations.

12.6.1 Minimum send-out capacity

An overview of the results for processing the minimum flow is presented in table 39. For the Basic- and the Cold-model, the minimum flow is equal to the BOG flow. The Recondenser-model has a minimum flow of 6,3 times the BOG flow because the recondenser requires an LH_2 input to condensate the BOG. The minimum flow of the PC-model is assumed to be similar to the baseload function due to the fact that the power cycles require a constant LH_2 flow. Since the minimum flow of the PC-model is equal to the baseload function, this configuration is not evaluated in this section.

Table 39: An overview is given for the various processes to handle the minimum flow of the terminal.

Minimum flow process	η_{loss} [%]	E_{kg} [kJ/kg]	Minimum flow
Basic-model	3,1	4360	BOG
Cold-model	0,86%	1220	BOG
Recondenser-model	0,18	260	6,3*BOG
PC-model	-	-	Baseload

The Basic-model requires significantly more energy to process the BOG flow compared to the other configurations. This can be explained by the fact that this terminal design utilizes LP compressors that cannot operate below -170°C. Therefore the compression takes place at higher temperatures which requires more power. Furthermore, the HP compressor needs intermittent cooling, and an additional heat exchanger is necessary to cool the compressed hydrogen BOG flow before it can be supplied to the grid. For the other configurations, it is assumed that compression is possible at -250°C. Therefore, these results represent the benefit of BOG compression at extremely low temperatures.

In addition, the BOG process can be handled even more efficiently by using a recondenser to condensate the hydrogen BOG. With this configuration, the hydrogen BOG can be pumped to desired pressure of the grid instead of using the HP compressors. However, as mentioned before, the minimum flow for this terminal design is significantly larger.

Lastly, the BOG flow is influenced by the type of technology used to insulate the storage tanks. The overall BOG generation is more than three times as high during normal operations when implementing membrane insulation instead of vacuum (see table 23. Therefore, the minimum flow of the terminal configuration using membrane insulated tanks is also higher. However, as mentioned in section 12.1.1, during the ship unloading process, the BOG flow is quite similar because the BOG generation due to the ship unloading procedures is such a large factor. Since this results in the largest BOG flow, the process equipment needed to handle the BOG flow is not influenced by the insulation method used for the storage tanks.

12.6.2 Baseload

The results for handling the baseload by the different terminal designs are summarized in this section. These results are influenced by the isolation method of the tanks; therefore, the terminal with vacuum and membrane tanks are both shown in table 40 and 41, respectively. For a more detailed understanding of the power requirements for handling the baseload send-out, illustrations have been provided in section 12.7.

Table 40: An overview is given for the baseload process, considering two membrane insulated tanks are utilized.

Baseload, Membrane	η_{loss} [%]	E_{kg} [kJ/kg]	P_{net} [kW]	SW mass flow [kg/s]	TRL-level
Basic-model	0,24	339	2716	1327	8
Cold-model	0,15	219	1757	1338	6
Recondenser-model	0,13	186	1490	1351	6
PC-model	-0,42	-599	-4800	1390	6

Table 41: An overview is given for the baseload process, considering two vacuum insulated tanks are utilized.

Baseload, Vacuum	η_{loss} [%]	E_{kg} [kJ/kg]	P_{net} [kW]	SW mass flow [kg/s]	TRL-level
Basic-model	0,16	224	1800	1352	8
Cold-model	0,13	191	1532	1354	6
Recondenser-model	0,13	178	1428	1359	6
PC-model	-0,46	-650	-5212	1407	6

As can be seen, with the vacuum insulated tanks, the overall net power input of the terminal decreases because less BOG needs to be processed. Especially for the Basic-model, the required overall power decreases significantly when utilizing vacuum insulated tanks instead of membrane technology. This can be explained by the fact that this configuration processes the BOG least efficiently. Furthermore, the lower total net power requirements also reflect the smaller efficiency losses and can be translated into lower OPEX. Therefore, investing in a more expensive vacuum insulated tank might be desirable for the LH_2 terminal.

However, for the terminal employing a recondenser, the difference between the insulation methods is significantly smaller. In addition, the required power input to supply hydrogen at baseload rate to the grid is lower compared to the Basic- and Cold-model, even when using the membrane insulated tanks. This indicates that when the terminal is assumed to have a baseload capacity to the grid, a membrane insulated tank combined with a recondenser is a very suitable option. In this case, the CAPEX and OPEX are low since the membrane insulated tank solution is assumed to be considerably cheaper than the vacuum tank, as described in section 6.3.

When the terminal employs power cycles, the send-out process is most efficient because it produces energy instead of consuming it. The net power generation is significant, and regarding the environmental regulations, it could be desirable to have an energy positive hydrogen import terminal. However, this configuration has also side effects such as the considerably large minimum flow, as mentioned before. Furthermore, it increases the process complexity of the terminal, and -as will be discussed in the next section- it requires additional equipment.

The seawater consumption for all terminal configurations is comparable. The TRL level for each configuration is defined at six except for the Basic-model. This TRL level six is assumed, as these configurations utilize the hydrogen compressors that operate below -170°C. As mentioned in chapter 8, manufacturers are not yet able to design compressors that can compress hydrogen at -250°C for various reasons. They noted that

further research is necessary to develop these compressors. In the Basic-model, all types of equipment can be delivered by manufacturers, except the ORV and the control equipment in the vacuum insulated pipes. As discussed in section 9.3, it is assumed that a similar type of Super-ORV used for LNG evaporation can be used for LH_2 applications. However, for LH_2 application, additional research is necessary for the material selection of this process equipment. As mentioned in section 5.4, the valves and other control equipment for the vacuum insulated pipes larger than 12 inches in diameter have not yet been developed. Therefore the TRL level for the Basic-model has been set at eight. Note that for the TRL level, the storage tank designs are not considered.

12.6.3 Required amount of process equipment

This section provides an overview of the amount of equipment needed to handle the BOG flow, the baseload and maximum send-out capacity. For the BOG process, the flow during unloading procedures is taken as the basis for calculation as this requires most equipment. Furthermore, note that backup equipment is not taken into account in these results.

Although vacuum insulated tanks result in a more efficient process, it appears that the amount of equipment required to process the various flows is not affected by the chosen insulation technology of the tank. These results indicate that vacuum insulated tanks result in lower operational costs as the send-out process is more efficient. However, the required amount of equipment and thus the investment costs are comparable for the assumed terminal capacity, besides the capital costs for the storage tank itself.

Table 42: An overview is given for the required process equipment needed to process the maximum BOG flow, so during unloading procedures. * Please note that the ORV, is partially used for the BOG flow, but also for the LH_2 evaporation process. So actually, no additional ORV is required to process the hydrogen BOG flow.

BOG equipment	LP-comp. [#}	LP-comp. cold [#]	HP-comp [#]	HP-comp. cold [#]	Heater [#]	Cooler [#]	Recondenser [#]	(ORV)* [#]
Basic-model	3	0	1	0	1	1	0	(0)
Cold-model	0	3	0	3	0	0	0	(1)
Recondenser-model	0	3	0	0	0	0	1	(1)
PC-model	0	3	0	3	0	0	0	(1)

To handle the BOG flow, the Basic-model requires two additional heat exchangers. One is needed to heat the BOG flow to -170°C, and the second one has to cool the compressed hydrogen before it can be supplied to the grid. Compared to the Cold- and PC- configurations, it only requires one HP compressor that can handle large mass throughputs. This is because the compressor design used in the Basic-model is not a labyrinth compressor as it operates at higher temperatures.

For the other configurations, it is assumed that the LP and HP compressors are vertical labyrinth compressors with comparable throughput. Therefore, three devices for both the HP and LP compressor are required to process the flow. However, when employing a recondenser, the HP compressor is eliminated, as seen in table 42. To heat the BOG flow, the ORV is utilized. Since the same ORV can be used for the LH_2 flow, no additional HEXs are required.

As is shown in table 43 below, the amount of equipment to handle the LH_2 stream is similar for each configuration except for the PC-model. This is because these three configurations process the LH_2 stream in the same way. Furthermore, it can be seen that considerably more process equipment is required to make the LH_2 terminal suitable for the Peakshaver function, which results in the maximum send-out capacity of the terminal. Especially for the HP pumps, because these pumps need to have three in series to be able to increase the pressure to the requirements of the grid.

Although the PC-model only needs one ORV to evaporate the baseload due to the higher inlet temperature of hydrogen (-157°C, instead of -245°C), the overall amount of equipment for these configurations is considerably more, as it employs two Rankine cycles in series. The amount of equipment needed for these Rankine cycles is presented in table 37.

Table 43: An overview is given for the required process equipment needed to process the liquid stream at the terminal. *The PC-model also requires equipment for the power cycles, as presented in table 37.

Equipment	**Baseload capacity**			**Max. send-out capacity**		
LH_2 stream	Sub. pump [#]	HP pump [#]	ORV [#]	Sub. pump [#]	HP pump [#]	ORV [#]
Basic-model	2	3	2	4	9	4
Cold-model	2	3	2	4	9	4
Recondenser	2	3	2	4	9	4
PC-model*	2	3	1	4	9	4

12.7 Overview power requirements for send-out process

This section provides an overview of the send-out efficiency and the power requirements of the various process components at the LH_2 terminal for the baseload send-out function.

For all four terminal configurations, the overall send-out efficiency is presented in a Sankey diagram at the left side of the four figures shown below. The efficiency loss is thereafter separated into the three process components that require power: the BOG compressors, LH_2 pumps, and seawater pumps (for the HEXs). At the right side of the figures, the terminal configuration is illustrated, with the percentage of overall net power (P_{net}) required for the various process components in red. The hydrogen mass flow is depicted in blue.

Besides the baseload function, it is assumed that the two storage tanks are membrane insulated. The results of the baseload function, with membrane insulated tanks obtained before, is depicted again in table 44.

Table 44: An overview is given for the baseload process, considering two membrane insulated tanks are utilized.

Baseload, Membrane	η_{loss} [%]	E_{kg} [kJ/kg]	P_{net} [kW]	SW mass flow [kg/s]
Basic-model	0,24	339	2716	1327
Cold-model	0,15	219	1757	1338
Recondenser-model	0,13	186	1490	1351
PC-model	-0,42	-599	-4800	1390

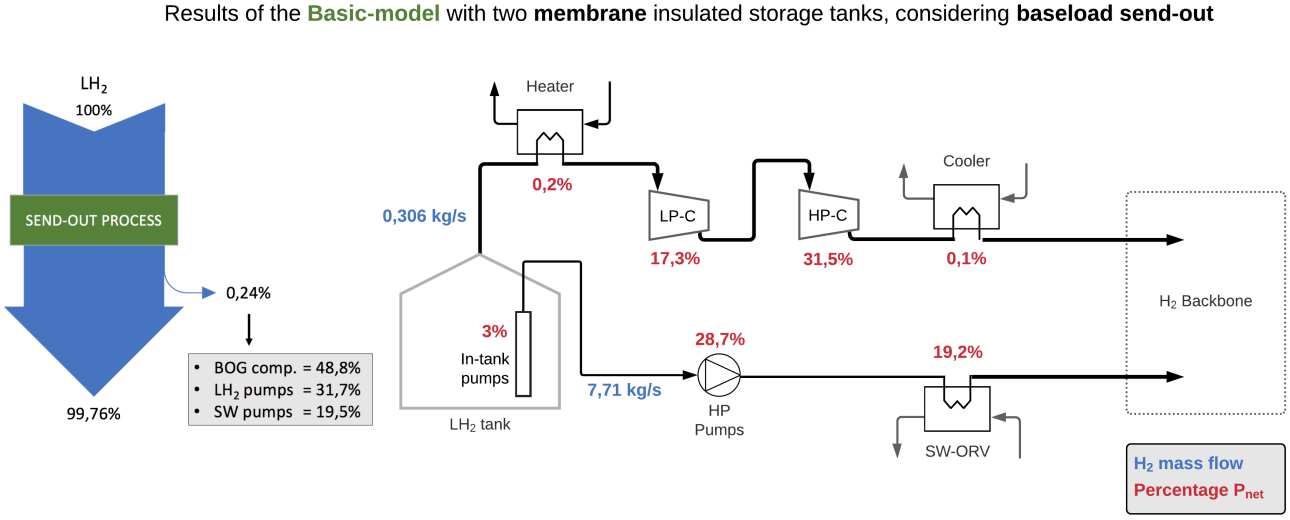

Figure 63: Overview of the energy efficiency and power requirements of the Basic-model for baseload send-out.

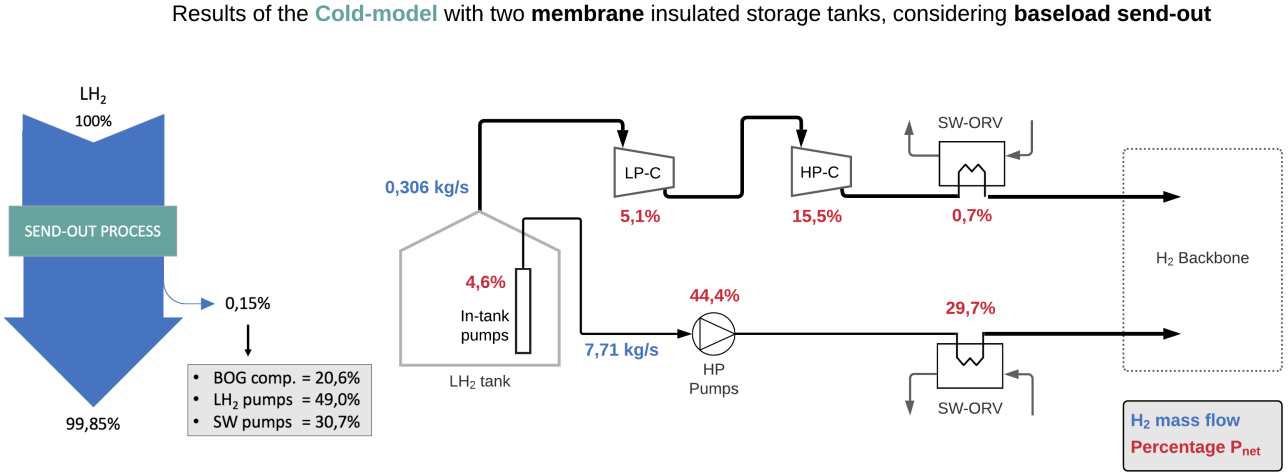

Figure 64: Overview of the energy efficiency and power requirements of the Cold-model for baseload send-out.

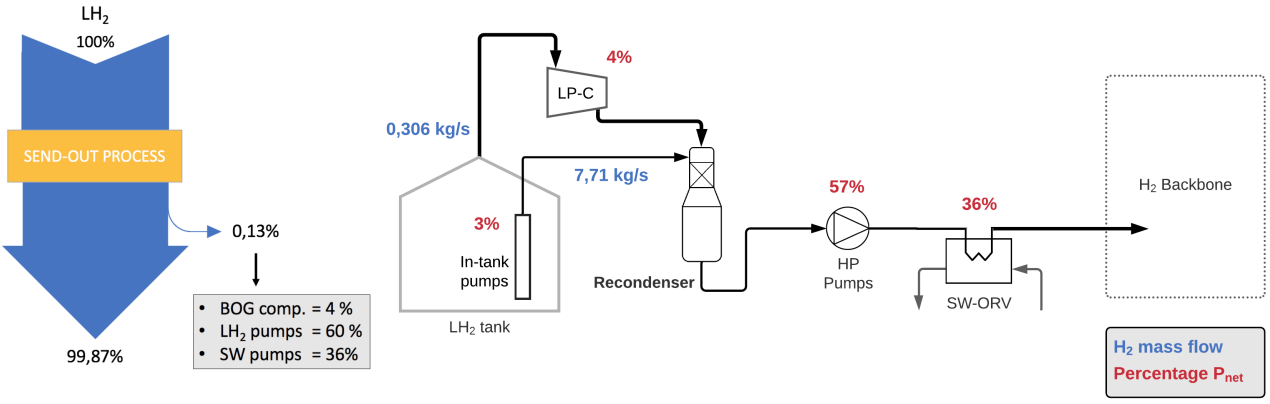

Figure 65: Overview of the energy efficiency and power requirements of the Recondenser-model for baseload send-out.

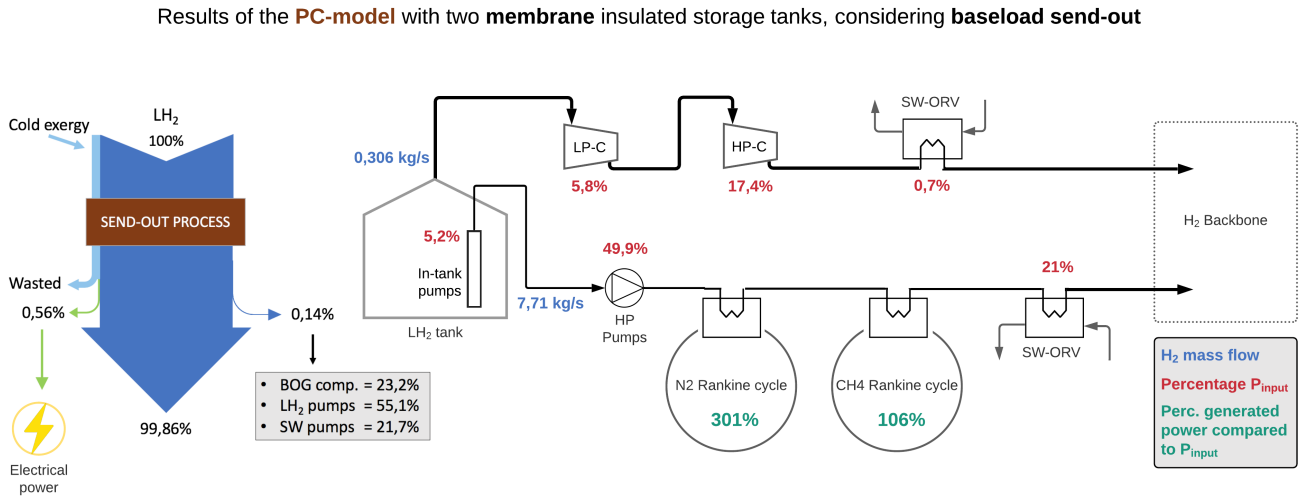

Figure 66: Overview of the energy efficiency and power requirements of the PC-model for baseload send-out. (In green the generated power of the power-cycles is presented, which is described as a percentage of the overall net power input.)

12.8 Discussion

In this section, general discussion regarding the evaluated cases are discussed.

BOG calculations

The first point of discussion is the generated hydrogen boil-off gas at the terminal. Several sources at the receiving terminal result in BOG generation as discussed in chapter 5, 8. However, for the BOG calculations, assumptions have been made reading the BOG sources. BOG formation at non-operational equipment such as the LH_2 pumps is not taken into account. Nevertheless, considering the terminal has the baseload and Peak-shaver function, it will happen that some parallel-connected LH_2 pumps will not be utilized during baseload operations.

Furthermore, during unloading, it is assumed that the vapour return flow (from the storage tank to the ship's tank) does not require treatment and is equal to the unloaded liquid volume flow. Not requiring treatment is only possible when the pressure in the storage tank is higher than the operating pressure of the ship's tank; otherwise, a compressor is needed. Considering that the current BOG compressors cannot operate below -170°C, this would require additional heating and cooling before the BOG can be supplied back to the ship's tank. Secondly, the assumption that the vapour return is equal to the unloaded liquid volume flow depends on many things. Again, the operating pressures of both tanks are a factor and the heat ingress into the vapour return line. As many factors influence this process, small changes can affect the assumption made. Since the vapour return flow is significant (10,000 m^3/h), this can substantially affect the total BOG flow during unloading.

BOG compressors
The hydrogen BOG inlet conditions for the "cold" LP compressor significantly affect the design specifications and power requirements for this compressor. A slight increase in temperature results in a considerably lower density of the BOG flow, as shown in figure 33. Due to the lower density, the volume flow will increase significantly. However, precisely defining these inlet conditions is difficult. It is assumed that the BOG leaving the tank is a saturated vapour, and transported through a vacuum insulated pipe (heat flux of 9,8 W/m) to the LP compressor. Nevertheless, during a particular operation, the conditions of the BOG leaving the tank could be slightly above the saturated vapour conditions.

LH_2 pumps
The isentropic efficiency for the LH_2 pumps is considered at a constant value. Nevertheless, for the centrifugal pumps used, the actual efficiency and the generated head is influenced by the volume throughput. As the highest efficiency is considered in the simulation, the actual pumping power could potentially be higher.

Furthermore, the centrifugal LH_2 pumps require a minimum throughput. This minimum throughput is not considered in these calculations. However, since the designed LH_2 pumps by Nikkiso have a minimum throughput equal to 3,10 kg/s, this would be a limiting factor for the minimum flow of the Recondenser-model. Because when the terminal employs a recondenser, the minimum send-out capacity of the terminal is partly handled with the LH_2 pumps. Thus, when using a recondenser, smaller LH_2 pumps are desirable if the terminal's minimum send-out rate is a requirement.

HEX-SW
The calculations for the seawater consumption of the vaporizers is assuming the seawater inlet and outlet conditions of 15/10°C. The temperature difference of 5°C is set for environmental regulations. However, during winter, these temperatures will be lower, meaning more seawater and therefore more pumping power is required to evaporate the LH_2, as is shown in figure 45. On the other hand, when a heat source heats the seawater before entering the vaporizer, less seawater is necessary because, in this case, the temperature difference of seawater can be higher than 5°C without violating environmental regulations. Therefore, utilizing nearby heat waste could improve the terminal efficiency. Furthermore, the number of required ORV could be decreased in that case.

13 Conclusion

This research represents the first investigation into the possibility to reuse the current LNG Peakshaver, which will become obsolete in the near future, as an LH_2 terminal. The focus of this research is on defining the characteristics of the relevant processes and the needed equipment of an LH_2 terminal and analysing how the differences with the current exploitation of the LNG-PS can be addressed.

The sub-questions raised in this report are used to provide a comprehensive conclusion of the project. Together they contribute to delivering the research objective:

To determine how the current LNG-Peakshaver can be retrofitted to receive, store and process liquid hydrogen in an energy-efficient way.

Each sub-question is covered in this chapter.

1. **What are the physical and chemical properties that influence the processes, and how do they vary between hydrogen and natural gas?**

Liquid hydrogen has a lot of similarities with liquefied natural gas; but there are also many differences in the properties of both substances. The properties of LH_2 that differ most from LNG and influence the process are discussed in chapter 3.

The most obvious property affecting the process is the temperature of LH_2, which is around 90 degrees Celsius lower than LNG. Due to the lower temperature, the formation of liquid oxygen is possible. Liquid oxygen is not acceptable in situations where chemicals are being processed because it causes hazardous situations. Therefore enhanced insulation is necessary when processing LH_2. For example, the LH_2 pipelines have to be vacuum insulated. The colder temperature also has an effect is on the material selection as some materials will become brittle. Therefore, the inner nickel-steel tank of the existing LNG storage tank cannot store LH_2. Stainless steel 304L or 316L is recommended for LH_2 application.

The insulation for an LH_2 tank has to be ten times better to reach the same boil-off rate as an LNG tank. This results from the lower temperature, but is primarily due to the lower value for the latent heat of vaporization of hydrogen.

The density of hydrogen in comparison with LNG is much smaller. In the liquid phase, the density of hydrogen is more than six times lower; in the vapour phase, it is almost eight times lower. The lower density influences the pumping and compression processes. Furthermore, it also has an effect on the energy density of hydrogen. Although the energy of LH_2 per unit mass is significantly larger than LNG, because of the low density, the energy per unit volume of hydrogen is 2,3 times lower than in the case of LNG. Therefore more volume capacity is needed in order to store the same amount of energy. If both tanks are used, the proposed LH_2 terminal can store 1150 TJ instead of 2700 TJ for LNG (given the HHV).

Processing hydrogen has other safety restrictions concerning the ATEX class for the process equipment. This is because of the large window for explosion danger when spilling hydrogen in the atmosphere and due to the fact that the minimum ignition energy is lower.

2. **Under which conditions is the liquid hydrogen delivered (by the large-scale maritime LH_2 vessels) to the proposed LH_2 terminal?**

The first designed large-scale LH_2 vessels will transport the liquid hydrogen in type-B tanks, meaning there is no pressure build-up inside the tanks. For this reason, the hydrogen will be delivered at a pressure just above

atmospheric, and a temperature of -253°C. Furthermore, it can be assumed that the para-hydrogen concentration will be above 98%, meaning the spin-isomer conversion will not lead to additional BOG at the LH_2 terminal.

3. **What are the process conditions for hydrogen in the hydrogen network?**

The proposed LH_2 terminal is assumed to supply the hydrogen to the Hydrogen Backbone. The maximum operating pressure of the Backbone is set at 50 bar, and the minimum temperature at 5°C. There are also quality specifications for the purity of the hydrogen; however, as LH_2 is extremely pure, this is not a constraint for the LH_2 terminal.

4. **Which factors impact the send-out capacity of the future LH_2 terminal and how does this influence the design of the terminal?**

A significant advantage of an LH_2 import terminal is the easily adjustable send-out rate of the terminal. In this way, an LH_2 terminal can provide flexibility to the hydrogen grid, which is not possible for the other hydrogen carriers. Offering flexibility is valuable for the hydrogen grid, for example, to absorb the fluctuating hydrogen production from wind energy in the Netherlands. However, since the hydrogen import is considered contractually bound in the initial phase of H_2 import, it is necessary also to have a baseload hydrogen supply to the grid. For this reason, a terminal that can deliver a baseload to the grid, with also additional capacity to offer flexibility to the grid, is most desired. The baseload and maximum send-out capacity (Peakshaver + baseload) are defined in section 4.3.

5. **What type of process equipment is suited to process LH_2, considering the process conditions of the terminal and can the current LNG equipment be reused for this?**

The LNG process equipment is not suitable for handling the LH_2 processes because the properties of LH_2 differ too much from those of LNG.

LH_2 pump
The designs for the LH_2 pumps are very similar to those for LNG applications, but for LH_2 special inducers are required to prevent cavitation damage in the centrifugal pumps. Furthermore, three pot mounted pumps (HP-pump) in series are needed to increase the LH_2 pressure to 50 bar. This is due to the lower density of LH_2, resulting in a smaller head delivered by the centrifugal pump. For LNG, only one HP-pump is sufficient to increase the pressure up to 80 bar.

BOG compressor
Currently, BOG compressor manufacturers are not able to design compressors to operate below -170°C. This is mainly because they only design BOG compressors for LNG applications. Extensive research is needed to determine whether hydrogen compression at lower temperatures is possible with regard to material selection and the hydrogen density problem. The rapidly decreasing density of hydrogen BOG at a slight temperature rise under these extremely low temperature conditions is considered a problem to be overcome. Furthermore, for the BOG compressor, a reciprocating type of compressor is considered. Developing this "cold" compressor is essential for the LH_2 terminal, as it will significantly improve the terminal's efficiency.

Vaporizers
To evaporate the LH_2, a so-called Super-ORV is selected. This heat exchanger utilizes seawater as the heat source. The super-ORV is an enhanced ORV design to improve the heat transfer as it minimizes the ice formation at the outside of the tubes. Since the temperature of LH_2 is lower, this type of design is considered the most promising. However, note that this process component is not yet developed for LH_2 application.

6. **Can the LNG storage tank be retrofitted to store LH_2 and if so, how can this be achieved?**

The aim is to reuse the current LNG storage tank. Due to the lower temperature of LH_2, the tank has to be retrofitted, as the insulation and the material of the inner tank are not suited for LH_2 storage. Two insulation techniques have been investigated, a vacuum design and implementing membrane technology at the inside of the current LNG tank. The existing LNG tank cannot be reused for the vacuum designed tank, only the concrete construction could be reused. An advantage of using a vacuum insulated tank is that the BOR will be very low, 0,043%/day.

The other solution, implementing membrane insulation panels on the inside of the LNG tank, does offer the possibility to reuse the entire LNG tank. This makes it a relatively cheaper solution, however the BOR of the retrofitted tank is higher, namely 0,31%/day. Adding additional insulation at the inside of the LNG storage tank seems feasible because the density of LH_2 is considerably lower than LNG, which provide the opportunity to add mass at the inside of the tank. Nevertheless, further research is required to determine the feasibility of this conversion solution.

7. **What are the required para- and ortho-hydrogen conditions for the supply to the Hydrogen Backbone and how does this affect the processes at the terminal?**

It is concluded that the para- to ortho-hydrogen conversion is not desired at the terminal, as long as there is no grid requirement on this topic. Although the HHV of the supplied para-hydrogen is in the worst case 0,36% lower than "normal" hydrogen, accommodating the catalytic endothermic conversion reaction at the terminal requires a significant amount of additional process equipment and power input. These factors make it unfeasible to have this conversion at the terminal site.

8. **What is the potential of utilizing the thermal exergy during LH_2 regasification?**

The thermal exergetic potential of LH_2 is a considerable value, namely 5,2% of the total exergy. In comparison, for LNG, it is 0,9%. Therefore, utilizing this thermal exergy is an important factor to look into. In this research employing power cycles are investigated to utilize the cold exergy. Implementing these power cycles is possible because a baseload send-out capacity is assumed. It has been concluded that using a nitrogen and a methane Rankine cycle in series is the most suitable way of recovering the cold exergy. The overall thermal efficiency of these two cycles in series is equal to 64,2%. By recovering the cold exergy in this way, the LH_2 terminal can be energy positive. Considering the environmental regulations, this could be desired; however, additional process equipment is needed to accommodate these power cycles.

9. **What are the possibilities for processing the LH_2 and related boil-off gas most efficiently and what is the total energy consumption?**

A more detailed evaluation of the various configurations is provided in section 12. However, considering the baseload requirements of the terminal, it is concluded that the Recondenser-model in combination with the retrofitted membrane insulated storage tank is the most promising. Due to the recondenser, the BOG flow can be processed relatively efficient. Therefore, the additional BOG due to the higher BOR of the membrane tank has little effect on the overall efficiency losses of the terminal. And the membrane retrofitted storage tank will be considerably cheaper than the newly constructed vacuum tank.

When a requirement of the LH_2 terminal is a low minimum send-out rate, in that case, the Cold-model is desired with a vacuum tank design. The minimum flow of the terminal is low, and it processes the BOG relatively efficient. However, note that these two configurations require compressors that can handle temperatures as low as -252 °C.

Extensive research is necessary to determine the cost-efficiency of utilizing cold exergy with power cycles. If these results are promising or, in case the terminal would be a pilot terminal to show the benefits of LH_2, employing the PC-model (Power cycle) would be of great interest.

14 Recommendation

In this chapter, the recommendations are outlined. The recommendations are regarding follow-up research for Gasunie to be able to handle LH_2 at the LNG-PS in the future and for their Hydrogen Backbone. In addition, recommendations are provided for the industry.

Gasunie

- The energy efficiency for the different terminal configurations has been evaluated in this study. With these results, a selection has been made with regard to the best terminal configuration. However, to determine which terminal configuration is the most feasible to build, it is vital to examine the cost-efficiency. An important factor to be defined is the costs for the (retrofitted) storage tanks. Furthermore, analysing the cost efficiency for the power cycles is of great interest to determine if this is a feasible solution.
- In this study, the scale of the terminal is based on the two existing storage tanks, as the reuse of these tanks is considered desirable. However, before it is possible to determine whether retrofitting these tanks for LH_2 application is desirable, it is crucial to decide on the wanted storage capacity of a future LH_2 terminal, as there is limited space to build storage tanks. The desired storage capacity is influenced by various factors described in section 4.3. One factor necessary to determine is the send-out function of the terminal, for example, the peakshaver function. Therefore, follow-up research is advised to investigate the required storage capacity and send-out function of a future LH_2 terminal. Besides the storage tank, the desired send-out function also significantly influences the process equipment selection.
- Recommendations for the specifications of the Hydrogen Backbone constructed by Gasunie. Currently, the minimum hydrogen inlet temperature to the grid is set at 5°C, which is similar to the natural gas grid. For the natural gas grid, this value is set at 5°C to make sure the gas will not drop below 0°C as a result of the positive JT-coefficient. Due to the positive JT-coefficient, the temperature of natural gas decreases when transporting through pipelines. However, for hydrogen gas in the grid, the JT-coefficient is negative, meaning the temperature increases slightly when transporting through pipes. Therefore, an inlet temperature of 0°C for the Hydrogen Backbone needs to be considered. This would improve the efficiency of the LH_2 terminal.
- No requirements have been defined on the para-hydrogen concentration for the Hydrogen Backbone. However, the energy content of para-hydrogen is slightly lower than "normal" hydrogen (0,36% of the HHV). It is recommended for Gasunie to make a decision on this topic.
- In this research, safety requirements have not been considered, however this is essential to be able to build an LH_2 terminal. One of the topics which must be addressed is determining the safety zone for a large-scale LH_2 storage tank. This is vital to decide on whether both storage tanks are available for LH_2 storage. Nevertheless, at the moment, there are no regulations set on this topic.
- Synergy with nearby plants is not considered. Nevertheless, utilizing heat waste or maybe other synergy possibilities could improve the LH_2 terminal case significant. Therefore it is recommended to investigate these options.

For industry in general

- The retrofit solution of the LNG storage tank with membrane insulation panels is very promising. Investigating whether this solution is feasible is valuable for a transition from LNG into a fossil-free LH_2 industry.
- Besides the LH_2 pumps (which can be delivered by Nikkiso Cryo Inc.), additional research is required for the BOG compressor, Super-ORV and vacuum insulated pipelines.

  Currently, the BOG compressors cannot operate below -170°C. However, utilizing a compressor that can handle temperatures as low as -250°C would significantly increase the efficiency of an LH_2 terminal. Therefore it is considered vital to develop these compressors for future LH_2 terminals.

It is assumed that the Super-ORV is a well-suited solution for the evaporation process. However, the existing equipment is dedicated to LNG applications. Therefore, research is needed to develop a Super-ORV dedicated to LH_2 usage.

Operating equipment in vacuum insulated pipelines (such as valves) with a diameter greater than 10 inches is not commercially available. Since the LH_2 terminal requires vacuum-insulated piping up to 32 inches in diameter, it is necessary to develop this equipment.

- The thermal exergy of LH_2 is a significant factor of the total exergy, namely 5,2% (for LNG, it is only 0,9%). There are multiple options available to utilize this exergy. An in-depth study to define suitable solutions to recover the thermal exergy would be of great interest for an LH_2 terminal. Usually, thermal exergy recovery is not feasible considering the cost efficiency. However, developing a universal exergy recovery process, which can be applied to any LH_2 terminal, can lower the CAPEX, potentially making it a viable solution.

References

[1] M. Farid, M. Keen, M. Papaioannou, I. Parry, C. Pattillo, and A. Ter, "After Paris: Fiscal, Macroeconomic, and Financial Implications of Climate Change," tech. rep., 2016.

[2] E. Union.

[3] Commission European, "A European Green Deal." https://ec.europa.eu/info/strategy/priorities-2019-2024/european-green-deal. Accessed: 2020-07-03.

[4] A. van Wijk, "The Green Hydrogen Economy in the Northern Netherlands," tech. rep., 2017. http://profadvanwijk.com/wp-content/uploads/2017/04/NIB-BP-EN-DEF-webversie.pdf.

[5] Ministerie van Economische Zaken en Klimaat, "Kabinetsvisie Waterstof," tech. rep., 2020. https://www.rijksoverheid.nl/documenten/kamerstukken/2020/03/30/kamerbrief-over-kabinetsvisie-waterstof.

[6] Deltalinqs, "Annexes to the H-vision Main Report," pp. 1–110, 2019.

[7] N. Rijk and J. Van Dinther, "ROTTERDAM HYDROGEN HUB," tech. rep., 2019.

[8] J. Rotmans, "Hydrogen for the Port of Rotterdam in an International Context," tech. rep., 2020. https://www.portofrotterdam.com/sites/default/files/drift-hydrogen-for-the-port-of-rotterdam-in-an-international-context-a-plea-for-leadership.pdf?token=3ySt8rOD.

[9] E. Wiebes, "Beantwoording feitelijke vragen Kabinetsvisie waterstof," tech. rep., 2020. https://www.rijksoverheid.nl/documenten/kamerstukken/2020/06/04/beantwoording-kamervragen-over-kabinetsvisie-waterstof.

[10] Port of Rotterdam, "WATERSTOF ECONOMIE IN ROTTERDAM START MET BACKBONE," 2020. https://www.portofrotterdam.com/sites/default/files/waterstofeconomie-in-rotterdam-factsheet.pdf?token=-ZrjwJcp.

[11] M. P. Bailey, "Large-scale green-hydrogen project under development in Oman." https://www.chemengonline.com/large-scale-green-hydrogen-project-under-development-in-oman/, 2021. Accessed: 2021-06-16.

[12] L. Collins, "Growing ambition: the world's 22 largest green-hydrogen projects." https://www.rechargenews.com/energy-transition/growing-ambition-the-worlds-22-largest-green-hydrogen-projects/2-1-933755, 2020. Accessed: 2021-06-16.

[13] A. van Wijk and F. Wouters, "50% Hydrogen for Europe: a manifesto – A sustainable energy supply for everyone," 2019. http://profadvanwijk.com/50-hydrogen-for-europe-a-manifesto/.

[14] J. R. Bartels and M. B. Pate, A feasibility study of implementing an ammonia economy. PhD thesis, 2008. https://lib.dr.iastate.edu/etd/11132.

[15] R. Moradi and K. M. Groth, "Hydrogen storage and delivery: Review of the state of the art technologies and risk and reliability analysis," International Journal of Hydrogen Energy, vol. 44, no. 23, pp. 12254–12269, 2019.

[16] The Royal Society, Ammonia: zero-carbon fertiliser, fuel and energy store. Policy Briefing. 2020. https://royalsociety.org/topics-policy/projects/low-carbon-energy-programme/green-ammonia/.

[17] USDrive, "Hydrogen Delivery Technical Team Roadmap," tech. rep., 2013. https://www.energy.gov/sites/prod/files/2014/02/f8/hdtt_roadmap_june2013.pdf.

[18] M. Niermann, S. Drünert, M. Kaltschmitt, and K. Bonhoff, "Liquid organic hydrogen carriers (LOHCs)-techno-economic analysis of LOHCs in a defined process chain," Energy and Environmental Science, vol. 12, no. 1, pp. 290–307, 2019.

[19] Air liquide, "Comparator | Gas Encyclopedia Air Liquide." https://encyclopedia.airliquide.com/compare-tool. Accessed: 2020-11-02.

[20] E. Kennedy, J. M. Botero, and J. Zonneveld, "Hydrohub HyChain 3," 2019.

[21] R. Terwel and J. Kerkhoven, "HyChain 2," tech. rep., 2019.

[22] Ø. Sekkesaeter, "Evaluation of Concepts and Systems for Marine Transportation of Hydrogen," tech. rep., 2019.

[23] R. Drnevich, "Hydrogen Delivery, Liquefaction & Compression," 2003. https://www1.eere.energy.gov/hydrogenandfuelcells/pdfs/liquefaction_comp_pres_praxair.pdf.

[24] U. Bossel and B. Eliasson, "Energy and Hydrogen Economy," tech. rep., 2002. https://afdc.energy.gov/files/pdfs/hyd_economy_bossel_eliasson.pdf.

[25] R. Agarwal, T. J. Rainey, S. M. Ashrafur Rahman, T. Steinberg, R. K. Perrons, and R. J. Brown, "LNG regasification terminals: The role of geography and meteorology on technology choices," Energies, vol. 10, no. 12, 2017.

[26] L. Yin and Y. Ju, "Review on the design and optimization of hydrogen liquefaction processes," Frontiers in Energy, vol. 14, no. 3, pp. 530–544, 2020.

[27] NCE MARITIME CLEANTECH, "Norwegian future value chains for liquid hydrogen," tech. rep., 2019. https://maritimecleantech.no/wp-content/uploads/2016/11/Report-liquid-hydrogen.pdf?fbclid=IwAR3uqivsh0dF3_VBQd8UB_0cgVtnf3XIM1of2xG7Y2WAS07e3OHzoTT-_9Q.

[28] GTS, "Het Transportnetwerk › Gasunie Transport Services." https://www.gasunietransportservices.nl/netwerk-operations/het-transportnetwerk. Accessed: 2020-12-18.

[29] Gasunie, "Waterstofbackbone › Gasunie New Energy." https://www.gasunienewenergy.nl/projecten/waterstofbackbone. Accessed: 2021-06-16.

[30] Dutch Government, "Afbouw gaswinning Groningen | Gaswinning in Groningen." https://www.rijksoverheid.nl/onderwerpen/gaswinning-in-groningen/afbouw-gaswinning-groningen, 2020. Accessed: 2021-06-15.

[31] Hydrogen Europe, "Vision on the Role of Hydrogen and Gas Infrastructure on the Road Toward a Climate Neutral Economy - A Contribution to the Transition of the Gas Market," no. April, 2019.

[32] NOS, "Kabinet: Gasunie gaat gasnetwerk ombouwen voor waterstof uit windenergie," 2021.

[33] Gasunie, "Webinar Hydrogen Infrastructure," 2020. https://www.gasunienewenergy.nl/projecten/waterstofbackbone/marktconsultatie.

[34] Port Of Rotterdam, "Havenmeester Havenkaart." https://portofrotterdam.maps.arcgis.com/apps/webappviewer/index.html?id=19a593c767cc4142a4ef07ac3fa7fbd8. Accessed: 2020-12-18.

[35] EMO, "About us - Europees Massagoed Overslag BV." https://www.emo.nl/en/about-us/. Accessed: 2020-12-17.

[36] E. De Rademaeker, B. Fabiano, S. S. Buratti, S. Rath, and M. Krol, "Comparative Risk Assessment for Different LNG-Storage Tank Concepts," The Italian Association of Chemical Engineering, pp. 103–108, 2013.

[37] A. Tandiroglu, "Temperature-dependent thermal conductivity of high strength lightweight raw perlite aggregate concrete," International Journal of Thermophysics, vol. 31, pp. 1195–1211, jun 2010.

[38] M. Strijbosch, "LNG-installatie," 2011. N.V. Nederlandse Gasunie.

[39] Engineering ToolBox, "Engineering ToolBox." https://www.engineeringtoolbox.com/. Accessed: 2020-11-02.

[40] H2tools, "Basic Hydrogen Properties | Hydrogen Tools." https://h2tools.org/hyarc/hydrogen-data/basic-hydrogen-properties. Accessed: 2020-10-07.

[41] Air Products, "Liquid hydrogen - Safetygram 9," tech. rep., 2014. https://www.airproducts.com/~/media/Files/PDF/company/safetygram-9.pdf.

[42] DESFA, "LNG Quality Specifications." www.desfa.gr/en/regulated-services/lng/users-information-lng/quality-specifications. Accessed: 2020-10-07.

[43] GIIGNL, "Basic Properties of LNG," 2019. https://giignl.org/sites/default/files/PUBLIC_AREA/About_LNG/4_LNG_Basics/giignl2019_infopapers1.pdf.

[44] R. Derwent, P. Simmonds, S. O'Doherty, A. Manning, W. Collins, and D. Stevenson, "Global environmental impacts of the hydrogen economy," International Journal of Nuclear Hydrogen Production and Applications, vol. 1, no. 1, p. 57, 2006.

[45] B. Vogel, T. Feck, J. U. Grooß, and M. Riese, "Impact of a possible future global hydrogen economy on Arctic stratospheric ozone loss," Energy and Environmental Science, vol. 5, no. 4, pp. 6445–6452, 2012.

[46] G. Myhre, D. Shindell, F.-M. Bréon, W. Collins, J. Fuglestvedt, J. Huang, D. Koch, J.-F. Lamarque, D. Lee, B. Mendoza, T. Nakajima, A. Robock, G. Stephens, T. Takemura, and H. Zhang, "Anthropogenic and natural radiative forcing," in Climate Change 2013 – The Physical Science Basis: Working Group I Contribution to the Fifth Assessment Report of the Intergovernmental Panel on Climate Change, pp. 659–740, 2013. doi: 10.1017/CBO9781107415324.018.

[47] UF, "Liquid Oxygen » Environmental Health & Safety » University of Florida." http://www.ehs.ufl.edu/programs/lab/cryogens/oxygen/, 2016.

[48] Hydrogen Tools, "Vacuum-Jacketed Piping | Hydrogen Tools." https://h2tools.org/bestpractices/vacuum-jacketed-piping. Accessed: 2020-12-02.

[49] Q. FAN and G. MANI, "12 - Dyeable polypropylene via nanotechnology," in Nanofibers and Nanotechnology in Textiles (P. J. Brown and K. Stevens, eds.), Woodhead Publishing Series in Textiles, pp. 320–350, Woodhead Publishing, 2007.

[50] B. Tesfa, F. Gu, R. Mishra, and A. D. Ball, "LHV predication models and LHV effect on the performance of CI engine running with biodiesel blends," Energy Conversion and Management, vol. 71, pp. 217–226, 2013.

[51] A. v. Wijk, "Verbal communication, supervisor TU Delft," 2021.

[52] O. R. Hansen, "Liquid hydrogen releases show dense gas behavior," International Journal of Hydrogen Energy, vol. 45, pp. 1343–1358, 1 2020.

[53] Ventinet, "ATEX informatie - VENTINET." https://ventinet.nl/kennisbank/general-atex-information/, 2018.

[54] D. Jonah, "The Joule-Thomson Effect | Sandhill Analytics." https://www.sandhillanalytics.com/cfdanywhere/joule-thomson. Accessed: 2020-12-02.

[55] The Editors of Encyclopaedia Britannica, "Joule-Thomson effect," Encyclopædia Britannica, 2017. https://www.britannica.com/science/Joule-Thomson-effect.

[56] D. Haeseldonckx, Concrete transition issues towards a fully-fledged use of hydrogen as an energy carrier. PhD thesis, 2009.

[57] D. Haeseldonckx and W. D'haeseleer, "The use of the natural-gas pipeline infrastructure for hydrogen transport in a changing market structure," International Journal of Hydrogen Energy, vol. 32, pp. 1381–1386, 7 2007.

[58] G. Buntkowsky, B. Walaszek, A. Adamczyk, Y. Xu, H. H. Limbach, and B. Chaudret, "Mechanism of nuclear spin initiated para-H2 to ortho-H 2 conversion," Physical Chemistry Chemical Physics, vol. 8, pp. 1929–1935, 4 2006.

[59] G. Petitpas, S. M. Aceves, M. J. Matthews, and J. R. Smith, "Para-H2 to ortho-H2 conversion in a full-scale automotive cryogenic pressurized hydrogen storage up to 345 bar," International Journal of Hydrogen Energy, vol. 39, pp. 6533–6547, 4 2014.

[60] B. P. Pedrow, "PARAHYDROGEN-ORTHOHYDROGEN CONVERSION ON CATALYST LOADED SCRIM FOR VAPOR COOLED SHIELDING OF CRYOGENIC STORAGE VESSELS," tech. rep., 2016.

[61] A. Laouir, "Performance analysis of open-loop cycles for LH2 regasification," International Journal of Hydrogen Energy, vol. 44, pp. 22425–22436, 8 2019.

[62] H. You, J. Ahn, S. Jeong, and D. Chang, "Effect of ortho-para conversion on economics of liquid hydrogen tanker with pressure cargo tanks," Ships and Offshore Structures, vol. 13, pp. 79–85, 2018.

[63] A. Züttel, A. Borgschulte, and L. Schlapbach, "Hydrogen as a Future Energy Carrier - Google Boeken," in Hydrogen as a Future Energy Carrier, pp. 165 – 172, 2008.

[64] E. Karlsson, Catalytic ortho- to Para-Hydrogen conversion in liquid hydrogen. PhD thesis, 2017.

[65] O. S. Burheim, "Hydrogen for Energy Storage," in Engineering Energy Storage, pp. 147–192, Academic Press, jan 2017.

[66] S. Kamiya, M. Nishimura, and E. Harada, "Study on introduction of CO2 free energy to Japan with liquid hydrogen," Physics Procedia, vol. 67, no. July, pp. 11–19, 2015.

[67] M. Wanner, "Process and device for determining the para content of a hydrogen gas stream," 1996. United States Patent (19); nr: 5,580,793.

[68] R. N. Brown, Compressors selection and sizing | Second edition. Butterworth-Heinemann, 1997.

[69] M. Giardino, "Test Facility Barges and Boats - NasaCRgis." https://crgis.ndc.nasa.gov/historic/Test_Facility_Barges_and_Boats, 2010.

[70] J. Ahn, H. You, J. Ryu, and D. Chang, "Strategy for selecting an optimal propulsion system of a liquefied hydrogen tanker," International Journal of Hydrogen Energy, vol. 42, pp. 5366–5380, 2 2017.

[71] Baird Maritime, "VESSEL REVIEW | Suiso Frontier – Japanese LH2 carrier sets the pace in hydrogen transport - Baird Maritime." https://www.bairdmaritime.com/ship-world/tanker-world/gas-tanker-world/vessel-review-suiso-frontier-japanese-lh2-carrier-sets-the-pace-in-hydrogen-transport/, 2021. Accessed: 2021-06-14.

[72] G. Giacomazzi and J. Gretz, "Euro-Quebec Hydro-Hydrogen Project (EQHHPP): a challenge to cryogenic technology," Cryogenics, vol. 33, no. 8, pp. 767–771, 1993.

[73] U. Petersen and R. Krapp, "DESIGN AND SAFETY CONSIDERATIONS FOR LARGE-SCALE SEABORNE HYDROGEN TRANSPORT," Tech. Rep. 7, 1994.

[74] A. Abe, M. Nakamura, . I. Sato, H. Uetanq, and T. Fujitanit, "STUDIES OF THE LARGE-SCALE SEA TRANSPORTATION OF LIQUID HYDROGEN," Tech. Rep. 2, 1998.

[75] MossMaritime, "Liquid Hydrogen Bunker Vessel," no. March, 2019.

[76] THE MARITIME EXECUTIVE, "World's First Liquefied Hydrogen Carrier Launched." https://www.maritime-executive.com/article/world-s-first-liquefied-hydrogen-carrier-launched, 2019. Accessed: 2021-06-14.

[77] B. Jha, "LNG Tankers - Different Types And Dangers Involved." https://www.marineinsight.com/types-of-ships/lng-tankers-different-types-and-dangers-involved/, 2019. Accessed: 2020-11-25.

[78] S. Chakraborty, "Understanding The Design of Liquefied Gas Carriers." https://www.marineinsight.com/naval-architecture/understanding-design-liquefied-gas-carriers/, 2020. Accessed: 2020-11-25.

[79] De wereld van waterstof, "Infrastructuur - Longread Waterstof." https://www.dewereldvanwaterstof.nl/gasunie/infrastructuur/, 2019. Accessed: 2020-10-08.

[80] Gasunie, "Hydrogen backbone." https://www.gasunie.nl/en/expertise/hydrogen/hydrogen-backbone, 2021. Accessed: 2021-06-28.

[81] J. Miyazaki, T. Kajiyama, K. Matsumoto, H. Fujiwara, and M. Yatabe, "Ultra high purity hydrogen gas supply system with liquid hydrogen," International Journal of Hydrogen Energy, vol. 21, no. 5, pp. 335–341, 1996.

[82] A. d. Bakker, "Verbal communication, supervisor Gasunie," 2021.

[83] S. Ruester, "Changing contract structures in the international liquefied natural gas market: A first empirical analysis," Revue d'Economie Industrielle, vol. 127, no. 3, pp. 89–112, 2009.

[84] A. Pavlou, Factors Determining LNG Throughput at the Port of Rotterdam. PhD thesis, 2014.

[85] Maersk, "Search for Shipping and Vessel Schedules." https://www.maersk.com/schedules/pointToPoint. Accessed: 2021-03-26.

[86] AIS Marine Traffic, "MarineTraffic: Global Ship Tracking Intelligence | AIS Marine Traffic." https://www.marinetraffic.com/. Accessed: 2021-03-26.

[87] L. Bachus, "Everything You Need to Know about NPSH, and Some Things you Didn't." https://empoweringpumps.com/everything-you-need-to-know-about-npsh-and-some-things-you-didnt/, 2020. Accessed: 2021-03-30.

[88] L. van Cappellen, H. Croezen, and F. Rooijers, "Feasibility study into blue hydrogen," tech. rep., 2018.

[89] J. W. Fawcett, "H21 North of England," tech. rep., 2018. doi: 10.1093/nq/s12-V.99.317-i.

[90] Gasunie, "Data offshore wind energy 2015 | not publicly available," 2015.

[91] P. De Laat, "Overview of Hydrogen Projects in the Netherlands - TKI Nieuw Gas," 2020. https://www.topsectorenergie.nl/sites/default/files/uploads/TKIGas/publicaties/OverviewHydrogenprojectsintheNetherlandsversie1mei2020.pdf.

[92] Gasunie, "Moving towards 2030 and 2050 with hydrogen - handout," 2016.

[93] C. J. Lee, Y. Lim, C. Park, S. Lee, and C. Han, "Synthesis of unloading operation procedure for a mixed operation of above-ground and in-ground liquefied natural gas storage tanks using dynamic simulation," Industrial and Engineering Chemistry Research, vol. 49, no. 17, pp. 8219–8226, 2010.

[94] S. Mokhatab, J. Y. Mak, J. V. Valappil, and D. A. Wood, "Chapter 6: Process Control and Automation of LNG Plants and Import Terminals," in Handbook of Liquefied Natural Gas, pp. 259–296, 2014.

[95] M. W. Shin, D. Shin, S. H. Choi, E. S. Yoon, and C. Han, "Optimization of the operation of boil-off gas compressors at a liquified natural gas gasification plant," Industrial and Engineering Chemistry Research, vol. 46, no. 20, pp. 6540–6545, 2007.

[96] Y. Li and Y. Li, "Dynamic optimization of the Boil-Off Gas (BOG) fluctuations at an LNG receiving terminal," Journal of Natural Gas Science and Engineering, vol. 30, pp. 322–330, 2016.

[97] M. Zlatkovikj, Using cold energy of the LNG in the integrated process of gasification and electric energy production. PhD thesis, 2017. https://fenix.tecnico.ulisboa.pt/downloadFile/281870113704248/ThesisMilanZlatkovikjFinal.pdf.

[98] JAXA, "World's First Loading Arm for Ship-to-Shore Transfer of Liquefied Hydrogen Developed." https://global.jaxa.jp/press/2019/04/20190418a.html, 2019. Accessed: 2021-05-23.

[99] A. Benito, "Accurate determination of LNG quality unloaded in Receiving Terminals: An Innovative Approach," 2009.

[100] Dobrota, B. Lalić, and I. Komar, "Problem of Boil - off in LNG Supply Chain," Transactions on Maritime Science, vol. 2, no. 2, pp. 91–100, 2013.

[101] R. Sedlaczek, Boil-off in large- and small-scale LNG chains. PhD thesis, 2008. https://citeseerx.ist.psu.edu/viewdoc/download?doi=10.1.1.470.6116{&}rep=rep1{&}type=pdf.

[102] Demaco Holland B.V., "Vacuum Insulated Transfer Lines (VIP)." https://demaco-cryogenics.com/products/vacuum-insulated-transfer-lines/. Accessed: 2021-05-19.

[103] Anup Kumar Deyin, "Pipe Schedule Chart: Pipe Schedule 40 dimensions." https://whatispiping.com/pipe-schedule/, 2016. Accessed: 2021-05-24.

[104] H. Arabnejad, S. A. Shirazi, B. S. Mclaury, and J. R. Shadley, "A guideline to calculate erosional velocity due to liquid droplets for oil and gas industry," in Proceedings - SPE Annual Technical Conference and Exhibition, vol. 7, pp. 4882–4893, Society of Petroleum Engineers (SPE), 2014.

[105] Ronald Dekker - Demaco, "Interview about vacuum insulated LH_2 pipes," 2021. verbal communication.

[106] Jan Bezuijen, "Verbal communication, Process engineer at LNG-PS," 2020.

[107] BRITISH STANDARD, "Installation and equipment for liquefied natural gas-Design of onshore installations," 2007. http://www.golng.eu/files/upload/10.1.1.470.7021.pdf.

[108] J. Andersson and S. Grönkvist, "Large-scale storage of hydrogen," International Journal of Hydrogen Energy, vol. 44, no. 23, pp. 11901–11919, 2019.

[109] C. San Marchi, "Metals for cryogenic hydrogen service," 2018. https://www.osti.gov/servlets/purl/1523775.

[110] H. Lee, Y. Shao, S. Lee, G. Roh, K. Chun, and H. Kang, "Analysis and assessment of partial reliquefaction system for liquefied hydrogen tankers using liquefied natural gas (LNG) and H2 hybrid propulsion," International Journal of Hydrogen Energy, vol. 44, pp. 15056–15071, 6 2019.

[111] De Vriese Robbé, "Static calculations LNG tank at LNG-PS | not publicly available," tech. rep., 1976.

[112] S. Jallais, "Pre-normative REsearch for Safe use of Liquid HYdrogen (PRESLHY)," tech. rep., 2018. https://www.hysafe.info/wp-content/uploads/sites/3/2018/09/PRESLHY-D2.3-LH2-Installation-description.pdf.

[113] M. Nishimura, "Interview regarding the LH2 terminal in Kobe, Japan," 2020. verbal communication.

[114] K. S. E. Flores, Study of Hydrogen Sorption/Desorption Effect on Austenitic Iron-Based Alloys. PhD thesis, 2019.

[115] F. Gregory, "Safety standard for hydrogen and hydrogen systems," tech. rep., 1997. https://ntrs.nasa.gov/api/citations/19970033338/downloads/19970033338.pdf.

[116] L. T. H. Nguyen, J. S. Hwang, M. S. Kim, J. H. Kim, S. K. Kim, and J. M. Lee, "Charpy impact properties of hydrogen-exposed 316l stainless steel at ambient and cryogenic temperatures," Metals, vol. 9, no. 625, pp. 1–14, 2019.

[117] K. M. Subodh and Z. G. John, "Review of Current State of the Art and Key Design Issues With Potential Solutions for Liquid Hydrogen Cryogenic Storage Tank Structures for Aircraft Applications," tech. rep., 2006. https://ntrs.nasa.gov/citations/20060056194.

[118] J. Sass, J. Fesmire, Z. F. Nagy, S. Sojourner, D. Morris, and S. Augustynowicz, "THERMAL PERFORMANCE COMPARISON OF GLASS MICROSPHERE AND PERLITE INSULATION SYSTEMS FOR LIQUID HYDROGEN STORAGE TANKS," Advances in Cryogenic Engineering: Transactions of the Cryogenic Engineering Conference — CEC, vol. 53, pp. 1375–1382, 2008.

[119] J. Zheng, L. Chen, J. Wang, X. Xi, H. Zhu, Y. Zhou, and J. Wang, "Thermodynamic analysis and comparison of four insulation schemes for liquid hydrogen storage tank," Energy Conversion and Management, vol. 186, no. December 2018, pp. 526–534, 2019.

[120] L. Hastings, A. Hedayat, and T. Brown, "Analytical modeling of variable density multilayer insulation for cryogenic storage," Tech. Rep. May, 2003.

[121] W. L. Johnson, "Optimization of layer densities for multilayered insulation systems," AIP Conference Proceedings, vol. 1218, no. 2010, pp. 804–811, 2010.

[122] Gaztransport Technigaz, "GST®, the membrane Full Integrity System for LNG Land Storage Tanks | GTT." https://gtt.fr/applications/land-storage. Accessed: 2021-06-01.

[123] Cryostar, "Email-contact," 2021.

[124] U.S. Department of Energy, "Pumps," in DOE Fundamentals Handbook: Mechanical Science, 1993. https://engineeringlibrary.org/reference/pumps-doe-handbook.

[125] NPTEL, "Mechanical Engineering - Fluid Machinery - Lecture 34." https://nptel.ac.in/courses/112/104/112104117/#, 2009. Accessed: 2021-05-15.

[126] Nikkiso Cryo Inc, "Email contact," 2021.

[127] M. Weeda, A. Elgowainy, M. Ball, R. B. Suez, A. Chmura, O. Ehret, T. Hasegawa, H. Iskov, H. Kurokawa, P. Mulard, A. Pigneri, M. Schiller, M. Sloth, and U. Hafseld, "Large-Scale Hydrogen Delivery Infrastructure," tech. rep., 2015. http://ieahydrogen.org/Activities/Task-28/Task-28-report_final_v2_ECN_12_2_v3.aspx.

[128] Cryostar, "Hydrogen Expanders and Pumps," 2019. https://www.sintef.no/globalassets/project/hyper/presentations-day-2/day2_1005_hautdidier_cryostar.pdf.

[129] Michael Smith Engineers, "Useful information on NPSH, NPSHA and NPSHR." https://www.michael-smith-engineers.co.uk/resources/useful-info/npsh. Accessed: 2021-05-15.

[130] Elliott Group, "Suction vessel mounted pumps." https://www.elliott-turbo.com/SuctionVesselMounted. Accessed: 2021-05-16.

[131] EnggCyclopedia, "How to read and use Pump Performance Curves." https://www.enggcyclopedia.com/2011/09/pump-performance-curves/. Accessed: 2021-05-15.

[132] E. S. Menon, "Series and parallel piping and power required," in Pipeline Planning and Construction Field Manual, ch. Chapter 9:, pp. 177–204, Elsevier Inc., 2011.

[133] "Optimal design of boil-off gas reliquefaction process in LNG regasification terminals," Computers and Chemical Engineering, vol. 117, no. March, pp. 171–190, 2018.

[134] A. Montemayor, J. D. Kumana, and S. P. Kothari, "Predict Storage Tank Heat Transfer Precisely," Chemical Engineering Magazine, pp. 1–16, 1982.

[135] M. Miana, R. Legorburo, D. Díez, and Y. H. Hwang, "Calculation of Boil-Off Rate of Liquefied Natural Gas in Mark III tanks of ship carriers by numerical analysis," Applied Thermal Engineering, vol. 93, no. October 2015, pp. 279–296, 2016.

[136] AMARINE-BLOG, "What is Boil off Gas and Estimating of BOG rate." https://amarineblog.com/2020/11/16/what-is-boil-off-gas-and-estimating-of-bog-rate/. Accessed: 2021-05-19.

[137] R. G. Scurlock, Stratification, Rollover and Handling of LNG, LPG and Other Cryogenic Liquid Mixtures. 2016.

[138] Neuman-Esser, "correspond by email - compressor manufacturer," 2021.

[139] Aspen Plus, "Aspen Plus | Leading Process Simulation Software | AspenTech." https://www.aspentech.com/en/products/engineering/aspen-plus. Accessed: 2021-05-05.

[140] S. S. Makridis, "Hydrogen storage and compression | Chapter 1," in Methane and Hydrogen for Energy Storage, pp. 1–28, 2016.

[141] E. Stamatakis, E. Zoulias, G. Tzamalis, Z. Massina, V. Analytis, C. Christodoulou, and A. Stubos, "Metal hydride hydrogen compressors: Current developments and early markets," Renewable Energy, vol. 127, pp. 850–862, 2018.

[142] J. Zou, N. Han, J. Yan, Q. Feng, Y. Wang, Z. Zhao, J. Fan, L. Zeng, H. Li, and H. Wang, "Electrochemical Compression Technologies for High-Pressure Hydrogen: Current Status, Challenges and Perspective," Electrochemical Energy Reviews, vol. 3, no. 4, pp. 690–729, 2020.

[143] E. A. Fosson, Design and analysis of a hydrogen compression and storage station. PhD thesis, 2017.

[144] Department of Energy, "Gaseous Hydrogen Compression." https://www.energy.gov/eere/fuelcells/gaseous-hydrogen-compression.

[145] H. Heshmat, "Oil-Free Centrifugal Hydrogen Compression Technology Demonstration," 2014. https://www.hydrogen.energy.gov/pdfs/review14/pd016_heshmat_2014_o.pdf.

[146] H. V. Reddy, V. S. Bisen, H. N. Rao, A. Dutta, S. S. Garud, I. A. Karimi, and S. Farooq, "Towards energy-efficient LNG terminals: Modeling and simulation of reciprocating compressors," Computers and Chemical Engineering, vol. 128, pp. 312–321, sep 2019.

[147] Burckhardt Compression, "Special designed compressor for the proposed terminal, designed by Burckhardt," 2021.

[148] Burckhardt Compression, "Laby ® Compressors - Contactless Labyrinth Sealing for highest availibility," tech. rep. https://www.burckhardtcompression.com/solution/compressor-technologies/laby-compressor/.

[149] Burckhardt Compression, "Process Gas Compressors - Comprehensive API 618 Compressor Portfolio," tech. rep., 2016. https://www.burckhardtcompression.com/solution/compressor-technologies/process-gas-compressor-api-618/.

[150] V. Chadha, A. G. Baruah, and S. Bhandari, "Capacity control of reciprocating compressors," 2016.

[151] JFE Engineering, "In-line BOG Recondenser," 2017.

[152] S. P. B. Lemmers, "Simplify BOG recondenser design and operation—Part 1." http://www.gasprocessingnews.com/features/201406/simplify-bog-recondenser-design-and-operation\T1\textemdashpart-1.aspx. Accessed: 2021-03-15.

[153] Mitsubishi Power Ltd., "Mitsubishi Power Commences Development of World's First Ammonia-fired 40MW Class Gas Turbine System – Targets to Expand Lineup of Carbon-free Power Generation Options, with Commercialization around 2025 –." https://power.mhi.com/news/20210301.html, 2021. Accessed: 2021-05-18.

[154] S. Patel, "Siemens' Roadmap to 100% Hydrogen Gas Turbines." https://www.powermag.com/siemens-roadmap-to-100-hydrogen-gas-turbines/, 2020. Accessed: 2021-05-18.

[155] D. H. program, "Hydrogen Fuel Cells," tech. rep., 2006.

[156] S. Marandi, F. Mohammadkhani, and M. Yari, "An efficient auxiliary power generation system for exploiting hydrogen boil-off gas (BOG) cold exergy based on PEM fuel cell and two-stage ORC: Thermodynamic and exergoeconomic viewpoints," Energy Conversion and Management, vol. 195, no. May, pp. 502–518, 2019.

[157] Y. A. Hussain, "Pressure Changers." https://www.just.edu.jo/{~}yahussain/files/pressurechangers.pdf, 2016. Accessed: 2021-05-20.

[158] N. Hall, "Enthalpy." https://www.grc.nasa.gov/www/k-12/airplane/enthalpy.html, 2015. Accessed: 2020-12-14.

[159] University of Florida, "Liquid Oxygen » Environmental Health & Safety » University of Florida." http://www.ehs.ufl.edu/programs/lab/cryogens/oxygen/, 2016. Accessed: 2020-05-04.

[160] Sumitomo, "LNG vaporizer | Sumitomo Precision Products Co., Ltd.." https://www.spp.co.jp/netsu/en/products/lng/. Accessed: 2020-12-13.

[161] Osaka Gas Co. Ltd, "High-performance open rack LNG vaporizer SUPERORV." https://www.osakagas.co.jp/en/rd/technical/1198901{_}6995.html. Accessed: 2021-05-12.

[162] A. Atienza-márquez, Exergy recovery from LNG-regasification for polygeneration of energy. PhD thesis, 2020.

[163] C. Qi, C. Yi, B. Wang, W. Wang, and J. Xu, "Thermal performance analysis and the operation method with low temperature seawater of super open rack vaporizer for liquefied natural gas," Applied Thermal Engineering, vol. 150, no. August 2017, pp. 61–69, 2019.

[164] A. Oosterkamp, "Study of soil heat transfer of a natural gas pipeline," International Journal of Offshore and Polar Engineering, vol. 27, no. 1, pp. 90–101, 2017.

[165] J. Essler, C. Haberstroh, H. T. Walnum, D. Berstad, P. Nekså, J. Stang, S. A. Energi, L. Decker, P. Treite, and L. A. Kryotechnik, "Report on Technology Overview and Barriers to Energy- and Cost-Efficient Large Scale Hydrogen Liquefaction," Tech. Rep. 278177, 2012.

[166] H. S. Taylor, "Catalysis." https://www.britannica.com/science/catalysis, 2018. Accessed: 2021-05-10.

[167] J. W. Leachman, R. T. Jacobsen, S. G. Penoncello, and E. W. Lemmon, "Fundamental equations of state for parahydrogen, normal hydrogen, and orthohydrogen," Journal of Physical and Chemical Reference Data, vol. 38, no. 3, pp. 721–748, 2009.

[168] R. M. Bliesner, Parahydrogen-Orthohydrogen Conversion for Boil-Off Reduction From Space Stage. PhD thesis, 2013.

[169] Molecular Products Inc., "Technical datasheet: Ionex® – Type O-P Catalyst." https://www.molecularproducts.com/wp-content/uploads/2017/02/OP-Catalyst-166{_}Rev-D{_}Technical-Datasheet{_}OP-Catalyst.pdf. Accessed: 2021-05-11.

[170] D. Weitzel, W. Loebenstein, J. Draper, and O. Park, "Ortho-para catalysis in liquid-hydrogen production," Journal of Research of the National Bureau of Standards, vol. 60, no. 3, p. 221, 1958.

[171] J. Eckroll, Concepts for Large Scale Hydrogen Liquefaction Plants. PhD thesis, 2017.

[172] M. Bracha, G. Lorenz, A. Patzelt, and M. Wanner, "Large-scale hydrogen liquefaction in Germany," International Journal of Hydrogen Energy, vol. 19, no. 1, pp. 53–59, 1994.

[173] G. Eigenberger, "Fixed-bed reactors," 1992.

[174] A. L. Woodcraft, "Predicting the thermal conductivity of aluminium alloys in the cryogenic to room temperature range," Cryogenics, vol. 45, no. 6, pp. 421–431, 2005.

[175] Gate terminal, "Technical datasheet: ORV at Gate terminal."

[176] E. A. Roszak and M. Chorowski, "Exergy analysis of combined simultaneous Liquid Natural Gas vaporization and Adsorbed Natural Gas cooling," Fuel, vol. 111, pp. 755–762, 2013.

[177] L. Zhao, J. Zhang, X. Wang, J. Feng, H. Dong, and X. Kong, "Dynamic exergy analysis of a novel LNG cold energy utilization system combined with cold, heat and power," Energy, vol. 212, p. 118649, 2020.

[178] I. Dincer and M. A. Rosen, "Chapter 3 - Chemical Exergy," in Exergy, pp. 37–40, 2013.

[179] "High-Level Interface — CoolProp 6.4.1 documentation." http://www.coolprop.org/coolprop/HighLevelAPI.html. Accessed: 2021-03-11.

[180] MATLAB, version 9.3.0 (R2017b). Natick, Massachusetts: The MathWorks Inc., 2017.

[181] A. Atienza-Márquez, J. C. Bruno, and A. Coronas, "Cold recovery from LNG-regasification for polygeneration applications," Applied Thermal Engineering, vol. 132, pp. 463–478, mar 2018.

[182] Y. Fujiwara, T. Asakura, T. Yamamoto, and M. Yamamoto, "LNG cold energy supply for CO2 reduction and energy conservation in Mitsui chemicals ethylene plant," in International Gas Research Conference Proceedings, pp. 1058–1073, 2011.

[183] K. Jiang, "Economic analysis of LNG cold energy utilization," in Energy Solutions to Combat Global Warming, vol. 33, pp. 119–132, Springer Verlag, 2017.

[184] A. Atienza-Márquez, J. C. Bruno, A. Akisawa, M. Nakayama, and A. Coronas, "Fluids selection and performance analysis of a polygeneration plant with exergy recovery from LNG-regasification," Energy, vol. 176, pp. 1020–1036, 2019.

[185] A. Atienza-Márquez, "Interview regarding thermal exergy utilization," 2021. verbal communication.

[186] T. Yamamoto and Y. Fujiwara, "The accomplishment of 100 % utilisation of LNG cold energy," in 25th World Gas Conference, pp. 1–19, 2012.

[187] R. F. García, J. C. Carril, J. R. Gomez, and M. R. Gomez, "Combined cascaded Rankine and direct expander based power units using LNG (liquefied natural gas) cold as heat sink in LNG regasification," Energy, vol. 105, pp. 16–24, 2016.

[188] J. M. Calm and G. C. Hourahan, "Physical, safety, and environmental data for refrigerants," HPAC Heating, Piping, Air Conditioning, vol. 71, no. 8, pp. 27–29, 1999.

[189] C. Sánchez, R. Juárez, J. Sanz, and M. Perlado, "Design and analysis of helium Brayton power cycles for HiPER reactor," in Fusion Engineering and Design, vol. 88, pp. 2679–2683, North-Holland, oct 2013.

[190] B. G. Miller, "Clean Coal Technologies for Advanced Power Generation," in Clean Coal Engineering Technology, pp. 251–300, Elsevier, jan 2011.

[191] E. D. Lavric, H. Weyten, J. De Ruyck, V. Pleşu, and V. Lavric, "Delocalized organic pollutant destruction through a self-sustaining supercritical water oxidation process," Energy Conversion and Management, vol. 46, no. 9-10, pp. 1345–1364, 2005.

[192] M. Mehrpooya, M. M. M. Sharifzadeh, and M. A. Rosen, "Optimum design and exergy analysis of a novel cryogenic air separation process with LNG (liquefied natural gas) cold energy utilization," Energy, vol. 90, pp. 2047–2069, 2015.

[193] A. R. Smith and J. Klosek, "A review of air separation technologies and their integration with energy conversion processes," Fuel Processing Technology, vol. 70, no. 2, pp. 115–134, 2001.

[194] S. Ivanova and R. Lewis, "Producing nitrogen via pressure swing adsorption," Chemical Engineering Progress, vol. 108, no. 6, pp. 38–42, 2012.

[195] Linde, "Nitrogen Generation by Pressure Swing Adsorption," tech. rep., 2016. https://www.linde-engineering.com/de/images/HA{_}N{_}1{_}1{_}e{_}09{_}150dpi{_}NB{_}tcm20-6131.pdf.

[196] H. Asakura, D. Kato, N. Saji, and H. Ohya, 80 K centrifugal compressor for helium refrigeration system, vol. 37. Publ by Plenum Publ Corp, 1991.

[197] Aspen, "Aspen simulation software." https://www.aspentech.com/. Accessed: 2020-12-18.

[198] K. I. Al-Malah, "Introducing Aspen Plus," in Aspen Plus®, pp. 1–47, John Wiley & Sons, Inc., sep 2016.

[199] Aspen Technology, "Aspen Plus ® : Process Simulation for Chemicals | Brochure," 2018.

[200] Aspen Technology Inc., "Aspen Physical Property System: Physical Property Methods," tech. rep., 2013.

[201] H. R. Azizabadi, M. Ziabasharhagh, and M. Mafi, "Applicability of the common equations of state for modeling hydrogen liquefaction processes in Aspen HYSYS," Gas Processing Journal, vol. 9, no. 1, pp. 11–27, 2021.

[202] Pumpfundamentals, "What is head?." https://www.pumpfundamentals.com/whatishead.htm, 2019. Accessed:2020-12-11.

[203] Hydrogen Fuel Cell Engines and Related Technologies, "Module 1: Hydrogen Properties," Hydrogen Fuel Cell Engines, p. 41, 2001. http://www1.eere.energy.gov/hydrogenandfuelcells/tech_validation/pdfs/fcm01r0.pdf.

[204] P. Islam, "Heat Exchangers." https://www.researchgate.net/profile/Md_Islam228/post/What_is_the_Heat_transfer_coefficient_in_case_of_cooling_at_280K_and_in_case_of_heating_at_380K/attachment/5a87761db53d2f0bba526cfc/AS%3A594817859985408%401518827037774/download/HeatExchangers.pdf.

[205] M. Y. Lee, "Innovative way to recondense boil-off-gas | Sulzer." https://www.sulzer.com/en/shared/about-us/innovative-way-to-recondense-boil-off-gas, 2017. Accessed: 2021-05-31.

[206] Y. E. Yuksel, M. Ozturk, and I. Dincer, "Analysis and assessment of a novel hydrogen liquefaction process," International Journal of Hydrogen Energy, vol. 42, no. 16, pp. 11429–11438, 2017.

[207] G. Valenti and E. Macchi, "Proposal of an innovative, high-efficiency, large-scale hydrogen liquefier," International Journal of Hydrogen Energy, vol. 33, no. 12, pp. 3116–3121, 2008.

[208] Kawasaki Heavy Ind., "Large Scale LH Supply Chain Project & H Gas Turbine Demonstration," 2019.

APPENDIX

A
Global overview of the processes at the LNG-Peakshaver

A.1 Process flow diagram LNG-PS

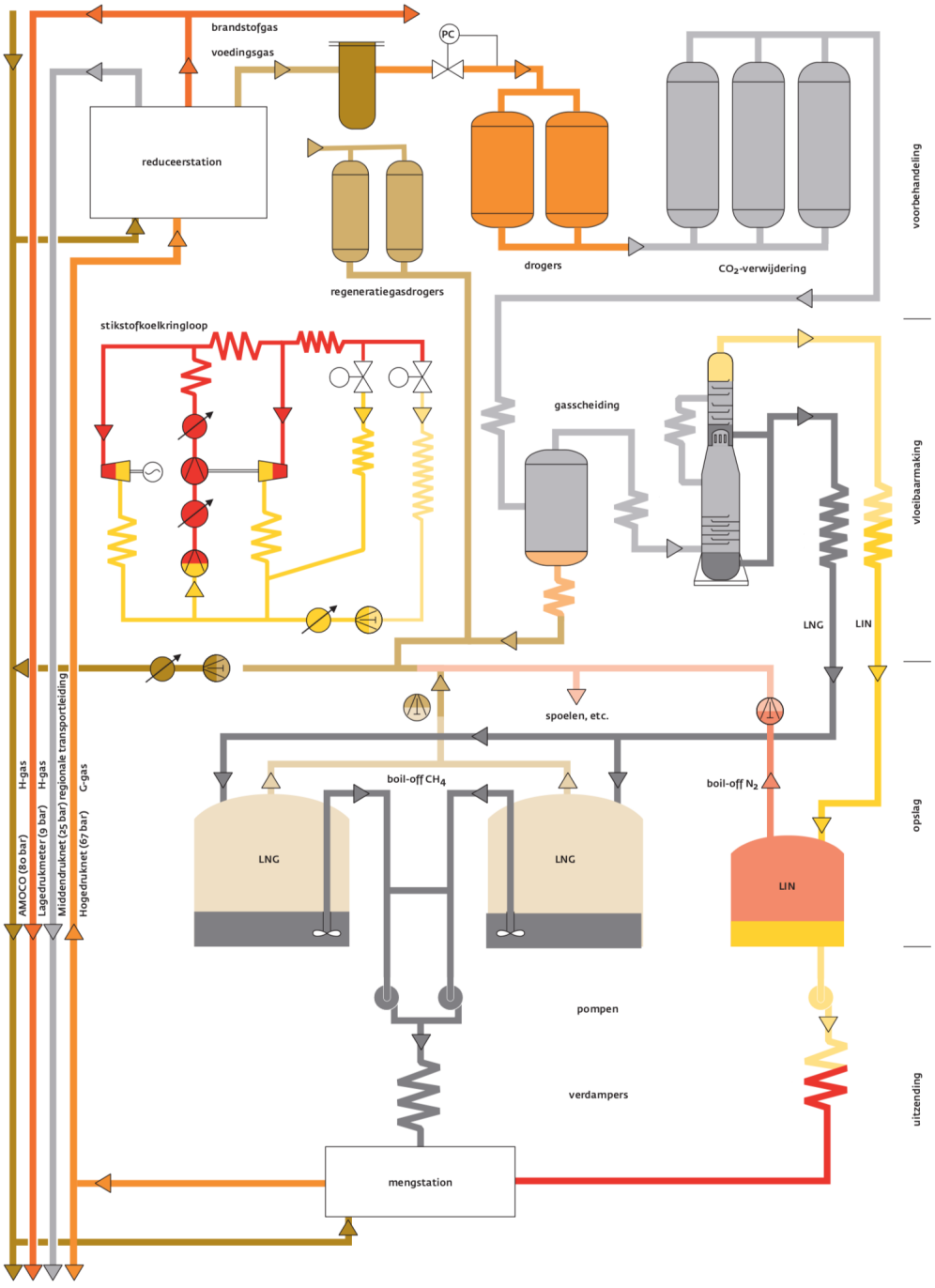

Figure 67: The process flow diagram of the LNG-PS [38].

B
Process equipment current LNG-PS

Process equipment data is confidential and not publicly available.

C
LH_2 centrifugal pump

C.1 Performance chart LH_2 centrifugal pumps CryoStar

In the figure below is a performance chart of the submerged centrifugal LH_2 pumps designed by CryoStar. Those submerged pumps have an electrical motor and a seal-less design, allowing cold stand-by for immediate start. The design is based on: API 610, ISO 13709 and IGC 11/82 [128].

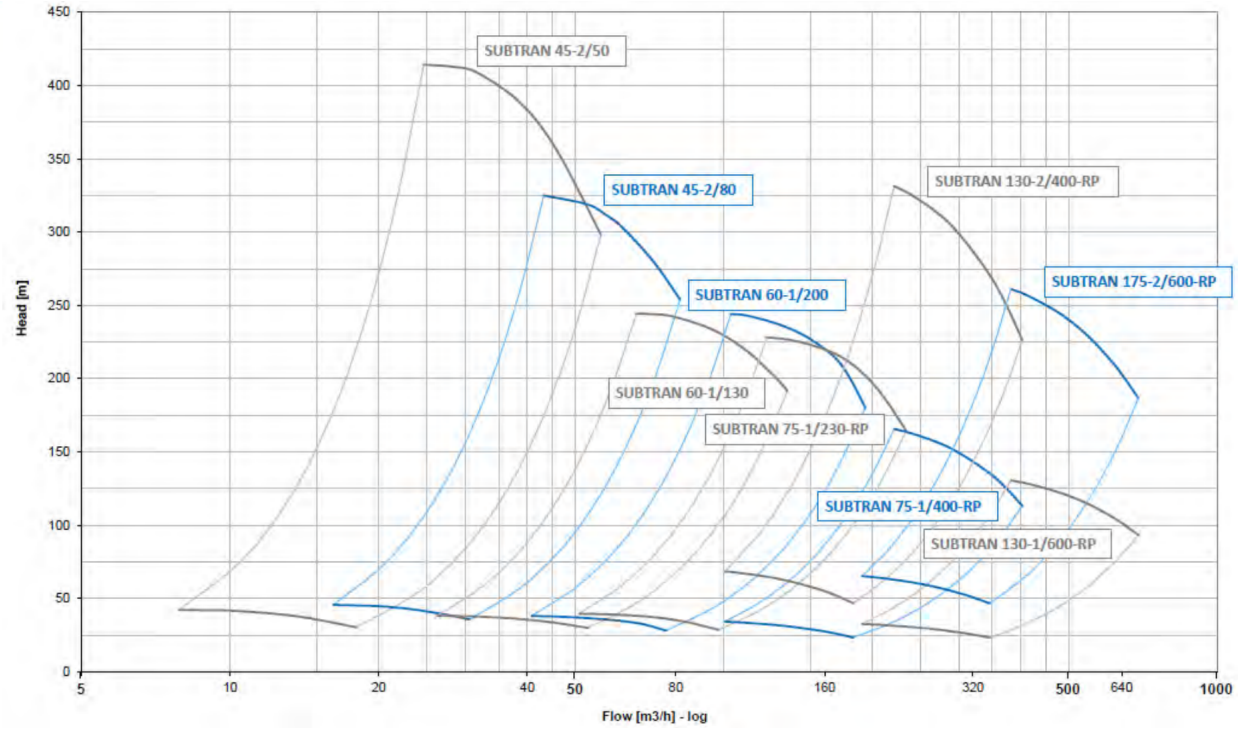

Figure 68: Performance chart of various centrifugal submersible pumps for liquid hydrogen by CryoStar [128].

From the figure it can be concluded that the SUBSTRAN 175-2/600-RP has a volume flow of around 600 m3/h, with a head of 225 meter. The head of the pump is another way to describe the pressure increase of the pump [202]. Calculating the head to the pressure increase can be done with formula 34. For a head of 225 meter, results in a pressure increase of 1,56 bar. Because the specific gravity of LH_2 is 0,0708 [203].

$$p = 0,0981 * h * SG \quad [Pa] \tag{34}$$

p	pressure (Pa)
h	head (m)
SG	specific gravity of the fluid

D Hydrogen Backbone

D.1 H_2 quality specification for the Hydrogen Backbone

Constituents	Specification 1	Specification 2	Specification 3	Opm.
Hydrogen fuel index	≥98,0 mol%	≥99,0 mol%	≥99,5 mol%	1
Total hydrocarbons including methane	≤1000 µmol/mol	≤1000 µmol/mol	≤1000 µmol/mol	2
Oxygen (O_2)	0,1-0,2 mol%	0,1-0,2 mol%	0,1-0,2 mol%	3
Sum of Inerts	≤2 mol%	≤1,0 mol%	≤0,5 mol%	4
Carbon dioxide (CO_2)	≤20 µmol/mol	≤20 µmol/mol	≤1 µmol/mol	5
Carbon monoxide (CO)	≤20 µmol/mol	≤20 µmol/mol	≤1 µmol/mol	6
Total sulphur incl H_2S	≤5 µmol/mol	≤5 µmol/mol	≤1 µmol/mol	7
Formic acid	≤10 µmol/mol	≤10 µmol/mol	≤1 µmol/mol	8
Formaldehyde (HCOH)	≤10 µmol/mol	≤10 µmol/mol	≤1 µmol/mol	8
Ammonia (NH_3)	≤10 µmol/mol	≤10 µmol/mol	≤1 µmol/mol	8
Halogenated compounds	≤0,05 µmol/mol	≤0,05 µmol/mol	≤0,05 µmol/mol	9
Water dewpoint	-8 °C bij 70 bara	-8 °C bij 70 bara	-8 °C bij 70 bara	10
All other impurities	disclaimer	disclaimer	disclaimer	11
Temperature	5-30 °C	5-30 °C	5-30 °C	12

Figure 69: Detailed description of the impurity constraints of the three cases for Gasunie's market consultation study [33].

E
Data and results of the thermodynamic cycles

The results of the various thermodynamic cycles are depicted in this Appendix chapter. For each cycle separately, the configuration is shown with the corresponding thermodynamic data of each state point of the cycle. In addition, some general values of the HEX's within the cycle are given to provide insight for future research [204]. These data and results are obtained with Aspen Plus [197].

E.1 Helium Brayton cycle

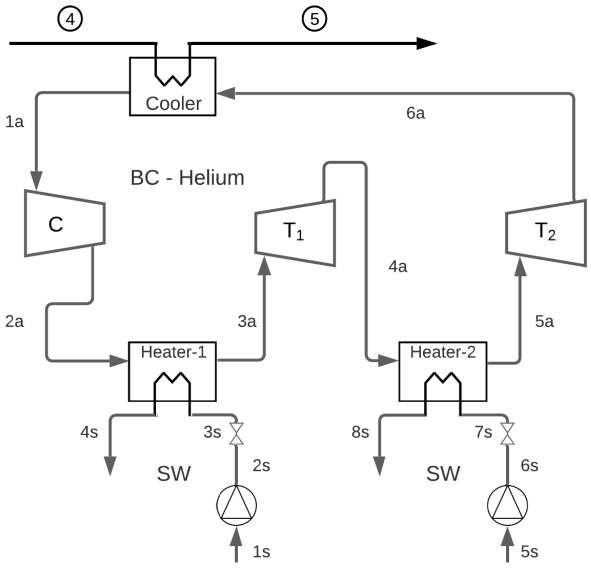

Figure 70: Overview of the proposed configuration of the Brayton cycle, with helium as the working fluid..

Table 45: Thermodynamic data of each state point of the helium Brayton cycle

N°	Fluid	m, [kg/sec]	T, [°C]	p, [bar]	h, [kJ/kg]	s, [kJ/kg*K]
4	LH2	3,46	-245,00	54,00	-3802,96	-51,19
5	LH2	3,46	-194,52	54,00	-2973,21	-34,38
1a	Helium	4,51	-190,00	4,00	-1115,73	-9,49
2a	Helium	4,51	-102,96	17,00	-659,37	-8,77
3a	Helium	4,51	5,00	17,00	-98,33	-6,22
4a	Helium	4,51	-40,11	10,00	-334,94	-6,03
5a	Helium	4,51	5,00	10,00	-100,61	-5,12
6a	Helium	4,51	-67,47	4,00	-478,93	-4,78
1s	Water	117,99	14,00	1,01	-15912,03	-9,22
2s	Water	117,99	14,04	6,00	-15911,37	-9,22
3s	Water	117,99	14,11	3,00	-15911,37	-9,22
4s	Water	117,99	9,00	3,00	-15932,80	-9,29
5s	Water	49,29	14,00	1,01	-15912,03	-9,22
6s	Water	49,29	14,04	6,00	-15911,37	-9,22
7s	Water	49,29	14,11	3,00	-15911,37	-9,22
8s	Water	49,29	9,00	3,00	-15932,80	-9,29

Table 46: Data of the HEXs used in the helium Brayton cycle

HEX	Duty [kW]	UA [kJ/s*K]	LMTD [°C]	MITA [°C]	HOT NTU	Cold NTU
Cooler	2870,93	33,42	85,90	55,00	1,43	0,59
Heater 1	-2529,38	61,68	41,01	9,11	0,12	2,63
Heater 2	-1056,47	44,49	23,75	9,11	0,22	1,90

E.2 Nitrogen Rankine cycle

In this section, the three different configurations of the nitrogen Rankine cycle is depicted, with related results of the flows and HEX values. First, the normal RC set-up is discussed. Thereafter the enhanced RC with LIN production is provided, with 0,5 kg/s LIN production. Lastly, the nitrogen Rankine cycle with a recuperator HEX is evaluated.

E.2.1 Nitrogen Rankine cycle - normal

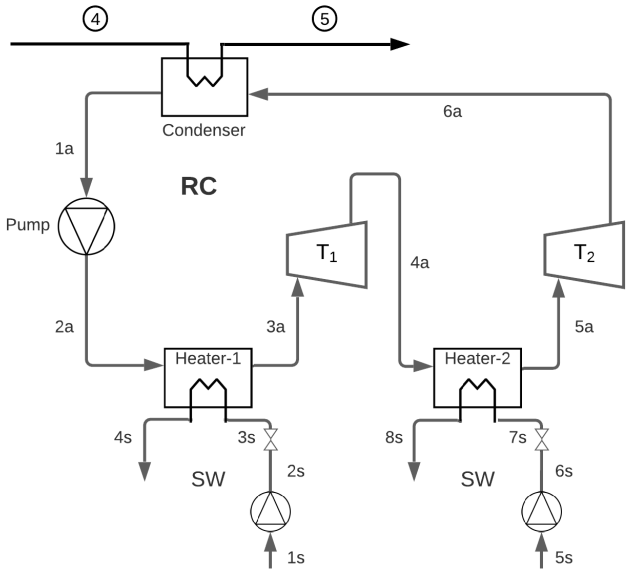

Figure 71: Overview of the proposed configuration of the Rankine cycle, with nitrogen as the working fluid.

Table 47: Thermodynamic data of each state point of the nitrogen Rankine cycle.

N°	Fluid	m, [kg/sec]	T, [°C]	p, [bar]	h, [kJ/kg]	s, [kJ/kg*K]
4	LH2	3,46	-245,00	54,00	-3802,96	-51,19
5	LH2	3,46	-194,52	54,00	-2973,22	-34,38
1a	Nitrogen	11,09	-189,52	2,00	-418,54	-3,84
2a	Nitrogen	11,09	-185,34	81,00	-404,98	-3,80
3a	Nitrogen	11,09	5,00	81,00	-40,15	-1,44
4a	Nitrogen	11,09	-53,76	32,00	-95,08	-1,39
5a	Nitrogen	11,09	5,00	32,00	-28,88	-1,12
6a	Nitrogen	11,09	-127,11	2,00	-159,77	-0,95
1s	Water	188,83	14,00	1,01	-15912,03	-9,22
2s	Water	188,83	14,04	6,00	-15911,37	-9,22
3s	Water	188,83	14,11	3,00	-15911,37	-9,22
4s	Water	188,83	9,00	3,00	-15932,80	-9,29
5s	Water	34,26	14,00	1,01	-15912,03	-9,22
6s	Water	34,26	14,04	6,00	-15911,37	-9,22
7s	Water	34,26	14,11	3,00	-15911,37	-9,22
8s	Water	34,26	9,00	3,00	-15932,80	-9,29

Table 48: Data of the HEXs used in the nitrogen Rankine cycle.

HEX	Duty [kW]	UA [kJ/s*K]	LMTD [°C]	MITA [°C]	HOT NTU	Cold NTU
Condenser	2870,90	80,82	35,52	20,35	1,76	1,42
Heater 1	-4047,71	53,49	75,68	9,11	0,07	2,52
Heater 2	-734,47	26,21	28,02	9,11	0,18	2,10

E.2.2 Nitrogen Rankine cycle - LIN production

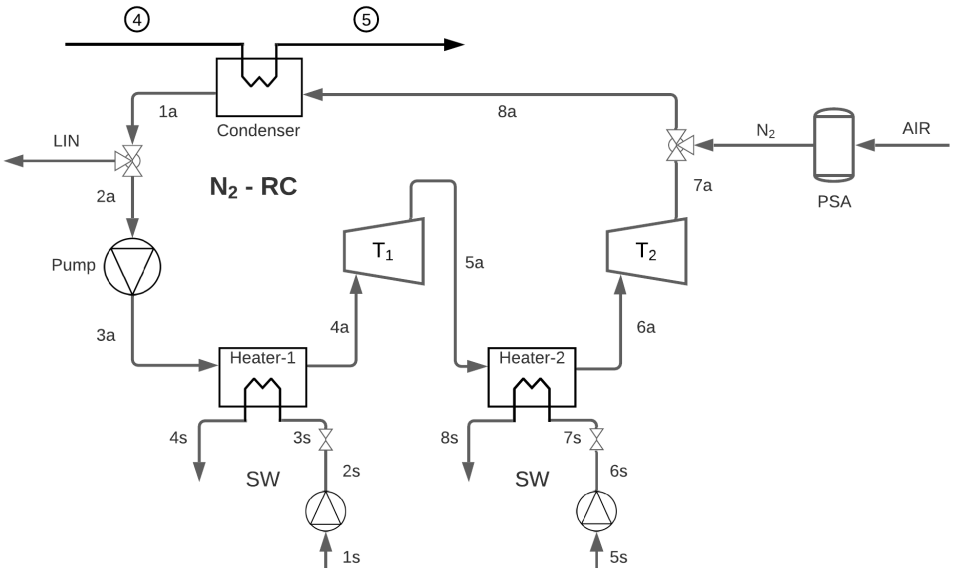

Figure 72: Overview of the proposed configuration of the enhanced nitrogen Rankine cycle, with additional LIN production.

Table 49: Thermodynamic data of each state point of the enhanced nitrogen Rankine cycle, with 0,5 kg/s LIN production.

N°	Fluid	m, [kg/sec]	T, [°C]	p, [bar]	h, [kJ/kg]	s, [kJ/kg*K]
4	LH2	3,46	-245,00	54,00	-3802,96	-51,19
5	LH2	3,46	-194,52	54,00	-2973,22	-34,38
N2	Nitrogen	0,50	40,00	2,00	15,20	-0,15
LIN	Nitrogen	0,50	-189,52	2,00	-418,54	-3,84
1a	Nitrogen	10,76	-189,52	2,00	-418,54	-3,84
2a	Nitrogen	10,26	-189,52	2,00	-418,54	-3,84
3a	Nitrogen	10,26	-185,34	81,00	-404,98	-3,80
4a	Nitrogen	10,26	5,00	81,00	-40,15	-1,44
5a	Nitrogen	10,26	-53,76	32,00	-95,08	-1,39
6a	Nitrogen	10,26	5,00	32,00	-28,88	-1,12
7a	Nitrogen	10,26	-127,11	2,00	-159,77	-0,95
8a	Nitrogen	10,76	-119,42	2,00	-151,64	-0,90
1s	Water	174,48	14,00	1,01	-15912,03	-9,22
2s	Water	174,48	14,04	6,00	-15911,37	-9,22
3s	Water	174,48	14,11	3,00	-15911,37	-9,22
4s	Water	174,48	9,00	3,00	-15932,81	-9,29
5s	Water	31,73	14,00	1,01	-15912,03	-9,22
6s	Water	31,73	14,04	6,00	-15911,37	-9,22
7s	Water	31,73	14,11	3,00	-15911,37	-9,22
8s	Water	31,73	9,01	3,00	-15932,77	-9,29

Table 50: Data of the HEXs used in the enhanced nitrogen Rankine cycle, with 0,5 kg/s LIN production.

HEX	Duty [kW]	UA [kJ/s*K]	LMTD [°C]	MITA [°C]	HOT NTU	Cold NTU
Condenser	2870,90	77,50	37,04	22,08	1,89	1,36
Heater 1	-3741,95	49,45	75,67	9,11	0,07	2,52
Heater 2	-678,99	24,23	28,03	9,11	0,18	2,10

E.2.3 Nitrogen Rankine cycle - Recuperator

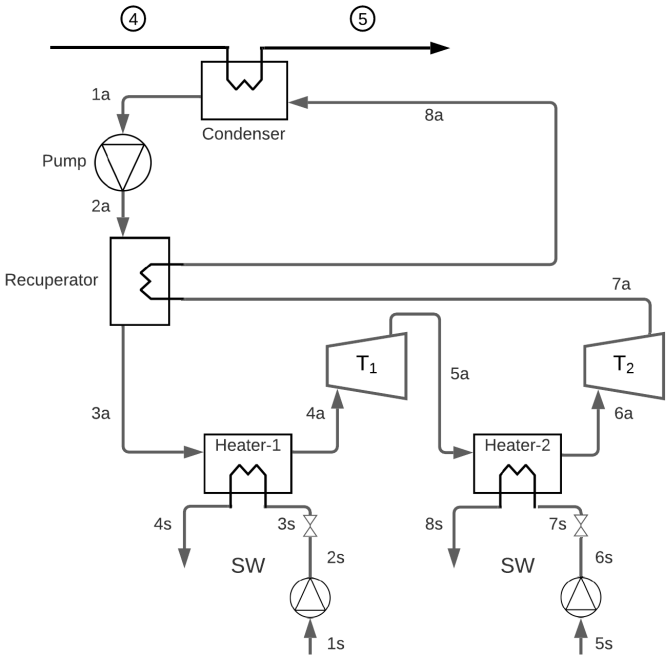

Figure 73: Overview of the proposed configuration of the nitrogen Rankine cycle, with recuperator.

Table 51: Overview of the process results of the nitrogen Rankine cycle, with recuperator.

Cycle	Qin [kW]	Net Power [kW]	Thermal Efficiency	Wnet / mLH2 [kWh / ton]	mWF / Wnet [kg / kWh]	Required SW flow [kg / s]	Pump/turb1/turb2 [bar]
N2-RC-Recuperator	2870,92	2146,54	74,8%	172,33	22,65	241,50	81/34/2

Table 52: Thermodynamic data of each state point of the nitrogen Rankine cycle with recuperator.

N°	Fluid	m, [kg/sec]	T, [°C]	p, [bar]	h, [kJ/kg]	s, [kJ/kg*K]
4	LH2	3,46	-245,00	54,00	-3802,96	-51,19
5	LH2	3,46	-194,52	54,00	-2973,22	-34,38
1a	Nitrogen	13,51	-189,52	2,00	-418,54	-3,84
2a	Nitrogen	13,51	-185,34	81,00	-404,98	-3,80
3a	Nitrogen	13,51	-163,89	81,00	-360,88	-3,35
4a	Nitrogen	13,51	5,00	81,00	-40,15	-1,44
5a	Nitrogen	13,51	-50,40	34,00	-91,99	-1,39
6a	Nitrogen	13,51	5,00	34,00	-29,37	-1,14
7a	Nitrogen	13,51	-129,11	2,00	-161,90	-0,97
8a	Nitrogen	13,51	-170,11	2,00	-206,00	-1,33
1s	Water	202,11	14,00	1,01	-15912,03	-9,22
2s	Water	202,11	14,04	6,00	-15911,37	-9,22
3s	Water	202,11	14,11	3,00	-15911,37	-9,22
4s	Water	202,11	9,00	3,00	-15932,80	-9,29
5s	Water	39,46	14,00	1,01	-15912,03	-9,22
6s	Water	39,46	14,04	6,00	-15911,37	-9,22
7s	Water	39,46	14,11	3,00	-15911,37	-9,22
8s	Water	39,46	9,00	3,00	-15932,80	-9,29

Table 53: Data of the HEXs used in the nitrogen Rankine cycle with recuperator.

HEX	Duty [kW]	UA [kJ/s*K]	LMTD [°C]	MITA [°C]	HOT NTU	Cold NTU
Condenser	2870,90	108,78	26,39	11,63	0,74	1,91
Heater 1	-4332,32	61,99	69,88	9,11	0,07	2,42
Heater 2	-845,84	31,29	27,03	9,11	0,19	2,05
Recuperator	595,66	25,44	23,41	15,22	1,75	0,92

E.3 Methane Rankine cycle

Table 54 and 55 depict the most suited Rankine cycle values, considering the constraints determined in section 10.6. However, if the pressure regime of the methane RC could be higher, the net power production could be increased. This is shown with the second methane RC, which has similar pressure conditions as the proposed methane RC by Atienza-Márquez et al. [184]. The pressure outlet conditions of the cycle are 105,3/32/7,5 bar for respectively the pump and the two turbines in series. Because the outlet pressure of the second turbine is 7,5 bar, the boiling point of methane rises to -130°C. This makes it possible to utilize more cold exergy of the LH2 flow, as the hydrogen can be heated up to 135°C instead of only -157°C for the lower pressure regime cycle. Although the net power production is higher, the thermal efficiency is significantly lower. The corresponding values of the methane RC operating in the higher pressure regime are shown below in Appendix E.3.2.

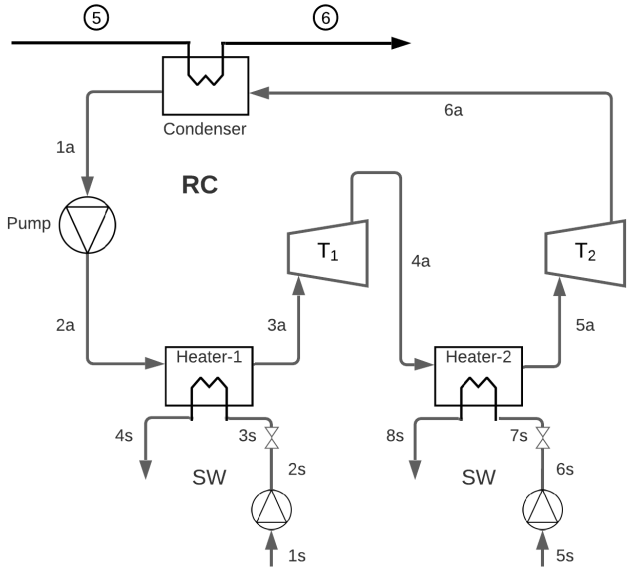

Figure 74: Overview of the proposed Rankine cycle configuration, which applies to both methane and ethylene as working fluid.

E.3.1 Methane Rankine cycle

Table 54: Thermodynamic data of each state point of the methane Rankine cycle.

N°	Fluid	m, [kg/sec]	T, [°C]	p, [bar]	h, [kJ/kg]	s, [kJ/kg*K]
5	LH2	3,46	-194,00	54,00	-2966,20	-34,29
6	LH2	3,46	-157,52	54,00	-2495,66	-29,39
1a	Methane	2,86	-152,53	2,00	-5524,40	-11,43
2a	Methane	2,86	-148,24	81,00	-5498,65	-11,38
3a	Methane	2,86	5,00	81,00	-4785,69	-7,70
4a	Methane	2,86	-51,31	32,00	-4868,67	-7,64
5a	Methane	2,86	5,00	32,00	-4725,68	-7,06
6a	Methane	2,86	-117,92	2,00	-4954,75	-6,78
1s	Water	95,06	14,00	1,01	-15912,03	-9,22
2s	Water	95,06	14,04	6,00	-15911,37	-9,22
3s	Water	95,06	14,11	3,00	-15911,37	-9,22
4s	Water	95,06	9,00	3,00	-15932,80	-9,29
5s	Water	19,06	14,00	1,01	-15912,03	-9,22
6s	Water	19,06	14,04	6,00	-15911,37	-9,22
7s	Water	19,06	14,11	3,00	-15911,37	-9,22
8s	Water	19,06	9,00	3,00	-15932,80	-9,29

Table 55: Data of the HEXs used in the methane Rankine cycle.

HEX	Duty [kW]	UA [kJ/s*K]	LMTD [°C]	MITA [°C]	HOT NTU	Cold NTU
Condenser	1628,07	73,77	22,07	10,08	1,57	1,65
Heater 1	-2037,62	35,20	57,89	9,10	0,09	2,65
Heater 2	-408,67	14,86	27,50	9,10	0,19	2,05

E.3.2 Methane Rankine cycle - High pressure regime

Table 56: Overview of the process results of the methane Rankine cycle, operating in the higher pressure regime.

Cycle	Qin [kW]	Net Power [kW]	Thermal Efficiency	Wnet / mLH2 [kWh / ton]	mWF / Wnet [kg / kWh]	Required SW flow [kg / s]	Pump/turb1/turb2 [bar]
Methane RC - HP	2630,71	803,21	30,5%	64,48	20,46	165,31	105,3/32/7,5

Table 57: Thermodynamic data of each state point of the methane Rankine cycle, operating in the higher pressure regime.

N°	Fluid	m, [kg/sec]	T, [°C]	p, [bar]	h, [kJ/kg]	s, [kJ/kg*K]
5	LH2	3,46	-194,00	54,00	-2966,20	-34,29
6	LH2	3,46	-135,05	54,00	-2205,88	-27,10
1a	Methane	4,57	-130,05	7,50	-5440,85	-10,81
2a	Methane	4,57	-122,86	105,30	-5405,72	-10,75
3a	Methane	4,57	5,00	105,30	-4815,53	-7,92
4a	Methane	4,57	-66,37	32,00	-4911,76	-7,84
5a	Methane	4,57	5,00	32,00	-4725,68	-7,06
6a	Methane	4,57	-70,51	7,50	-4864,61	-6,94
1s	Water	125,70	14,00	1,01	-15912,03	-9,22
2s	Water	125,70	14,04	6,00	-15911,37	-9,22
3s	Water	125,70	14,11	3,00	-15911,37	-9,22
4s	Water	125,70	9,00	3,00	-15932,80	-9,29
5s	Water	39,63	14,00	1,01	-15912,03	-9,22
6s	Water	39,63	14,04	6,00	-15911,37	-9,22
7s	Water	39,63	14,11	3,00	-15911,37	-9,22
8s	Water	39,63	9,00	3,00	-15932,80	-9,29

Table 58: Data of the HEXs used in the methane Rankine cycle, operating in the higher pressure regime.

HEX	Duty [kW]	UA [kJ/s*K]	LMTD [°C]	MITA [°C]	HOT NTU	Cold NTU
Condenser	2630,71	70,73	37,20	19,32	1,60	1,58
Heater 1	-2694,40	54,67	49,29	9,11	0,10	2,59
Heater 2	-849,52	26,31	32,29	9,11	0,16	2,21

E.4 Ethylene Rankine cycle

The configuration of the ethylene Rankine cycle is illustrated in figure 74. The corresponding data of the ethylene RC is shown below in table 59 and 60.

Table 59: Thermodynamic data of each state point of the methane Rankine cycle, operating in the higher pressure regime.

N°	Fluid	m, [kg/sec]	T, [°C]	p, [bar]	h, [kJ/kg]	s, [kJ/kg*K]
5	LH2	3,46	-194,00	54,00	-2966,20	-34,29
6	LH2	3,46	-101,90	54,00	-1765,41	-24,24
1a	Ethylene	8,67	-96,81	1,50	1227,67	-5,43
2a	Ethylene	8,67	-97,52	29,00	1234,19	-5,42
3a	Ethylene	8,67	5,00	29,00	1776,50	-3,17
4a	Ethylene	8,67	-43,94	12,88	1737,44	-3,14
5a	Ethylene	8,67	5,00	12,88	1816,62	-2,82
6a	Ethylene	8,67	-92,73	1,50	1707,07	-2,71
1s	Water	203,22	14,00	1,01	-16021,86	-9,49
2s	Water	203,22	14,04	6,00	-16021,20	-9,49
3s	Water	203,22	14,10	3,00	-16021,20	-9,49
4s	Water	203,22	9,00	3,00	-16044,33	-9,57
5s	Water	29,67	14,00	1,01	-16021,86	-9,49
6s	Water	29,67	14,04	6,00	-16021,20	-9,49
7s	Water	29,67	14,10	3,00	-16021,20	-9,49
8s	Water	29,67	9,00	3,00	-16044,33	-9,57

Table 60: Data of the HEXs used in the methane Rankine cycle, operating in the higher pressure regime.

HEX	Duty [kW]	UA [kJ/s*K]	LMTD [°C]	MITA [°C]	HOT NTU	Cold NTU
Condenser	4154,71	129,47	32,09	8,06	0,13	2,87
Heater 1	-4699,98	145,50	32,30	9,10	0,16	3,17
Heater 2	-686,20	27,52	24,93	9,10	0,21	1,96

F
BOG handling methods

In this Appendix chapter, the various BOG handling solutions are described. The process flows are shown, and in some cases, additional information is provided. The first three solutions have been analysed in this report. The other solutions have been discussed but require more in-depth investigation if deploying on the terminal is considered.

F.1 Normal BOG handling

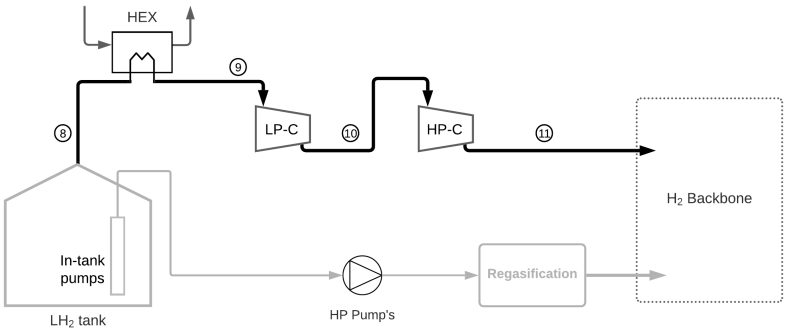

Figure 75: Process flow diagram of the Normal BOG handling solution.

In this case, the hydrogen BOG is processed with the compressors designed by Burckhardt. As is shown in the figure above, a HEX is used before the compressor because the LP-compressors cannot operate below -170°C. Heating the BOG before compression requires more energy input for the compressor. Therefore, processing the BOG in this way consumes a lot of energy.

Despite the high energy demands for the BOG process, there are also advantages when using this way of BOG handling. The first advantage is that the amount of hydrogen supply to the grid is small, as it is equal to the BOG flow. This is beneficial when the hydrogen demand of the grid is low. In that case, no unwanted hydrogen has to be delivered to the grid to keep the terminal safe. Furthermore, this way of processing the BOG is a straightforward process. These benefits also apply to the Cold BOG handling case.

F.2 Cold BOG handling

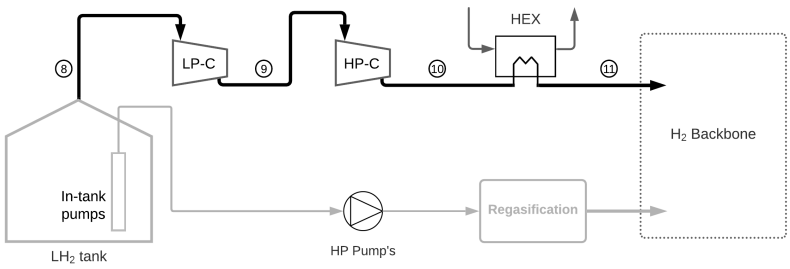

Figure 76: Process flow diagram of the Cold BOG handling solution.

For Cold BOG handling, it is assumed that compressors are capable of handling BOG at any temperature. So no additional heat transfer is needed before the BOG enters the LP-compressor. The temperature of the BOG leaving the HP-compressor will be below 0°C; therefore, a HEX is required after the compressor process. The benefit of this process is similar to the Normal BOG handling case. However, the energy demands for this method will be lower compared with the previous case since the compression takes place at lower temperatures.

F.3 BOG recondenser process

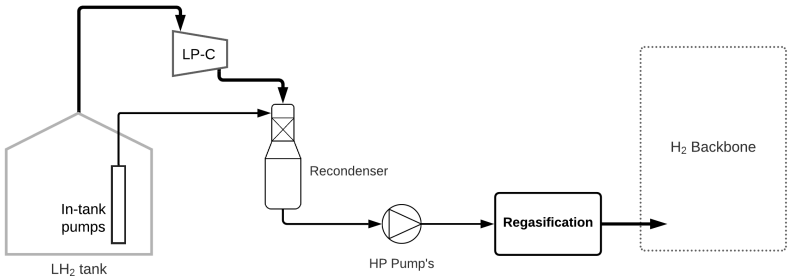

Figure 77: Process flow diagram of the BOG recondenser process.

The BOG recondenser process is already discussed in section 8.3. The benefits of handling the BOG in this manner is the fact that less energy has to be consumed since pumping requires less energy than gas compression.

The design of conventional BOG recondenser at LNG terminals consists of two sections. The upper part of the condenser houses a packed-bed column, where the cocurrent downflow of BOG and the subcooled liquid have direct contact to recondense the BOG [152]. With a pressure drop of around 10 mbar [205]. In the lower part of the recondenser, a holdup section is implemented. This holdup section is necessary to provide a significant NPSH for the HP-pump [152]. Since the LH_2 leaving the recondenser is considered a less subcooled liquid, it also affects the $NPSH_A$ of the liquid. As explained in chapter 7, the $NPSH_A$ is necessary to prevent cavitation issues inside the pump.

F.4 BOG reliquefaction process

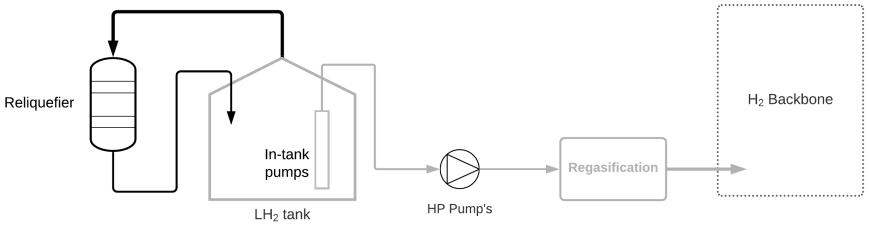

Figure 78: Process flow diagram of the actively reliquefaction process of the BOG.

In this case, the reliquefaction of the BOG flow is considered. This can be an exciting option because the hydrogen boil-off gas is already very cold and still in its para-hydrogen state. Furthermore, with this solution, no minimum hydrogen supply to the grid is necessary. This could be beneficial for the receiving terminal in the early stages of the hydrogen industry, as demand for the hydrogen grid could be low initially. As the figure 78 shows, the BOG flow is reliquefied with a reliquefaction process and is separate from the liquid stream. So the hydrogen supply to the grid is independent of the BOG flow. Therefore no minimum hydrogen supply to the grid is required.

For the reliquefaction process, first, the BOG flow has to be compressed up to 20 [206] till 40 bar [110]. Due to this compression, the temperature of the BOG flow increases as well. After this compression, the hydrogen BOG is cooled with a cooling cycle. The liquid for the cooling cycle is most often helium [207], because this liquid has a boiling point below the boiling point of hydrogen. After the hydrogen BOG is cooled down with multiple helium cooling cycles to 21 K [206] or 23 K [110], depending on the pressure of the BOG. The last phase in the reliquefaction process is the expansion of the hydrogen BOG. This expansion leads to a temperature decrease due to the positive Joule-Thomson coefficient of the hydrogen, explained in section 3. A wet expander is employed for the expansion process instead of a Joule-Thomson valve because it is more efficient [110].

The main disadvantage of this way of processing the boil-off gas is the very energy-consuming liquefaction process. The energy consumption of hydrogen liquefaction is around 20% of the HHV of hydrogen when atmospheric hydrogen is liquefied [26]. Luckily, the energy consumption for the reliquefaction process of the BOG flow is lower because of the already lower temperature and para-hydrogen concentration. So the ortho-para conversion at the liquefaction process is not necessary, which is 16% of the total work of the conventional liquefaction process [66]. When considering the same BOG reliquefaction as is done by Lee et al. in the article [110], then the energy consumption for the reliquefaction process of the hydrogen BOG is equal to 9.6% of the LHV. This 9.6% of the LHV is equivalent to 11,5 MJ/kg required for the reliquefaction process, which is still significant. Another disadvantage is the additional equipment and extra Helium fluid stream needed for processing the BOG flow in this way.

F.5 Electrical utilization of the BOG

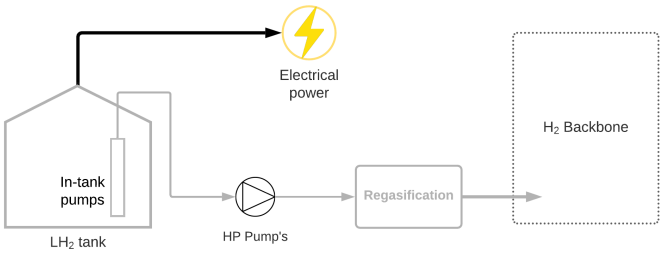

Figure 79: Process flow diagram of the Electrical utilization process of the hydrogen BOG.

As mentioned, utilising the boil-off gas into electricity can be done in two ways, using a fuel cell or a hydrogen gas turbine. Currently, the gas turbines are not capable of operating with 100% hydrogen input—multiple issues arising with 100% hydrogen input to the gas turbine. The hydrogen combustion temperature is higher than with natural gas, which creates hotspots [208]. These hotspots result in a higher NOx concentration in the emission. Furthermore, the flame propagation velocity of hydrogen is higher than natural gas. This could lead to flash back issues [208]. Nevertheless, various companies are doing investigations on this topic. They aim to have a commercially available 100% hydrogen gas turbine within a few years [153], [154].

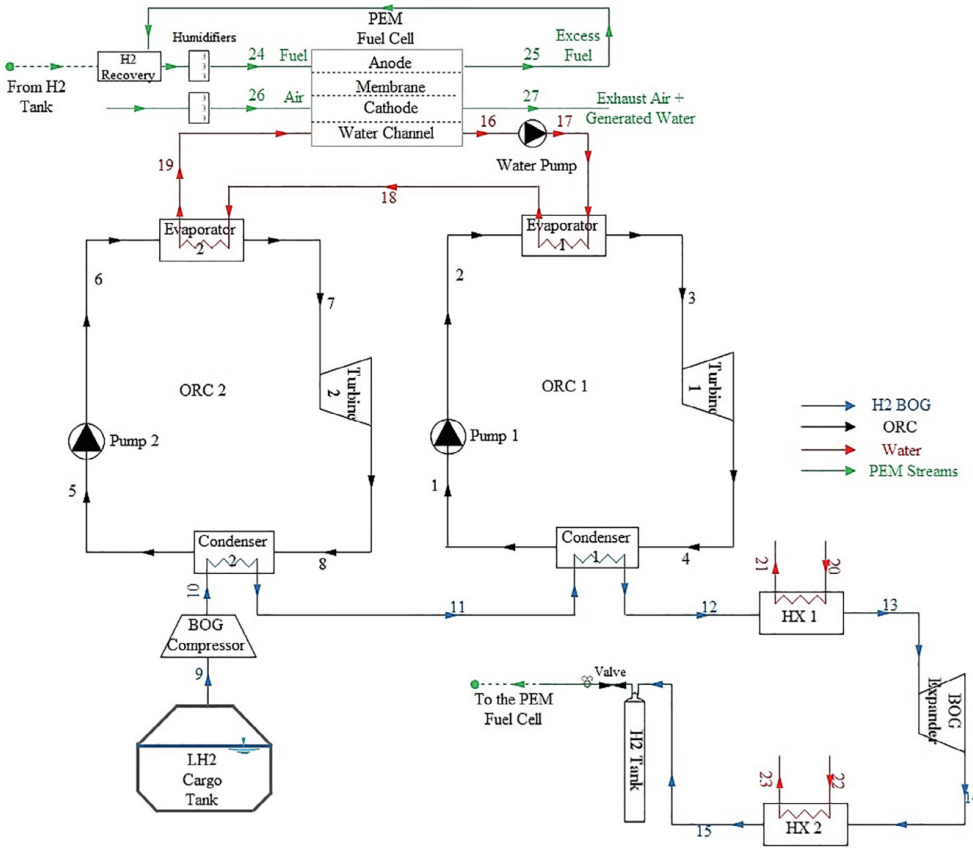

Figure 80: Flow diagram of a proposed system by [156], to convert hydrogen BOG into electricity

As explained, research has been done to convert hydrogen BOG into electricity by means of a fuel cell. The study done by Marandi et al., employs a fuel cell and two Organic Rankine Cycles operating as a heat recovery system to convert the BOG into electricity, as is depicted in figure 80 [156]. The PEM fuel cell has an energy efficiency of 45%, and the total system has an energy efficiency of 58%, meaning the heat recovery system increases the overall energy efficiency by 13%. The proposed design by Marandi et al. is a small-scale design in comparison with the requirements of the receiving terminal because the power output is 1353 kW with a hydrogen mass flow of only 0,019 kg/s.

The side effect of such a system is the additional equipment and processes at the terminal, which require extra space at the terminal site as well as a significant investment cost. The total cost rate for the 1353 kW power generation system explained above is 154,66 $/h [156]. For the large scale design, these costs will be significantly higher. Further in-depth research is required to investigate the real possibilities for the electrical utilisation of the hydrogen BOG. Multiple types of fuel cells are available besides the PEM fuel cell, and the design for the 100% hydrogen gas turbine is probably available before the LH_2 terminal is operational. The feasibility study for this form of BOG processing mainly depends on whether the price of the produced electricity is compatible with the electricity market price.

G
Aspen Plus models - LH_2 terminal configurations

In this Appendix, the Aspen models are provided for the various terminal configurations. The BOG and LH_2 streams are depicted separately. The Aspen Plus flowsheet is provided for each stream, with the corresponding input data and thermodynamic data of each flow.

G.1 BOG process flows

In this sections, the results for the various BOG processing streams are presented.

G.1.1 Basic-model (BOG process)

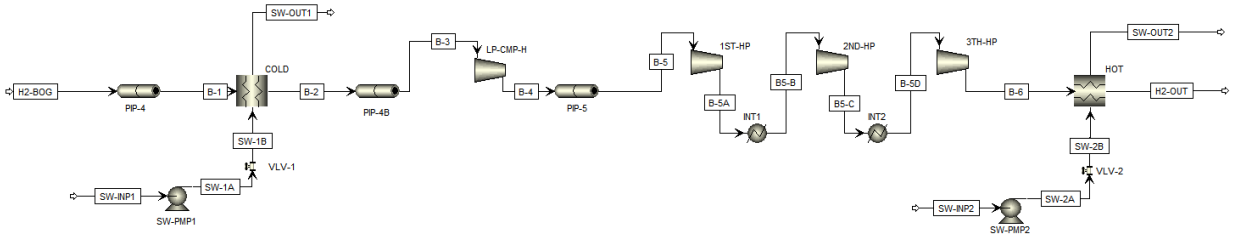

Figure 81: Basic-model, BOG processing scheme from Aspen Plus

Table 61: Thermodynamic data of each state point of the Basic-model, BOG processing scheme

N°	Fluid	T, [°C]	p, [bar]	h, [kJ/kg]	s, [kJ/kg*K]	ρ, [kg/m^3]
H2-BOG	H2	-252,69	1,04	-3482,18	-31,42	1,36
B-1	H2	-250,75	1,04	-3459,32	-30,35	1,22
B-2	H2	-170,00	1,04	-2591,32	-13,93	0,24
B-3	H2	-169,41	1,04	-2584,66	-13,86	0,24
B-4	H2	-49,36	6,58	-1047,75	-11,77	0,71
B-5	H2	-48,11	6,58	-1030,43	-11,70	0,71
B-5A	H2	48,92	19,81	352,81	-11,17	1,47
B5-B	H2	40,00	19,30	224,06	-11,47	1,48
B5-C	H2	101,45	35,46	1121,97	-11,39	2,25
B-5D	H2	40,00	34,60	231,50	-13,89	2,63
B-6	H2	75,83	50,00	758,62	-13,85	3,38
H2-OUT	H2	50,00	50,00	383,95	-14,96	3,65
SW-INP1	water	15,00	1,01	-15907,84	-9,20	999,10
SW-1A	water	15,03	4,00	-15907,44	-9,20	999,24
SW-1B	water	15,09	1,30	-15907,44	-9,20	999,10
SW-OUT1	water	10,09	1,30	-15928,40	-9,28	999,71
SW-INP2	water	15,00	1,01	-15907,84	-9,20	999,10
SW-2A	water	15,03	4,00	-15907,44	-9,20	999,24
SW-2B	water	15,09	1,30	-15907,44	-9,20	999,10
SW-OUT2	water	20,09	1,30	-15886,51	-9,13	998,20

Table 62: Input data for the Basic-model, BOG processing scheme

Stream/Block	Name on Scheme	Operating parameters	
Incoming BOG stream	H2-BOG	Vapour fraction and pressure	V = 1 p = 1,04 bar
Vacuum pipe 4	PIP-4	Length, diameter, heat flux	L = 202 m D = 12″ (40S) q = 9,8 W/m
BOG heating to -170°C, HEX	COLD	Seawater temperature change	ΔT_{SW} = -5°C
Vacuum pipe 4B	PIP-4B	Length, diameter, heat flux	L = 60 m D = 12″ (40S) q = 9,8 W/m
LP compressor	LP-CMP-H	Discharge pressure, isentropic efficiency	p = 6,58 bar n = 0,7176
Vacuum pipe 5	PIP-5	Length, diameter, heat flux	L = 50 m D = 24″ q = 30 W/m
HP comp. stage 1	1ST-HP	Discharge pressure, isentropic efficiency	p = 19,81 bar n = 0,88
HP comp. stage 2	2ND-HP	Discharge pressure, isentropic efficiency	p = 35,46 bar n = 0,97
HP comp. stage 3	3TH-HP	Discharge pressure, isentropic efficiency	p = 50 bar n = 0,97
Intermitted cooling	INT1, INT2	Output temperature	T = 40°C
BOG cooling to 50°C	HOT	Seawater temperature change	ΔT_{SW} = 5°C
Incoming SW stream	SW-INP1, SW-INP2	Temperature, pressure and mass flow	T = 15°C p = 1 atm m = Design-spec
Design spec: SW-INP1 mass flow	-	Variable: B-2 temperature; Manipul. varb.: SW-INP1	T_{B2} = -170°C
Design spec: SW-INP2 mass flow	-	Variable: H2-OUT temperature; Manipul. varb.: SW-INP2	$T_{H2\text{-}OUT}$ = 50°C
SW pump	SW-PMP1, SW-PMP2	Discharge pressure, isentropic efficiency	p = 4 bar n = 0,75
SW pressure at HEX	VLV-1, VLV-2	Outlet pressure	p = 1,3 bar

G.1.2 Cold-model (BOG process)

Note: This way of BOG processing is also used in the PC-model.

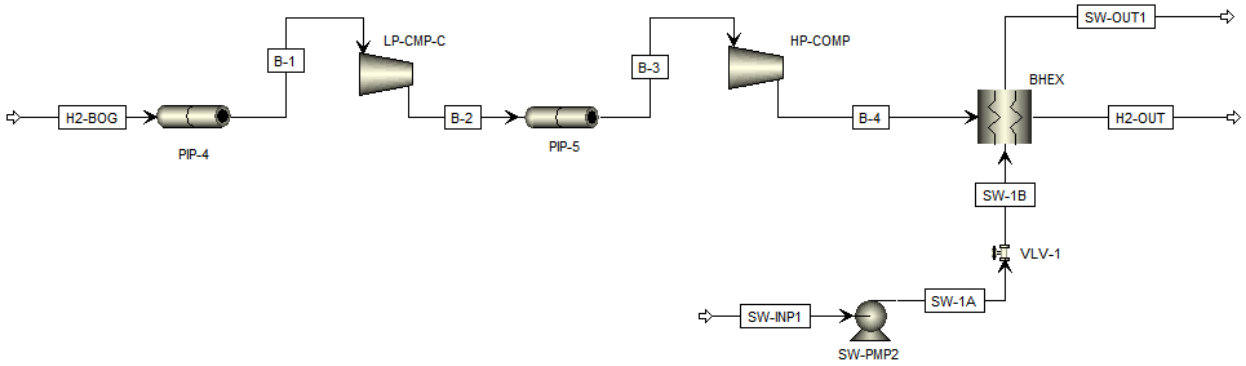

Figure 82: Cold-model, BOG processing scheme from Aspen Plus

Table 63: Thermodynamic data of each state point of the Cold-model, BOG processing scheme

N°	Fluid	T, [°C]	p, [bar]	h, [kJ/kg]	s, [kJ/kg*K]	ρ, [kg/m^3]
H2-BOG	H2	-252,69	1,04	-3482,18	-31,42	1,36
B-1	H2	-252,65	1,04	-3481,57	-31,39	1,36
B-2	H2	-222,85	6,58	-3187,88	-29,61	3,35
B-3	H2	-222,71	6,58	-3186,31	-29,58	3,33
B-4	H2	-142,78	50,00	-2304,31	-27,51	9,04
H2-OUT	H2	5,02	50,00	-265,36	-17,13	4,23
SW-INP1	water	15,00	1,01	-15907,84	-9,20	999,10
SW-1A	water	15,03	4,00	-15907,44	-9,20	999,24
SW-1B	water	15,09	1,30	-15907,44	-9,20	999,10
SW-OUT1	water	10,09	1,30	-15928,40	-9,28	999,71

Table 64: Input data for the Cold-model, BOG processing scheme

Stream/Block	**Name on Scheme**	**Operating parameters**	
Incoming BOG stream	H2-BOG	Vapour fraction and pressure	V = 1 p = 1,04 bar
Vacuum pipe 4	PIP-4	Length, diameter, heat flux	L = 202 m D = 12" (40S) q = 9,8 W/m
LP compressor (can handle extremely low temperatures)	LP-CMP-C	Discharge pressure, isentropic efficiency	p = 6,58 bar n = 0,7176
Vacuum pipe 5	PIP-5	Length, diameter, heat flux	L = 50 m D = 24" q = 30 W/m
HP compressor	HP-COMP	Discharge pressure, isentropic efficiency	p = 50 bar n = 0,7176
BOG heating, with ORV	BHEX	Seawater temperature change	ΔT_{SW} = -5°C
Incoming SW stream	SW-INP1	Temperature, pressure and mass flow	T = 15°C p = 1 atm m = Design-spec
Design spec: SW-INP1 mass flow	-	Variable: H2-OUT temperature; Manipul. varb.: SW-INP1	$T_{H2\text{-}OUT}$ = 5°C
SW pump	SW-PMP1	Discharge pressure, isentropic efficiency	p = 4 bar n = 0,75
SW pressure at ORV	VLV-1	Outlet pressure	p = 1,3 bar

G.1.3 Recondenser-model (BOG process)

In this section, the effect of the operating pressures of the recondenser is presented, and after that, the results of the Aspen simulation model.

When processing the BOG with a recondenser, an LH_2 flow is required to condensate the hydrogen BOG. As mentioned before, the operating pressure of the recondenser affects the required LH_2/BOG ratio, and also influences the energy efficiency of the process. An overview of these process characteristics for using the recondenser at different pressures is provided in table 65. The results are presented from 4 to 8 bar as these are the pressure ranges of the submerged pump and compressor. The overview shows that a lower operating pressure of the recondenser requires less energy for the BOG compressor, which results in a more efficient process. However, this lower pressure also results in a larger LH_2/BOG ratio, and thus in a higher minimum flow rate. The desired operating pressure of the recondenser depends on the send-out requirements of the terminal. Although the efficiency of the BOG processing stream decreases at a higher operating pressure, the overall efficiency loss is still significantly lower than the other options to process the BOG flow.

Table 65: Shows the effect of the recondenser operating pressure on the BOG process.

Operating press. Recondenser	**LH_2/BOG ratio**	η_{loss} **[%]**	E_{kg} **[kJ/kg]**	**Perc. comp. work [%]**
4	9,2	0,14%	204	9%
5	7,7	0,15%	217	12%
6	6,7	0,16%	231	15%
7	5,9	0,17%	245	18%
8	5,3	0,18%	260	21%

Note: The thermodynamic data results are shown for the minimum send-out rate, with the recondenser operating at 8 bar, and the BOG flow is equal to 0,306 kg/s.

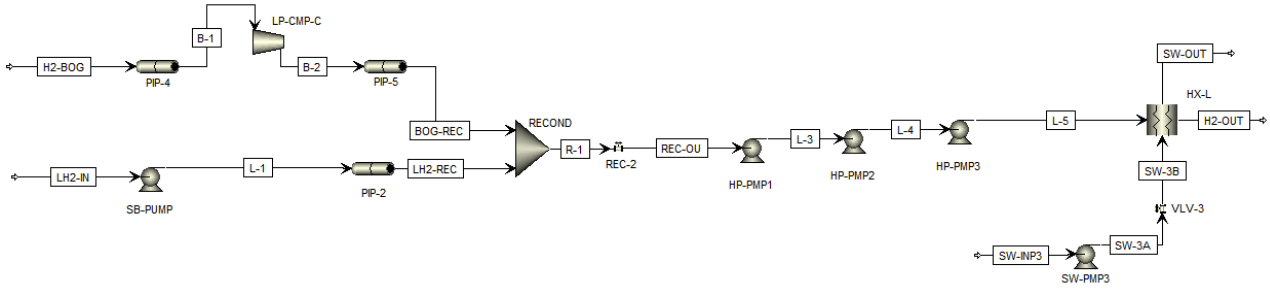

Figure 83: Recondenser-model, BOG processing scheme from Aspen Plus

Table 66: Thermodynamic data of each state point of the Recondenser-model, BOG processing scheme. Note the operating pressure of the recondenser is at 8 bar.

N°	Fluid	T, [°C]	p, [bar]	h, [kJ/kg]	s, [kJ/kg*K]	ρ, [kg/m^3]
H2-BOG	H2	-252,69	1,04	-3482,18	-31,42	1,36
B-1	H2	-252,54	1,04	-3480,30	-31,33	1,35
B-2	H2	-217,91	8,00	-3138,31	-29,43	3,68
BOG-REC	H2	-217,48	8,00	-3133,41	-29,34	3,65
LH2-IN	LH2	-252,85	1,07	-3931,99	-53,41	70,94
L-1	LH2	-252,02	8,00	-3917,41	-53,18	70,91
LH2-REC	LH2	-251,90	8,00	-3916,19	-53,12	70,77
R-1	LH2	-243,20	8,00	-3792,34	-48,35	54,71
REC-OU	LH2	-243,21	7,99	-3792,34	-48,35	54,70
L-1	LH2	-252,02	8,00	-3917,41	-53,18	70,91
L-3	LH2	-240,29	23,99	-3748,68	-47,88	55,45
L-4	LH2	-237,52	39,99	-3705,62	-47,46	56,05
L-5	LH2	-234,84	55,99	-3663,01	-47,08	56,57
H2-OUT	H2	5,00	55,99	-263,18	-17,60	4,72
SW-INP3	water	15,00	1,01	-15907,84	-9,20	999,10
SW-3A	water	15,03	4,00	-15907,44	-9,20	999,24
SW-3B	water	15,09	1,30	-15907,44	-9,20	999,10
SW-OUT	water	10,09	1,30	-15928,40	-9,28	999,71

Table 67: Input data for the Recondenser-model, BOG processing scheme

Stream/Block	**Name on Scheme**	**Operating parameters**	
Incoming BOG stream	H2-BOG	Vapour fraction and pressure	V = 1 p = 1,04 bar
Vacuum pipe 4	PIP-4	Length, diameter, heat flux	L = 202 m D = 12" (40S) q = 9,8 W/m
LP compressor (can handle extremely low temperatures)	LP-CMP-C	Discharge pressure, isentropic efficiency	p = Recon. operating pressure n = 0,7176
Vacuum pipe 5	PIP-5	Length, diameter, heat flux	L = 50 m D = 24" q = 30 W/m
Incoming LH_2 stream	LH_2-IN	Temperature and pressure	T = 20,3 K p = 0,0574 barg m = design-spec
Submerged pump	SB-PUMP	Discharge pressure, isentropic efficiency	p = Recon. operating pressure n = 0,67
Vacuum pipe 2	PIP-2	Length, diameter, heat flux	L = 202 m D = 12" (40S) q = 9,8 W/m
Recondenser (Mixer)	RECOND	Pressure drop	p = 0 bar
Recondenser pressure drop	REC-2	Pressure drop	Δp = 10 mbar
Design spec: $NPSH_A$ of the HP-pump	-	Variable: the $NPSH_A$ of the HP-PMP1 Manipul. varb.: LH_2-IN	$NPSH_A$ = 2,5 m
High pressure pump	HP-PUMP (1,2,3)	Pressure increase, isentropic efficiency	Δp =16 bar n = 0,67
Incoming SW stream	SW-INP3	Temperature, pressure and mass flow	T = 15° p = 1 atm m = Design-spec
SW ORV	HX-L	Seawater temperature change	ΔT_{SW} = -5°
Design spec: SW-INP3 mass flow	-	Variable: H2-OUT temperature; Manipul. varb.: SW-INP3	$T_{H2\text{-}OUT}$ = 5°
SW pump	SW-PMP3	Discharge pressure, isentropic efficiency	p = 4 bar n = 0,75
SW pressure at ORV	VLV-3	Outlet pressure	p = 1,3 bar

G.2 LH_2 stream processing

G.2.1 Normal LH_2 processing

This way of LH_2 processing has been used in the Basic-model, Cold-model and Recondenser-model.

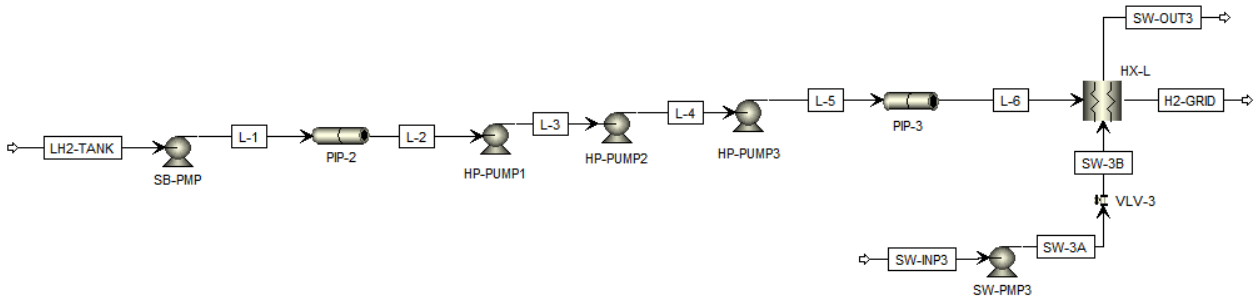

Figure 84: Normal LH_2 processing scheme from Aspen Plus, used in the Basic-, Cold- and Recondenser-model.

Table 68: Thermodynamic data of each state point of the Recondenser-model, BOG processing scheme. Note the operating pressure of the recondenser is at 8 bar.

N°	Fluid	T, [°C]	p, [bar]	h, [kJ/kg]	s, [kJ/kg*K]	ρ, [kg/m^3]
LH2-TANK	LH2	-252,85	1,07	-3931,99	-53,41	70,94
L-1	LH2	-252,25	6,07	-3921,47	-53,24	70,92
L-2	LH2	-252,22	6,07	-3921,18	-53,23	70,88
L-3	LH2	-250,32	22,07	-3887,49	-52,72	70,85
L-4	LH2	-248,44	38,07	-3853,78	-52,25	70,85
L-5	LH2	-246,58	54,07	-3820,08	-51,82	70,87
L-6	LH2	-246,54	54,07	-3819,70	-51,80	70,84
H2-GRID	H2	5,02	54,07	-263,72	-17,45	4,56
SW-INP3	water	15,00	1,01	-15907,84	-9,20	999,10
SW-3A	water	15,03	4,00	-15907,44	-9,20	999,24
SW-3B	water	15,09	1,30	-15907,44	-9,20	999,10
SW-OUT3	water	10,09	1,30	-15928,40	-9,28	999,71

Table 69: Input data for the Basic, Cold and Recondenser-model, LH_2 processing scheme

Stream/Block	Name on Scheme	Operating parameters	
Incoming LH_2 stream	LH_2-TANK	Temperature and pressure	T = 20,3 K p = 0,0574 barg
Submerged pump	SB-PMP	Pressure increase, isentropic efficiency	Δp = 5 bar n = 0,67
Vacuum pipe 2	PIP-2	Length, diameter, heat flux	L = 100 m D = 12" (40S) q = 9,8 W/m
High pressure pump	HP-PUMP (1,2,3)	Pressure increase, isentropic efficiency	Δp =16 bar n = 0,67
Vacuum pipe 3	PIP-3	Length, diameter, heat flux	L = 130 m D = 12" (40S) q = 9,8 W/m
Seawater ORV	HX-L	Seawater temperature change	ΔT_{SW} = -5°
Incoming SW stream	SW-INP3	Temperature, pressure and mass flow	T = 15° p = 1 atm m = Design-spec
Design spec: SW-INP3 mass flow	-	Variable: H2-GRID temperature; Manipul. varb.: SW-INP3	$T_{H2\text{-}GRID}$ = 5°
SW pump	SW-PMP3	Discharge pressure, isentropic efficiency	p = 4 bar n = 0,75
SW pressure at ORV	VLV-3	Outlet pressure	p = 1,3 bar

G.2.2 PC-model (LH_2-flow)

In this flowsheet, the two power cycles are not implemented; instead, a heater block (2RCS) is added to heat LH_2 flow to -157,7°. As the results are determined separately, adding the two power cycles into this flowsheet is not necessary. The results and flowsheet for the power cycles can be found in Appendix E.

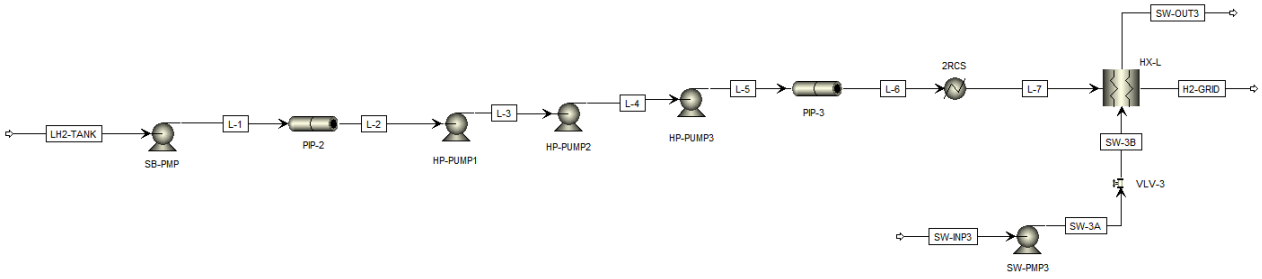

Figure 85: PC-model, simplified LH_2 processing scheme from Aspen Plus

Table 70: Thermodynamic data of each state point of the Recondenser-model, BOG processing scheme. Note the operating pressure of the recondenser is at 8 bar.

N°	Fluid	T, [°C]	p, [bar]	h, [kJ/kg]	s, [kJ/kg*K]	ρ, [kg/m^3]
LH2-TANK	LH2	-252,85	1,07	-3931,99	-53,41	70,94
L-1	LH2	-252,25	6,07	-3921,47	-53,24	70,92
L-2	LH2	-252,24	6,07	-3921,34	-53,24	70,90
L-3	LH2	-250,34	22,07	-3887,66	-52,73	70,87
L-4	LH2	-248,45	38,07	-3853,96	-52,26	70,87
L-5	LH2	-246,60	54,07	-3820,26	-51,83	70,89
L-6	LH2	-246,58	54,06	-3820,10	-51,82	70,87
L-7	H2	-157,70	54,06	-2498,00	-29,42	11,08
H2-GRID	H2	5,00	54,06	-264,02	-17,45	4,56
SW-INP3	water	15,00	1,01	-15907,84	-9,20	999,10
SW-3A	water	15,03	4,00	-15907,44	-9,20	999,24
SW-3B	water	15,09	1,30	-15907,44	-9,20	999,10
SW-OUT3	water	10,09	1,30	-15928,40	-9,28	999,71

Table 71: Input data for the PC-model, LH_2 processing scheme

Stream/Block	**Name on Scheme**	**Operating parameters**	
Incoming LH_2 stream	LH_2-TANK	Temperature and pressure	T = 20,3 K p = 0,0574 barg
Submerged pump	SB-PUMP	Pressure increase, isentropic efficiency	Δp = 5 bar n = 0,67
Vacuum pipe 2	PIP-2	Length, diameter, heat flux	L = 100 m D = 12" (40S) q = 9,8 W/m
High pressure pump	HP-PUMP (1,2,3)	Pressure increase, isentropic efficiency	Δp =16 bar n = 0,67
Vacuum pipe 3	PIP-3	Length, diameter, heat flux	L = 130 m D = 12" (40S) q = 9,8 W/m
Heat transfer with the two Rankine cycles	2RCS	Outlet temperature	T = -157,7°
Seawater ORV	HX-L	Seawater temperature change	ΔT_{SW} = -5°
Incoming SW stream	SW-INP3	Temperature, pressure and mass flow	T = 15° p = 1 atm m = Design-spec
Design spec: SW-INP3 mass flow	-	Variable: H2-GRID temperature; Manipul. varb.: SW-INP3	$T_{H2\text{-}GRID}$ = 5°
SW pump	SW-PMP3	Discharge pressure, isentropic efficiency	p = 4 bar n = 0,75
SW pressure at ORV	VLV-3	Outlet pressure	p = 1,3 bar